2007

Modeling spatial and temporal variations of surface moisture content and groundwater table fluctuations on a fine-grained beach, Padre Island, Texas

Yuanda Zhu
Louisiana State University and Agricultural and Mechanical College, yzhu2@lsu.edu

MODELING SPATIAL AND TEMPORAL VARIATIONS OF SURFACE MOISTURE CONTENT AND GROUNDWATER TABLE FLUCTUATIONS ON A FINE-GRAINED BEACH, PADRE ISLAND, TEXAS

A Dissertation
submitted to the Graduate Faculty of the
Louisiana State University and
Agricultural and Mechanical College
in partial fulfillment of
the requirements for the degree of
Doctor of Philosophy

in

The Department of Geography and Anthropology

By

Yuanda Zhu
B.S., Huazhong Agricultural University, 1998
M.S., Huazhong Agricultural University, 2001

December 2007

To Louisa and Min

ACKNOWLEDGEMENTS

I would like to thank everyone who offered their generous help in my PhD study. First and most, I want to thank my major professor, Dr. Steven L. Namikas, for accepting me as a graduate student and for his financial, academic and mental support and guidance throughout the program. From the initialization of this project, he led me through all the hurdles and difficulties I have confronted.

I would also thank Dr. Patrick A. Hesp, Dr. Michael D. Blum, and Dr. Barry D. Keim for serving on my committee and for their interest of this project. It took them much time to go through and to make helpful suggestions for the whole project.

Special thanks are given to Mr. Brandon L. Edwards who offered invaluable help for my field work in 2005 and 2006. I will never forget the extremely high temperatures, humidity, intense sunshine, strong wind and occasional thunder storms we experienced during my field work. I would also like to thank Mr. Phillip P. Schmutz and Dr. Diane P. Horn for their help in 2006 summer.

I would also thank Ms. Dana Sanders, Ms. Vicki Terry, Ms. Linda Strain, and Ms. Nedda Taylor for their help in my program of study.

I would also like to thank the staff of the Padre Island National Seashore for their kind help and some useful data I did not obtain in the field.

TABLE OF CONTENTS

LIST OF FIGURES

ABSTRACT

The basic goals of this study are to document, represent and model beach surface moisture dynamics. Achieving these goals requires that the dynamics be understood within the context of the key associated processes including evaporation and groundwater table fluctuations. Atmospheric parameters including wind speed, air temperature and relative humidity, evaporation, beach surface moisture content, groundwater table fluctuations and tidal oscillations were directly monitored in an eight-day field experiment.

Field measurements demonstrated that beach surface moisture content has a relatively high degree of variability in the cross-shore direction and a relatively low variability in the alongshore direction. The highest levels of variability were found in the middle beach, where daily fluctuations of up to 30% (volume) were common. Long-term variations in surface moisture content are controlled by water table fluctuations, while short-term variations are dominated by either evaporation or groundwater table fluctuations depending on the local water table depth.

Two traditional methods to estimate potential evaporation rates were tested, the mass-transfer method and the combined (energy-budget and mass-transfer together) approach. Results showed that the mass-transfer method produces consistent large errors in simulations, even with recalibration of the constants. Simulations utilizing the Penman equation provide much better agreement with field data. It was found that groundwater table fluctuations at the studied beach are mainly forced by tidal oscillations. The numerical solution of the linealized Boussinesq equation provides an accurate approach to simulate tide-forced beach groundwater table fluctuations. These simulations were found to be significantly improved by modeling the system as a sloping beach rather than using the traditional vertical beach approach.

Spatial and temporal variations in beach surface moisture were modeled using the numerically solved Richard's equation and the Force-Restore method. The Force-Restore method underestimates surface moisture contents when the water table is relatively shallow owing to an inherent defect in the model itself. The simulations employing the numerically solved Richard's equation agree closely surface moisture content from the field.

This study represent perhaps the first, certainly the most comprehensive, attempt that has been made to date, to explain intermediate-scale variability in beach surface moisture content in light of the microscale process that drive these dynamics. The findings of this study should be applicable to longer time periods, and larger spatial areas with similar environmental settings. However, more investigations regarding hydraulic properties of local sediment are needed to enhance the model applicability.

CHAPTER 1 INTRODUCTION

The major purposes of this chapter are to introduce and outline what this project is focused on and why it is important. Given that beach surficial moisture is generally controlled by a complex combination of hydrological and meteorological components, and that it usually exerts a significant influence on a variety of coastal processes (particularly aeolian sediment transport), a better understanding of the high degree of spatial and temporal variability in this environmental conditions represent the ultimate goal of this study.

1.1 Introduction

It is widely recognized that the moisture content of beach sediment is important to interstitial biological activity, coastal water resource budgets, beach stability, and to wind-blown sediment transport (McLachlan, 1989; Famiglietti *et al.*, 1998; Horn, 2002; Chen and Hu, 2004; Yang and Davidson-Arnott, 2005). Surface moisture content in particular is often cited as having an important influence on the entrainment of sand by wind, and several models of this influence have been proposed (Namikas and Sherman, 1995; Cornelis and Gabriels, 2003). However, application of such models to real world beaches is hampered by a lack of understanding of the nature and dynamics of spatial and temporal variability in surface moisture content. Although a small number of field investigations have provided limited data sets documenting surface moisture content at various beaches (e.g. Chepil, 1956; Svasek and Terwindt, 1974; Sarre, 1988; Nickling, 1989; Atherton *et al.*, 2001; Yang and Davidson-Arnott, 2005), there is no available guidance regarding how to represent or model the high degree of temporal and spatial variability in the surface moisture content of real beaches. This problem must be resolved before it will be

possible to realistically incorporate the role of surface moisture into the modeling and simulation of wind blown transport on real beaches.

1.2 Research Needs

Surface moisture content, as other investigators have noted (e.g., York *et al.*, 2002), is affected by many factors including rainfall, groundwater, evaporation, percolation and condensation. Most previous studies related to the variations of surficial soil moisture have generally focused on the water exchange between the unsaturated zone and the atmosphere (i.e. evaporation and precipitation), and neglected the effects of groundwater (Chen and Hu, 2004). Even in sophisticated models of land surface and soil hydrology, the input of groundwater has often been not considered. This omission is likely due to the fact that for most ecological systems the rainfall is typically the most significant input to surface moisture content. For beaches, however, frequent fluctuations in groundwater level may provide the major input to surface moisture. Unfortunately, the few reports available to date provide only a rough empirical relation between cycles of tide and surface moisture content (e.g., Atherton *et al.*, 2001). Further, these studies are generally limited into the swash or intertidal zones, and far from sufficient to establish a quantitative relation between these two parameters. Current knowledge about the relation between surface moisture content and water table fluctuations is simply too limited to provide a reliable picture of surface moisture content variations for beach systems, particularly for the backbeach areas that represent the most significant zone for aeolian sediment transport (e.g., Sherman *et al.*, 1998).

Beach groundwater oscillation forced by tides and waves has also been studied extensively by coastal engineers in recent decades (e.g., Nielson, 1990; Gourlay, 1992; Turner *et al.*, 1993; Li *et al.*, 1997; Jeng *et al.*, 2005). Although the phase of beach groundwater fluctuations has

been successfully modeled (Horn, 2002), predictions of depths and amplitudes of beach groundwater table usually have significant errors even in the best studies (see Raubenheimer *et al.*, 1999). Therefore, there is a need to further improve the accuracy in modeling groundwater table fluctuations and hence ground-surface moisture relations in real beach systems.

Most field studies of the effect of surface moisture content on sediment transport have employed traditional surface-scrape sampling strategies (e.g., Cornelis and Gabriels, 2003). Such methods are time consuming and always considerably disturb the original experimental surface, making detailed time-series data a practical impossibility (Atherton *et al.*, 2001). Furthermore, such traditional point measurement techniques do not represent the spatial distribution well since only a limited area can be satisfactorily monitored within an acceptable temporal framework (Walker *et al.*, 2001). Atherton *et al.* (2001) introduced a new effective approach for monitoring near-surface moisture content using the Delta-T moisture sensor. This kind of moisture sensor sends a microwave signal and analyzes the reflection to measure the dielectric constant of the soil and then records it as voltage that can be converted into volumetric moisture content by calibration. Yang and Davidson-Arnott (2005) further testified and modified this method to obtain reliable measurements in the upper 2 centimeters of sediment. This method will be used in this study to allow rapid and repeated measurements at a same location in the field with little disturbance of the surface, providing high enough spatial and temporal resolution over long enough time periods and large enough areas. The field measurements will provide a solid basis for model evaluation and for a better understanding of the moisture influence on aeolian sediment transport process on coastal beaches.

The mathematical description of the water transport dynamics on a real beach contains several main challenges. First, the governing equations for saturated water flow in the phreatic

zone and unsaturated water flow in the vadose zone are highly nonlinear, and the nonlinearity has both time dependent and averaged effects that have never been perfectly modeled at our current level of knowledge (Nielson, 1990). The second problem is that the local soil moisture profiles above a fluctuating water table might be extremely difficult to be predicted with any existing models due to the hysteresis (which leads to various soil water content at same hydraulic pressure) introduced by the highly frequent fluctuations of the water table. The Darcy law without consideration of hysteresis is widely used in previous studies, and provides the fundamental basis for almost all current studies of soil moisture modeling (e.g., York *et al.*, 2002; Chen and Hu, 2004). The third difficulty is that of the moving boundary position for groundwater fluctuations induced by tidal variations on a sloping beach face. This has previously been tackled analytically by Nielson (1990) and further investigated theoretically by Li *et al.* (2000), but most previous studies assumed a vertical beach face (e.g, Dominick *et al.*, 1971; Philip, 1973; Fang *et al.*, 1973) or treated it as a black box while acknowledging its strong nonlinear filtering effects on tidal waves (Nielson, 1990). In addition, the assumptions underlying studies of the two key aspects of this system are essentially distinct: vertical unsaturated water flow is assumed to be predominant in studies of soil moisture dynamics while horizontal saturated water flow is assumed to control the process of tide-induced water table fluctuation. Both of these approaches arbitrarily neglect flows in other directions for simplicity and convenience. Although two-dimensional or three-dimensional flow models have been introduced by some authors (e.g., Li *et al.*, 1996b; Jeng *et al.*, 2005a), they are not promising to date for practical use due to their complexity and concerns regarding their accuracy. As water transport is the essential part of surface moisture dynamics, the approaches to deal with these

challenges fundamentally determine the model performance in simulating the spatial and temporal variability in beach surface moisture content.

1.3 Research Objectives

To achieve the major goal–to develop of a realistic model of dynamic change in the surface moisture content of a real-world beach–five fundamental objectives have been set in this study as follows:

1) To document spatial and temporal variability in surface moisture content and then develop a high-resolution database for a real-world beach. High resolution measurements over time and space are essential to understand trends and amplitudes of surface moisture content changes, and potentially to be utilized to test existing models or develop new ones. However, as mentioned above, most previous studies of beach surface moisture usually employed a traditional drying-weighing approach and these records of surface moisture content have large gaps in time and often low spatial resolution. Therefore, a high-resolution database of surface moisture content is necessary and will provide the basis for further analysis in this project.

2) To obtain concurrent measurements of key processes and parameters influencing surface moisture content. Beach surface moisture dynamics are directly affected by water flows as capillary rise from groundwater, infiltration from precipitation and swash, and water molecular dispersion and movement as evaporation and condensation. Further, sediment characteristics determine rates and velocity of saturated and unsaturated water flows in a beach body, beach groundwater table fluctuates in response to tides and waves and inland hydraulic water pressure, and atmospheric parameters including solar radiation, air temperature, relative humidity and wind speed control the rates of and phase shift between evaporation and condensation (see Figure 1.1). Therefore, the variability in surface moisture content cannot be understood and

accurately modeled until these processes and parameters have been accurately measured or modeled.

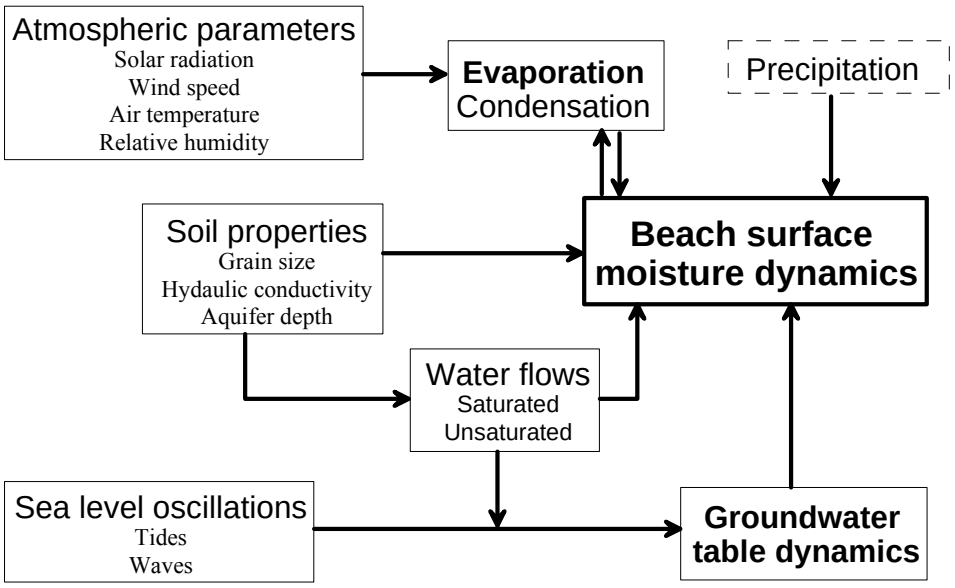

Figure 1.1 Key processes and parameters associated with beach surface moisture dynamics

3) To examine and test previous evaporation models and develop a feasible approach for evaporation estimation in coastal areas. A large number of evaporation models have been proposed and extended through structural modifications and constant recalibrations in many previous studies. However, atmospheric circulation patterns of coastal areas are quite unique in contrast to those of inland area, due to the combined influences at both water and land surfaces. Since existed evaporation models have usually been developed based on data obtained from inland areas, they need to be carefully tested and verified using field data from coastal areas.

4) To quantitatively model water table fluctuations forced by tides in a real, sloping beach. Groundwater level in a beach often fluctuates quickly responding to inland and oceanic hydraulic pressures and consequently plays a crucial role in regulating the status of beach surface moisture in that beach groundwater table is fairly shallow in general. Since measurements of groundwater table are usually not available or costly to obtain, it is necessary to develop an effective approach

to model and predict its elevation from tidal records (which can be easily obtained from other sources). Most previous studies have assumed that the beach face is vertical for simplicity (e.g, Dominick *et al.*, 1971; Philip, 1973; Fang *et al.*, 1973) or treated it as a black box (albeit acknowledging its strong nonlinear filtering effects on tidal waves). The nonlinearity introduced by a sloping beach was first tackled analytically by Nielson (1990), and then theoretically investigated by Li *et al.* (2000). However, very few of the theoretical works published in recent years have been tested using field data, an advance which this study will provide.

5) To develop a realistic model to predict spatial and temporal variations in beach surface moisture content using a coupled groundwater model and evaporation model with consideration of condensation and precipitation. Apparently, surface moisture dynamics involve a mutual interaction with all of these processes (as well as marine inputs, for a beach environment). Any process can become the controlling factor for moisture dynamics at a given time and location, under different environmental conditions. Although the effects of single factors have been studied intensively, the interactions between them remain unclear.

1.4 Outline of Project

This project mainly focuses on ways to enhance understanding of the spatial and temporal variability in beach surface moisture content, through quantitative simulations of these variations. The primary motivation is to establish a basis for subsequent modeling of moisture influence on coastal aeolian sediment transport. Major associated input and output processes, i.e., groundwater table fluctuations, precipitation, condensation and evaporation, are carefully considered and modeled. Several models are implemented and compared with each other to simulate the groundwater table dynamics and potential evaporation based on field-observed

atmospheric parameters, soil properties and tidal fluctuations. Eventually, beach surface moisture dynamics are simulated with coupled groundwater and evaporation models.

This research will provide valuable contributions to our understanding of beach hydrodynamics in several ways. First, the degree of variability in surface moisture content over various time (hours to weeks) and space (meters to dozens of meters) scales are assessed and analyzed based on field-obtained high-resolution measurements. Second, the most precise evaporation model is found for coastal areas that often has unique atmospheric conditions rather than inland areas. Third, tide-induced groundwater table fluctuations are documented and modeled for coasts of the Gulf of Mexico, particularly fine-grained beaches with micro tidal ranges. Fourth, the factors controlling beach surface moisture content variations are identified and the degrees of their dominance were analyzed. Finally, a realistic model combining a groundwater model, evaporation model and soil water retention curve is developed, requiring only a few inputs that can be obtained from routine data or easily measured in the field.

This dissertation is composed of eight chapters. The next chapter provides a review of selected literature. In Chapter 3, the environmental setting of the study site and methodology of this study will be introduced. In Chapter 4, spatial variability and temporal trends of beach surface moisture are evaluated based on high-resolution measurements obtained in the field. In Chapter 5, selected evaporation models are tested against field data to identify the most precise model for evaporation prediction at high temporal resolution. In Chapter 6, tide-induced beach groundwater table fluctuations are modeled numerically and analytically, and tested against field measured data. In Chapter 7, measured temporal and spatial variations of surface moisture content are simulated by combining the findings of the previous chapters, and the results are assessed. Chapter 8 provides a summary of and major conclusions for the whole project.

CHAPTER 2 REVIEW OF LITERATURE

This chapter reviews recent literature on the key topics associated with beach hydrology. Some general information and major research advances are included to provide a comprehensive understanding of the behaviors, controlling factors, and practical implications of relevant hydrological processes. Additional detail on specific topics is also incorporated in subsequent chapters as appropriate.

2.1 Introduction

As the interface of atmosphere and pedosphere, the soil surface has a unique role in conditioning hydrological and biological processes. Motions and disturbances in the atmospheric fluid at a variety of temporal and spatial scales are principally forced by the differential heating, and by friction at the surface (Entekhabi *et al.*, 1996). Further, soil surface acting as the upper boundary of vadose zone indirectly limits unsaturated water flow within soil body. Surface moisture is widely believed to be a crucial parameter in partitioning energy and affecting ecosystem structure and function (Wythers *et al.*, 1999). Thus, it is important to enhance the currently weak knowledge of surface moisture dynamics.

For a relatively simple beach system, surface moisture dynamics influences the presence of vegetation, the occurrence of aeolian sediment transport, and eventually the stability and evolution of beach dune topography. Beach surface moisture distribution usually exhibits an extremely high variability in both of time and space (Yang and Davidson-Arnott, 2005), which necessitates intensive and accurate measurements to make this complex phenomena fully understood. Until recently a method that is capable of making high-frequency or continuous measurements over time at the same spot has not been available (Atherton *et al.*, 2001). The

method to measure moisture content directly using newly-developed moisture sensor potentially allows the enhancement of beach surface moisture study.

In traditional groundwater and unsaturated water flow models that are based on the combination of Richard's equation and Darcy's law, evaporation (the major component of upper boundary conditions) is usually set to a constant value, or totally neglected. As a result, predicted water content at the soil surface could not sufficiently represent the cyclic variations induced by diurnal changes of evaporation (Maxwell and Miller, 2005). Conversely, most conventional "land surface" models to date use a parmeterization of the bottom layer either specified as a constant moisture content or a uniform potential gradient, ignoring the fluctuations of groundwater table (Chen and Hu, 2004). Thus, a satisfactory scheme to estimate surface moisture variations under conditions of high evaporative potential and a fluctuating water table is potentially of great utility.

2.2 Surface Moisture Content and Aeolian Sediment Transport

Investigations of the effects of soil moisture on aeolian sediment transport dates back to the early 1930s (e.g., Akiba, 1933). A number of subsequent field observation and wind tunnel studies thereafter have shown that surface moisture can exert very important impacts on both entrainment and transport of sediment by wind (Chepil, 1956; Belly, 1964; Azizov, 1977; Logie, 1982; Cornelis and Gabriels, 2003; Wiggs *et al.*, 2004; McKenna Neuman and Langston, 2006). Comprehensive and critical reviews of this topic have been made by Horikawa et al. (1982), Hotta et al. (1984), Namikas and Sherman (1995), and Cornelis and Gabriels (2003). Most laboratory wind tunnel studies (e.g. Sue, 1963; Horikawa et al., 1982; Nickling and McKenna Neuman, 1997; McKenna Neuman and Maljaas, 1997) are based on simulating the entrainment process at a variety of wind speeds and moisture contents for a particular sediment. However, the

results seldom can be extrapolated directly and adequately in terms of the texture of used materials and the high variability of some factors such as wind velocity and soil moisture content in natural systems. Field studies (e.g., Chepil, 1956; Belly, 1964; Cornelis and Gabriels, 2003; Sarre, 1988; Wiggs *et al.*, 2004) have suffered from the capability of instruments and technological limitation to obtain high resolution data over space and continuous measurements at the same spot, due to the utilization of traditional sampling approach. Few studies have addressed the time-dependent or space-dependent behavior of surface moisture, in terms of influences on aeolian sediment transport in either laboratory or field.

Relationships between moisture content and critical threshold velocity have received substantial attention from many researchers (e.g., Sarre *et al.*, 1989; Sherman *et al.*, 1998; Bauer and Davidson-Arnott, 2002; Wiggs *et al.*, 2004), although the exact nature of this phenomena is still not full understood or specified for natural systems (Namikas and Sherman, 1995). It is accepted that the existence of soil moisture increases the threshold velocity of wind required to initialize sediment motion because the capillary force induced by soil moisture increases the bonding force between soil particles and the resistance of soil grains against motion forced by wind (Nickling and McKenna Neuman, 1997). The findings of wind-tunnel (e.g., Chepil, 1956; McKenna Neuman and Nickling, 1989) and field (e.g., Jackson and Nordstrom, 1997) studies confirmed the general conceptual idea that threshold velocity increase with soil moisture content. Some studies also indicated that given a certain type of soil or sand and a certain velocity of wind, the aeolian sediment process would stop completely when the moisture content of that soil reached a critical value (Chepil, 1956; Sarre, 1988; Nickling, 1989). However, the "critical" moisture content has varied from 5% in the wind tunnel study of Belly (1964) to 14% in the field study of Sarre (1988). More surprisingly, the critical moisture content even assumed as a low

value of 1% (gravimetric) in the wind tunnel study of Chepil (1956), although this finding was never confirmed by other studies. Apparently, although moisture content has been cited as a particularly regulator of aeolian sediment transport, contradictory outcomes have also often been uncovered due to the differences in experimental approach adopted and material used, and more importantly, the high variability in surface moisture content in natural system.

Along with relating threshold velocity empirically to surface moisture content through field observation or laboratory work, some researchers also made efforts to establish models that simulate the relationship between aeolian transport rates and surface moisture content, empirically or theoretically (see reviews by Namikas and Sherman, 1995; Cornelis and Gabriels, 2003). Although almost all models are based on the idea that the presence of surface moisture increases the threshold velocity and decreases excess shear velocity for sediment transport, the predicted results of these models can differ from each other by orders of magnitude (Namikas and Sherman, 1995). These disparities can be attributed to differences in experimental procedures and equipment (e.g. measurement of sediment moisture content), the representation of the characteristics of the sediment, and the methodology used to determine the transport rate (Cornelis and Gabriels, 2003). Namikas and Sherman (1995) and Wiggs *et al.* (2004) also emphasized that measured soil moisture content employed in previous studies are static rather than dynamic representations of the moisture field. With evaporation and condensation, the surface moisture content may vary radically in space and through time and subsequently contribute dramatically to variability in sediment transport processes. This problem cannot be resolved until the spatial and temporal variability of surface moisture content can be both documented and modeled.

2.3 Budget of Beach Surface Moisture

Moisture storage in a natural soil body is due to molecular attraction, surface tension, and/or capillary force. Beach sediment is composed of granular particles of varying shape and size, although beach sediment is often well sorted. Between these particles are interconnected pore spaces that vary considerably in size and shape. Theoretically all of the pore spaces are filled with air in a completely dry soil and with water in a saturated one, but in most field situations the material is in an intermediate state, with some pore spaces filled with water and rest with air (Hanks, 1987). Water can be stored in soil owing to capillary force. Capillarity results from an attraction between water molecules (surface tension of water) and a larger attraction between water molecule and solid (sand or soil particles here) molecule to which water molecule is attached (Namikas and Sherman, 1995; Horn, 2005). The attraction between water molecules, as surface tension, keeps water molecules packed close to each other to maintain the water surface area as small as possible, while attraction between water molecule and solid molecule tries to hold as much water on solid surface as possible. Therefore, soil moisture content refers to the amount of water held by soil pore spaces when the adhesive forces and the cohesive forces are in an equilibrium state with gravity force (Namikas and Sherman, 1995). At low moisture content, small amount of water form bridges at the contact points of solid particles where the attraction from solid particles is strongest (Kim and Sture, 2004). Because of the presence of water bridges between the particles, surface tension force (which acts along the water-particle contact line) combined with the force due to pressure difference in outside and inside the bridge (which acts on the cross-sectional area) act as a bonding force (Kim and Sture, 2004). The bonding forces, thickness and curvatures of water bridges between solid (soil or sand)

particles change with moisture content, and the capacity of moisture content of a certain type of soil or sand depends on properties of the material (grain-size, porosity and packing rate).

Beach surface moisture dynamics actually is an essential part of beach hydrologic cycle. Like all the hydrologic cycles, beach surface moisture dynamics can be theoretically illustrated using a simple budget equation, $\Delta Storage = Input - Output$, where $\Delta Storage$ is the net change of water content of the soil matrix, *Input* includes infiltration and percolation from precipitation, condensation and capillary uplift from groundwater etc., and *Output* may include evaporation, transpiration, runoff, drainage, etc.

For a simple system like a beach, the content of surface moisture can increase through a number of input processes, including capillary rise from the subsurface, conditional condensation, and infiltration through occasional precipitation. Capillary water flow occurs when the hydraulic pressure between surface and subsurface changes, and maintains the status of surface moisture content that is determined by hydraulic pressure (negative to water table depth) within the sand column (Child, 1969). Condensation is a phase change of water molecules from vapor to liquid, and it occurs only when the air inside or outside of the soil surface is oversaturated, which is usually due to decreases of air temperature. Condensation is believed to be an important process influencing the diurnal variations in beach surface moisture content and hence the cease of aeolian sediment transports (Sherman, 1998), but the importance has not been quantified by any previous studies. Precipitation adds water directly to soil surface but the rate of subsequent infiltration and the increasing extent of moisture content is also affected by the original moisture content and surface properties. For a beach environment with shallow water table, the contribution of capillary rise from groundwater or subsurface layers to surface moisture variability seems to be underestimated in most previous work (e.g., Deardorff, 1977, 1978).

For a beach system with no vegetation, evaporation is the only output process for surface moisture (if the subsequent percolation after occasional precipitation events is not considered). Water molecules within the soil surface are not free but the capillary and absorption forces that bind the water molecules over the surface of soil grains can be overcome when certain conditions are reached (Hanks, 1987). As a result, water vapor can be released into the atmosphere. The process is commonly further divided into two stages, Stage One or the constant rate stage, and Stage Two, know as the falling rate stage. The evaporation rate is theoretically determined by the atmospheric conditions and the rate of soil-water transport. In Stage One, the evaporation rate is controlled by atmospheric factors such as relative humidity, air temperature and wind speed because the soil is moist enough. In Stage Two, the soil is too dry to maintain the atmospherically-determined potential evaporation rate, and hence the rate of soil-water transport rate becomes the predominant control on evaporation rates (Stewart and Broadbrige, 1999). Philip (1957) suggested a sharp transition of surface moisture content between these two stages of an evaporation cycle, while Wiegand and Taylor (1961) demonstrated a smooth change. Previous authors have related the rate of evaporation to the absolute humidity, or more commonly relative humidity in the context of vapor flux driven by vapor gradients. No doubt that evaporation constantly decreases the content of surface moisture, but the rate of evaporation depends on surface moisture content itself and the atmospheric conditions.

Clearly, variations in beach surface moisture are determined by the balance between water inputs and outputs. However, the inputs and outputs themselves are further affected by a variety of environmental factors.

2.4 Factors Controlling Soil Moisture Variability

Famileitti *et al.* (1998) summarized a number of factors that influence soil moisture variability, including topography, soil properties (i.e., grain size, porosity, and content of organic matter), vegetation type and density, mean moisture content of soil column, water table depth, rainfall, solar radiation and other meteorological parameters. Although this summarization was primarily based on field studies of near-surface moisture variability in soil at small spatial scales, it is still helpful in understanding moisture variability in beach system where specific observations are not available.

Topographical features including slope, aspect and relative elevation all have substantial impacts on the distribution of soil moisture within the surface layer. Topographical features not only influence moisture inputs through infiltration, drainage and runoff, they also modify near-bed airflow patterns and finally influence the rates of evaporation and transpiration. It is worth noting that some investigations showed contradictory results for the same topographic features in different environments. For example, Moore *et al.* (1988) found a significant correlation between topographical profile curvature and moisture content, while Niemann and Edgell (1993) found no relationship between curvature and surface moisture content. It is also worth noting that almost all relationships found between topographical features and surface moisture content are very weak although they may be statistically significant. Soil heterogeneity affects the distribution of soil moisture through variations in texture, packing rate, organic matter content, structure and the presence of macroporosity, all of which affect hydraulic conductivity and retention properties of soil column. Natural soils or sand often exhibit a spatial heterogeneity that is highly irregular, which prohibit the use of effective or average parameters for representing hydraulic processes (Russo *et al.*, 2001). Vegetation, on the one hand, has positive effects on

surface moisture content by decreasing evaporation through solar radiation absorption and reflection, but on the other hand has negative effects by increasing evapotranspiration through root uptake from subsurface layer and affecting hydraulic conductivity of soil by the presence of root system. In most cases, multiple environmental factors may combine with each other in affecting surface moisture content. Essentially, roughly flat, bare, and relatively well-sorted beaches provide ideal systems to study temporal and spatial variability in soil moisture content because influence of some factors (i.e., topography, vegetation and surface heterogeneity) is negligible.

Theoretically, the spatial distribution and temporal variations of surface moisture content on beaches are relatively easy to understand because of the simple environment: first, native sand on coastal beaches is often well-sorted, which means spatially homogeneous texture, porosity and then hydraulic conductivity (relative to the complex textures of natural soils); second, beaches usually have little vegetation due to high salinity,; and finally, the beach surface is commonly relative flat with low gradients. However, previous field investigation (Yang and Davidson-Arnott, 2005) and our preliminary studies (Namikas *et al.*, 2007) also indicated that the moisture content of beach surface can vary over a wide range (<1% to 30%, gravimetric) even over a very small distance (0.25 meter to meters). Their results indicated that even for simple systems like beaches, surface moisture content usually exhibits high variability and apparently need to be further investigated to understand and model its dynamics.

2.5 Beach Groundwater System

The configuration of beach water table has a pronounced effect on the direction and rate of groundwater flow (Gillham, 1984). Further, beach groundwater flow significantly affects swash sediment transport and hence beach stability (e.g., Grant, 1948; Emory and Foster, 1948; Turner

and Nielson, 1997; Li *et al.*, 1997). Erosion tends to occur with exfiltration due to higher beach water table relative to sea level, while accretion often takes place during infiltration because of low water table conditions (Chappell *et al.*, 1979; Weisman *et al*., 1995; Li *et al*., 1996a). Beach groundwater through capillary rise can contribute the major input to the beach surface moisture budget. Beach groundwater system is usually highly dynamic and affected by many factors including tides, waves and swash, and to a lesser extent by atmospheric exchanges (evaporation and rainfall) and exchanges with deeper aquifers (Horn, 2005). In a common sense, tidal oscillations are the major cause of beach groundwater fluctuations.

Like all groundwater systems, the beach can be divided into three zones: the vadose zone (also referred to as zone of aeration), the phreatic zone, and the capillary fringe (also referred to as the tension-saturated zone). The vadose zone is an unsaturated zone above the capillary fringe (Horn, 2002). The capillary fringe is a thin, saturated layer above the water table. The phreatic zone is a saturated zone located below the water table. The beach water table is defined as a dynamic surface where pore-water pressure equal to atmospheric pressure (Horn, 2002), therefore hydraulic pressure is positive in phreatic zone but negative in capillary fringe although they are both saturated. By definition, the height of capillary fringe above water table should be equal to that of the water surface in the largest pore of the beach sediment matrix (Gillham, 1984; Silliman *et al.*, 2002). In the studies of Nielson and Perrochet (2000) and Nachabe *et al.* (2002), however, the capillary fringe is defined as the layer where water in soil is held by capillary forces and whose soil moisture content is between the residual moisture content (also refers to the field capacity) and saturated moisture content. The height of capillary fringe by this definition, therefore, is much greater than that by Horn's definition, which may considerably affect the performance of groundwater models when capillary effect is considered. In this study, we will

follow Horn's definition because Horn's definition is more physically specified and can be calculated from grain-size composition of the material, while the definition in the studies of Nielson and Perrochet (2000) and Nachabe *et al.* (2002) involves the concept of field capacity, which is controversial and has low repeatability in field measurements.

A number of studies deal with the role of the capillary fringes as an interface between the vadose zone and the saturated zone below water table (e.g., Gillham, 1984; Li *et al.*, 1997). The results of laboratory experiments in the study of Silliman *et al.* (2002) show that fluid flow occurs regularly in the capillary fringe, both vertically and horizontally, and that active exchange of water exists between capillary fringe and water body below water table. Their results suggest that the capillary fringe may play a more significant role than usually assumed on fluid flow in the transition region from saturated to unsaturated zone.

Field evidences indicate that the elevation of the beach groundwater table is always somewhat higher than mean sea level, which is often refereed to as overheight, superelevation or outcrop. Horn (2005) attributes this phenomenon to the lag in the response of the beach ground water table to the higher falling rate of seawater surface. However, in some field observations, even when the still water level reached its highest position (e.g., high tide), the beach groundwater level is still higher. Therefore, sea water level oscillations may not be the only reason for the supperelevation. Gourlay (1992) and Turner *et al.* (1997) suggested that the combined effects of prevailing hydrodynamic conditions such as tidal elevation, wave run-up and rainfall, and characteristics of beach sediment, such as sediment porosity, size, shape and sorting, control the superelevation of beach groundwater table. Thus, all factors must be considered in the investigation of beach groundwater table fluctuations.

Field observations have also showed that the beach ground water table is not flat and acts as a damped free wave landward. Emery and Gale (1952) characterized the beach as a filter that allows larger or longer waves to pass. Both the magnitude and frequency of water table oscillations decrease as the waves propagate landward from the shoreline (Raubenheimer *et al.*, 1999). The landward distance to which the effects of sea water level fluctuations are discernible depends on its frequency (Braid *et al.*, 1998). The elevation of groundwater table in the beach is usually asymmetric and skewed in time (Raubenheimer *et al.*, 1999).When the tide level either in rising or falling is lower than the beach groundwater table, a slope of beach water table occurs in the zone near the shoreline, and potentially some amount of water will drain out from the beach water body though the part of beach face under the exit point (Horn, 2005). The gradient of this slope varies with the state of tidal fluctuation. Water table oscillations also have been shown to lag behind tidal oscillations by various time periods. The length of time lag is mainly controlled by, and increases with the hydraulic conductivity of beach sediments, which is controlled by the characteristics of sediment (Nielson, 1990; Jackson *et al.*, 1999). The asymmetry and time lag of beach groundwater table during the landward propagation of waves are the major challenges in modeling and need to be further investigated.

Beach water table fluctuations forced by tides or waves in beach systems have been studied extensively (e.g., Nielson, 1990; Turner, 1993; Li *et al.*, 1997), and have been comprehensively and critically reviewed by Nielsen *et al.* (1988), Gourlay (1992), Baird and Horn (1996), Turner *et al.* (1997) and Horn (2002 & 2005). A number of studies have been done involving simulation and prediction of the tide-induced fluctuations of the beach water table (e.g., Teo *et al.*, 2003; Jeng *et al.*, 2005 ab). The basic relationship in most of beach groundwater models is the

Boussinesq equation (Dominick, 1970 & 1971; Dominick *et al.*, 1973; Turner *et al.*, 1997; Horn, 2002 & 2005), which is originally derived from the Darcy's Law:

$$v_x = -K\frac{\partial h}{\partial x} \tag{2.1}$$

and the continuity equation:

$$\frac{\partial h}{\partial t} = \frac{1}{S_x}\frac{\partial}{\partial x}(hv_x) \tag{2.2}$$

where K is the hydraulic conductivity and S_x is specific yield, v_x is Darcy velocity and h the elevation of the free water surface (water table) above some lower-bounding aquitard, Substituting Equation (2.1) into Equation (2.2), it becomes the Boussinesq equation (Liu and Wen, 1997):

$$\frac{\partial h}{\partial t} = \frac{K}{S_x}\frac{\partial}{\partial x}(h\frac{\partial h}{\partial x}) \tag{2.3}$$

which is defined to describe transient horizontal flow. Under the assumption of prevailing hydrostatic conditions, this one-dimensional equation is sufficient to describe shore-normal groundwater flow (Nielsen, 1990). When the magnitude of water fluctuations is small compared with the depth h_0 of the aquifer, Equation (2.3) may be linearized to give

$$\frac{\partial h}{\partial t} = \frac{Kh_0}{S_x}\frac{\partial^2 h}{\partial x^2} \tag{2.4}$$

The assumptions of the Boussinesq equation includes: 1) horizontal flow dominates in the beach groundwater oscillation and vertical flow can be neglected, 2) density gradients are negligible, and 3) sand drains instantaneously (Raubenheimer *et al.*, 1999), 4) the ground water flow in a shallow aquifer can be described using the Dupuit-Forchheimer approximation (Braid *et al.*, 1998). The assumptions (1) and (2) supported by field studies from Baird et al. (1998) and Baubenheimer et al. (1999) respectively. However, the results of Robinson *et al.* (2005, cited in

Horn, 2005) indicated the magnitude of vertical groundwater flows might have be at same order as horizontal flows in the intertidal zone.

Almost all of studies of the Dominick *et al.* (1971), Nielson (1990), Hanslow and Nielson (1993), Turner (1993, 1995, 1997), Li *et al.* (1996, 2000, 2002), Baird *et al*. (1998), Cartwright and Nielson (2001) have shown that only with a small range of errors, the predicted results match reasonably well with observed beach water table oscillations forced by tide fluctuations, on any frequencies of semi-diurnal, diurnal or spring-neap tidal cycles. It is worth noting that predicted results are not applicable so far for fluctuation of higher frequency than semi-diurnal tidal cycle (e.g. wave run-up and swash). Although the effect of capillary fringe on water table fluctuation is often arbitrarily neglected in the studies directly using the Boussinesq equation (e.g., Turner, 1993; Li *et al.*, 1996 & 2000), evidences from field investigations testified the capillary force might impose a significant effect on the nonlinearity of water table fluctuations (Li *et al.*, 1997; Nielson and Perrochet, 2000). In cases the detailed dynamics of the capillary fringe itself are not of primary interest, the approach is to incorporate a simplified description of the capillary fringe in the water table equations. For example, Parlange and Brusaert (1987) combined the Green-Ampt model into the Boussinesq equation to describe the water table fluctuations in a shallow unconfined aquifer under the influence of capillarity. Nielson and Perrochet (2000), in another way, modified the Boussinesq equation using a complex term, dynamic porosity, to put the effect of capillarity into consideration.

2.6 Soil Moisture Profile with a Moving Water Table

As the beach groundwater table is always fluctuating, the soil moisture profile above may also change with it. In theory, the shape of the moisture profile above a moving water table is influenced by both the rate of infiltration at the soil surface and the rate of rise or fall of water

table (Childs and Poulovassilis, 1962). Assuming the soil matrix is uniform and isotropic, it must have a constant soil moisture characteristic curve under hydrostatic conditions. The curve, as shown in Figure 2.1, will shift up or down in response to the water table shifting. Thus, if the shape of the curve is known, the change in soil moisture in a profile can be easily calculated with knowledge of a single variable, the rate of rise or fall of the water table. In results, however, the shape of the moisture profile with a moving water table below is not necessarily the same as the static moisture profile. Rather, it tends to stretch out above a falling water table and be compressed above a rising one (Childs and Poulovassilis, 1962). The extension or compression depends on both the velocity of the water table shifting and the shape of the curve itself. Childs and Poulovassilis (1962) presented probably the first report that theoretically studied the relation between the moisture profile and moving water table. However, their study does not give a complete physical basis for this complex process since they assumed a constant difference of water head *dh* between the two moisture profiles (Figure 2.1). Based on that assumption, the moisture profile remains the same shape during the water table change. Their results therefore do not provide useful information about the extension or compression of the moisture profiles during water table falling or rising. In this study, moisture contents within the profile will be measured constantly along with groundwater table fluctuation, which may provide detail information to study the possible extension or compression of the moisture profile.

Soil moisture profile in a hydrostatic state is usually termed as *soil water retention curve* or *soil moisture characteristic curve*, describing the relation between matric potential and volumetric water content in a soil. The shape of the soil moisture characteristic curve is primarily controlled by the pore size distribution among soil, which is determined by grain size composition of soil. The relation between the soil moisture characteristic curve and phase

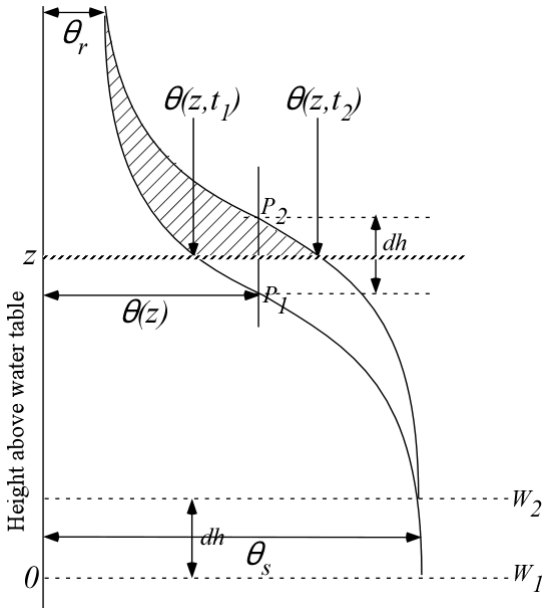

Figure 2.1 Two stages of a hypothetical moisture profile of constant shape over water table change (z is the position of the surface, dh is the height of water table (W) change between time t1 and t2, θr and θs are the residual and saturated moisture content respectively, θz is the moisture content at the position z, following Child and Poulovassilis, 1962)

configuration of soil water is illustrated in Figure 2.2. Air entry suction h_a is defined as the minimum value of suction that allows free air to enter soil pores during the drying process. When suction is less than h_a, the gas phase can exist only as entrapped air. When suction is greater than h_a, the occupation of the soil pores by free air gradually increases with the suction. When the volume of entrapped air is negligibly small, the soil in which the suction is less than h_a is considered saturated. Similarly, water entry suction h_w is defined as the maximum value of suction that allows water to enter soil pores when no free air remains in the soil pores during the wetting process. Air entry suction is close to but normally higher than water entry suction. The height of capillary fringe h_c in definition is equal to h_a (Miyazaki, 1993). If the soil water is in hydrostatic equilibrium, one probably can estimate moisture content from the depth above water table based on the characteristic of soil water profile, i.e., the soil retention curve (Child, 1969). Thus, the curve provides the basis to model the change of moisture profile as well as surface moisture content.

Various equations have been proposed for describing the characteristic curve (e.g., Brooks and Corey, 1964; van Genuchten, 1980; Miyazaki, 1993; Olyphant, 2003). Among these equations, the van Genuchten function, which is more widely accepted (e.g. Vogel *et al.*, 2001), is given by:

$$\Theta = [\frac{1}{1+(\alpha h)^n}]^m \qquad \textbf{(2.5)}$$

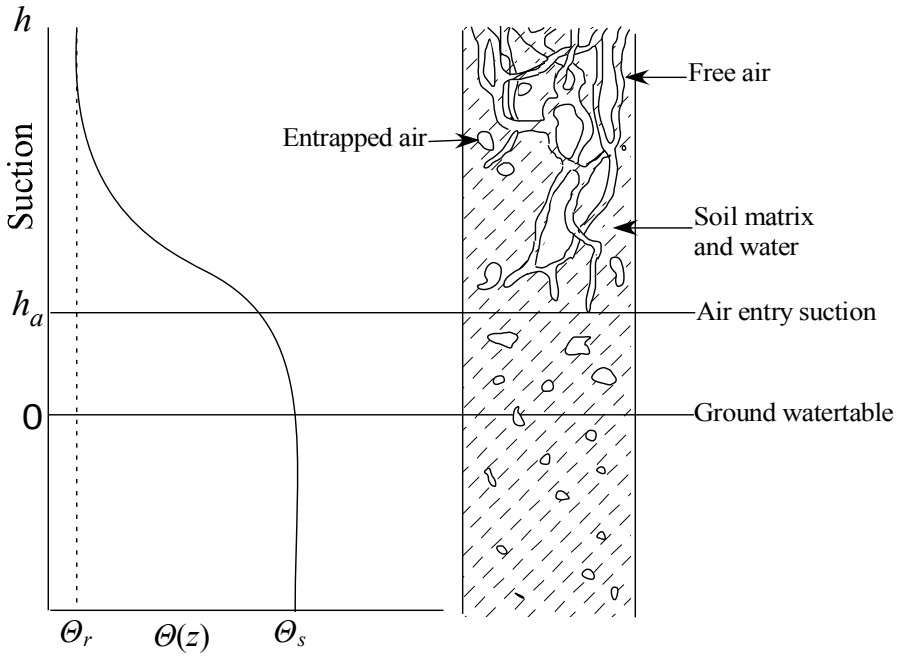

Figure 2.2 Soil moisture characteristic curve and sketch of soil water phase (see text for explanation, after Miyazaki, 1993)

in which α , *m*, and *n* are estimated parameter values, *h* is the suction, and Θ is the dimensionless water, transformed from the volumetric water content θ as:

$$\Theta = \frac{\theta - \theta_r}{\theta_s - \theta_r} \qquad \textbf{(2.6)}$$

where θ is water content at the position *h*, θ_r and θ_s are the residual and saturated water content respectively. The equation (2.5) may be rewritten in terms local volumetric water content θ as:

$$\begin{cases} \theta = \theta_r + \dfrac{\theta_s - \theta_r}{(1+\alpha h^n)^{1-\frac{1}{m}}} & for \quad z > h_a \\ \theta = \theta_s & for \quad z \le h_a \end{cases} \tag{2.7}$$

The model presented by Brooks and Corey (1964) is another widely used model in power function (see Nachabe, 2002; Nachabe *et al.*, 2004), given by:

$$\Theta = \frac{\theta - \theta_r}{\theta_s - \theta_r} = (\frac{h_a}{h})^{\lambda} \tag{2.8}$$

where λ is the pore-size distribution index, which can be easily estimated from soil texture data (Rawls *et al.*, 1993). The van Genuchten model will be employed in this study because it has a better representation of the field obtained moisture profile, particularly the part close to saturation.

The parameters required for these relationships are usually estimated by measuring the saturated hydraulic conductivity and assuming that coefficients and exponents of moisture retention and hydraulic conductivity are equal. Associated parameters traditionally are determined on laboratory measurements using permeameters, moisture extractors and pressure plate or membrane. Although laboratory techniques have been sophistically improved in recent years and more accurate results may be obtained, any laboratory-based analysis still has a major disadvantage: laboratory-determined hydraulic properties are often non-representative of field conditions since the samples are usually small and the collection of samples invariably introduces some disturbance of the in situ soil matrix (Child, 1969; Kool *et al.*, 1987; Olyphant, 2003). In recent years, several authors (e.g., Abbspour *et al.*, 2000; Jhorar *et al.*, 2002) have attempted to determine parameters of the characteristic curves by combining field measurements of system variables such as moisture content, pressure head, and water flux with an inverse method that couples a numerical flow model with a parameter optimization algorithm. Chen *et al.*

(1999) and Hwang and Powers (2003) validated the power of the approach of parameter optimization using inverse modeling and extended the inverse parameter estimation method to the modified multi-step outflow method for two-fluid (i.e., air-water, air-oil and oil-water) flow systems. In this study, the inverse method will be employed to determine the soil water retention curve of local sediment because it is more reliable to represent natural conditions.

The only previous study that attempted to associate moisture dynamics of the beach surface with water table fluctuations was provided by Atherton *et al.* (2001). That field investigation was restricted to the inter-tidal zone of a fine sand beach, and only considered relative short periods (8 hrs). It was found that surface moisture content decreased much more slowly than previously thought during falling tide, and it was suggested that capillary water may exist even in upper 6 cm of the beach sediment, implying that the capillary fringe might be underestimated in previous studies. This is clearly a need for additional research on this topic.

2.7 Water Flow in a Soil Column

Soil water retention curve describes the relationship between hydraulic pressure and moisture content of a given sand column under a hydrostatic state. It is water flow caused by pressure difference that leads to variations in moisture content. The rate of water flow in soil is determined by two factors: the force acting on each element of soil water volume and the resistance to flow offered by the soil pore space. As the configuration of pore space in a porous material, such as soil, is far too complex and unspecifiable in quantitative terms to permit the rate of fluid flow to be calculated by the Navier-Stokes equations (Child, 1969). The Darcy equation, which integrates individual water flow in each pore of various size and shape, is more explicitly developed and easier to use for both saturated and unsaturated flow (Miyazaki, 1993). It can be written as:

$$q = \frac{Q}{t} = -K\frac{dH}{dz} \quad \textbf{(2.9)}$$

where q, Q/t is the flux of water, and K is hydraulic conductivity of a porous medium, such as soil, and dH/dz is the gradient of hydraulic head in z direction.

Given any small parcel of soil, the continuity equation of water for three dimensions is given by:

$$d\theta dxdydz = -(\frac{\partial q_x}{\partial x} + \frac{\partial q_y}{\partial y} + \frac{\partial q_z}{\partial z})dxdydzdt \quad \textbf{(2.10)}$$

which can be rewritten as:

$$\frac{\partial \theta}{\partial t} = -(\frac{\partial q_x}{\partial x} + \frac{\partial q_y}{\partial y} + \frac{\partial q_z}{\partial z}) \quad \textbf{(2.11)}$$

Applying with Darcy law, (2.11) results in (Iwata *et al.*, 1988):

$$\frac{\partial \theta}{\partial t} = \frac{\partial}{\partial x}(K_x\frac{\partial H}{\partial x}) + \frac{\partial}{\partial y}(K_y\frac{\partial H}{\partial y}) + \frac{\partial}{\partial z}(K_z\frac{\partial H}{\partial z}) \quad \textbf{(2.12)}$$

In saturated soils, assuming hydraulic conductivity is constant and isotropic, and the soil matrix is incompressible, then $K_x = K_y = K_z = K_s$ (the saturated hydraulic conductivity), and the equation (2.15) can be transformed into the Laplace equation:

$$\frac{\partial^2 H}{\partial x^2} + \frac{\partial^2 H}{\partial y^2} + \frac{\partial^2 H}{\partial z^2} = 0 \quad \textbf{(2.13)}$$

Theoretically, the channels for water moving in an unsaturated material are those pores which are filled by water at the particular suction. The air-filled pores are ineffective since water can not pass through a pore without occupying it. The unsaturated material, therefore, can be treated as a new *saturated* material considering those air-filled pores as solid (Child, 1969). This is the basic assumption under which the Darcy law could be applied to unsaturated water flow. In

unsaturated soils, replacing hydraulic pressure H by matric head Ψ_m, the equation (2.12) becomes:

$$\frac{\partial\theta}{\partial t}=\frac{\partial}{\partial x}(K_x\frac{\partial\Psi_m}{\partial x})+\frac{\partial}{\partial y}(K_y\frac{\partial\Psi_m}{\partial y})+\frac{\partial}{\partial z}(K_z\frac{\partial\Psi_m}{\partial z}) \qquad \textbf{(2.14)}$$

which is Richard's equation. Introducing a term specific water capacity C, defined by:

$$C=\frac{d\theta}{d\Psi_m} \qquad \textbf{(2.15)}$$

the substitution of C into the equation of (2.14) gives the equation of flow with respect to θ as

$$\frac{\partial\theta}{\partial t}=\frac{\partial}{\partial x}(\frac{K_x}{C}\frac{\partial\theta}{\partial x})+\frac{\partial}{\partial y}(\frac{K_y}{C}\frac{\partial\theta}{\partial y})+\frac{\partial}{\partial z}(\frac{K_z}{C}\frac{\partial\theta}{\partial z}) \qquad \textbf{(2.16)}$$

Klute and Philip (see Iwata *et al.*, 1988) transformed the equation (2.16) of one dimension into an equation of the diffusion type which permitted a numerical solution,

$$\frac{\partial\theta}{\partial t}=\frac{\partial}{\partial x}(D\frac{\partial\theta}{\partial x}) \qquad \textbf{(2.17)}$$

where D is the liquid diffusivity defined by $K\,\partial\Psi/\partial\theta$ and $\partial\Psi/\partial\theta$ is called the differential water capacity, equal to the inverse of specific water capacity C (Miyazaki, 1993).

Given $\zeta=xt^{\frac{1}{2}}$, equation (2.17) can be rewritten as

$$-\frac{\zeta}{2}\frac{d\theta}{d\zeta}=\frac{d}{d\zeta}(D\frac{d\theta}{d\zeta}) \qquad \textbf{(2.18)}$$

Therefore, the partial differential equation (2.17) becomes the ordinary differential equation (2.21), which can be solved numerically, subject to given boundary and initial conditions (Iwata *et al.*, 1988).

For the case of isotropic, one-dimensional transient vertical flow, however, a gravitational term which involves K_z should be included one-dimensional form of equation 2.14 (Hanks and Ashcroft, 1980):

$$\frac{\partial \theta}{\partial t} = \frac{\partial}{\partial z}(K_z \frac{\partial(\Psi_m + \Psi_z)}{\partial z}) \quad \textbf{(2.19)}$$

which can be written as a diffusion type equation (Iwata *et al.*, 1988):

$$\frac{\partial \theta}{\partial t} = \frac{\partial}{\partial z}(D \frac{\partial \theta}{\partial z}) + \frac{\partial K}{\partial z} \quad \textbf{(2.20)}$$

The hydraulic conductivity of soil, *K*, decreases rapidly as the water content θ decreases from saturation. The unsaturated hydraulic conductivity is usually a highly nonlinear function of the dimensionless water content Θ, given as

$$K_{x,y,z} = K_s \Theta^n \quad \textbf{(2.21)}$$

where Θ is defined by the equation (2.6), and the estimated parameter *n* can be set equal to $(2+3\lambda)/\lambda$ if the Burdine model is adopted (Brooks and Corey, 1964; Nachabe, 2002).

Fluid flow in variably saturated porous media is often modeled using Richard's equation with a set of constitutive relations describing the relation among fluid pressures, saturations, and relative permeabilities (Farthing *et al.*, 2003). For a beach environment, one-dimensional, diffusion type equation (2.20) derived from Richard's equation (2.14) can be used to model the unsaturated flow in the sand column, because horizontal unsaturated flow can be neglected (no surface water flow or surface water head).

2.8 Summary and Conclusions

Beach surface moisture usually exhibits a high degree of spatial and temporal variability and plays an important role in coastal processes, particularly aeolian sediment transport. This variability is not well understood. Nor has it been thoroughly investigated, due to both the complexity introduced by the involved processes and limitations of instrumentation and approaches used in previous studies.

The spatial and temporal variability in beach surface moisture are affected to various degrees by all components of beach hydrological cycle, including capillary rise from groundwater, condensation, evaporation and precipitation, as well as hydraulic properties of beach materials. Although some of these associated processes have been quite well documented and modeled (at least for other environments), the dynamics of beach surface moisture itself is far from fully understood. On the other hand, advances achieved and models proposed by previous hydrological studies provide a solid basis from which this study can develop a realistic and quantitative approach to represent the variability of surface moisture content in a natural beach system.

CHAPTER 3 METHODOLOGY AND DATA

A brief introduction to the study area in regard to environmental setting, prevailing climatic conditions, and tide and wave conditions is given in this chapter to provide a broader context in which the present study is set. This is followed by a detailed description of the approaches, instruments, and methods employed in this study to measure and monitor key conditions including meteorological parameters, soil moisture content, and tide and groundwater elevations.

3.1 Description of Study Area

The study site was located within Padre Island National Seashore, Texas, on the northwest shore of the Gulf of Mexico, approximately 27.44^{o}N and 97.29^{o}W (Fig. 3.1). The Padre Island is the longest barrier island in the world, with a length of approximately 180 km and a width varying between 1 to 4 km. Most of the island is less than 6 m above sea level, although a few dunes stand up to 15 m high (Weise and White, 1991). Particularly, the beach at the study site is approximately 70 meters wide with almost no vegetation, and backed by a well established 1-2 m high foredune (Figure 3.2). Landward of the foredune, a well-vegetated system of hummocky dunes grades into a mix of tidal flats and marshes on the lagoon coast of the Laguna Madre (NPS, 2005). The native sediment is predominately very-well sorted, fine and very-fine quartz, with a mean size of approximately 0.14 mm (2.15 phi, Figure 3.3). Size distributions typically exhibit a coarse skew, with about 15-25% of samples falling into the very-fine size range, and less than 1% in the medium range.

The climate of Padre Island is classified as humid subtropical, but the rainfall averages ~85 cm a year. Snow and other forms of frozen precipitation are rare, with only trace amounts every 2 years on average (Bomar, 1983). The mean annual temperature is about 21.5 ^{o}C, with a typical

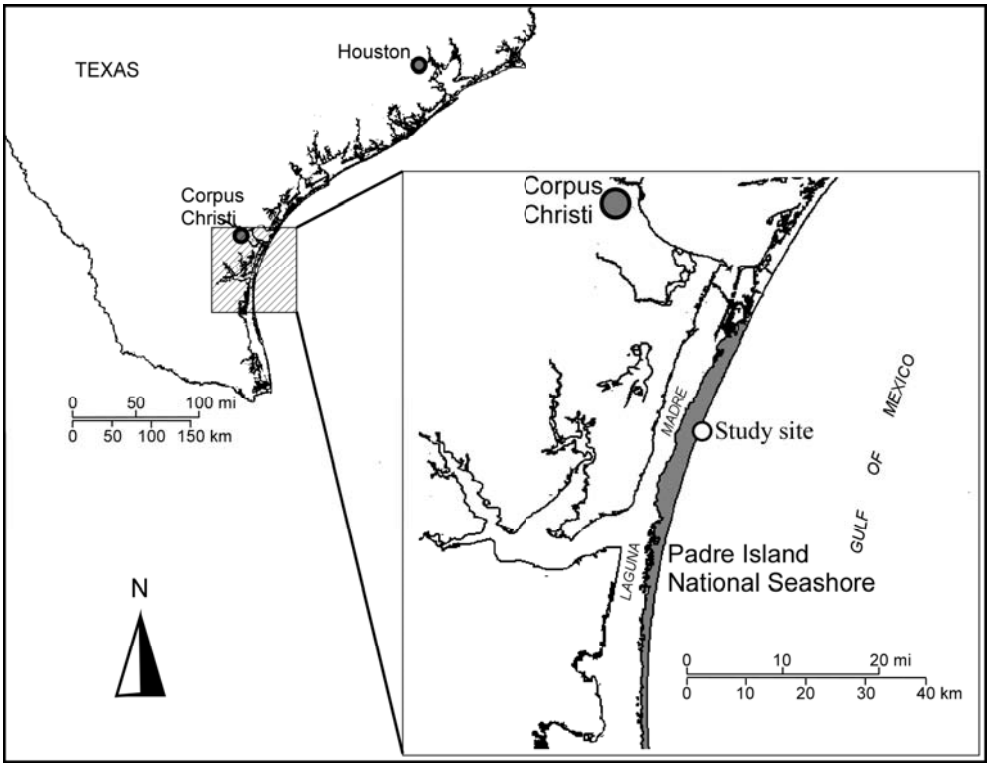

Figure 3.1 Map of the study site

Figure 3.2 Photo of the studied beach

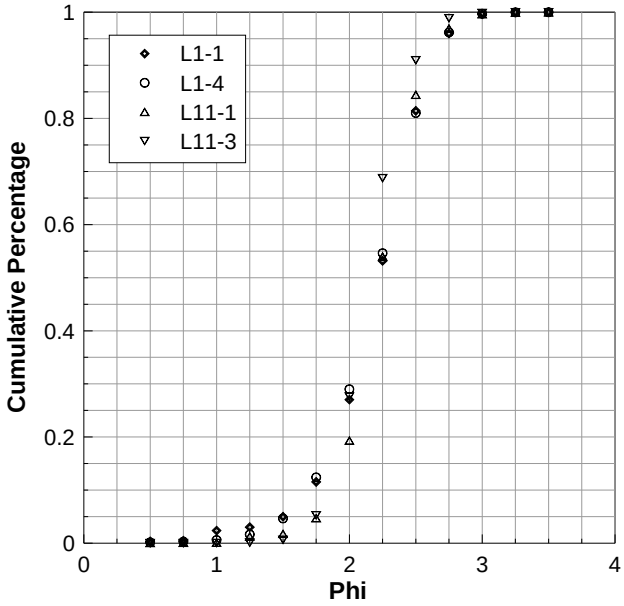

Figure 3.3 Grain-size parameters of local sediment

summer temperature range of 24-35 ^{o}C, and a winter range of 8-20 ^{o}C (NOAA, 2005). Prevailing winds have an average annual velocity of 5.4 m/s. Frequent and strong southeasterly winds usually dominate in spring through mid-summer and north northwesterly winds associated with cold front in fall and winter (Corpus Christi website, 2005). For the majority of the study period, winds were almost directly onshore from the southeast.

Incoming waves are generally 1-2 m high offshore and 10-30 cm high at the landward edge of the surf zone with period of 5-7 second. This coast experiences a micro tidal range (typically 0.3-0.8 m), with mixed but predominately diurnal tidal cycles (Weise and White, 1991).

3.2 Methodology

To model the spatial and temporal variability in surface moisture content, it is necessary to measure all related meteorological and hydrological processes including evaporation, condensation, precipitation and groundwater table fluctuations, as well as the hydraulic properties of the native sediment. Topographical conditions of the whole beach are also needed as reference for the calculation of water table depths.

3.2.1 Environmental Parameters

Wind speed was measured with two RM Young® Model 12102 cup anemometers installed at elevations 1 high and 2 m above the beach surface. A Qualimetrics® Model 2020 Micro Response Vane at the top of the weather tower (about 3 m) was used to monitor wind direction. Air temperature and relative humidity were measured using an Omega® HX303V Temperature/Humidity transmitter. A continuously recording rain gage was installed to monitor precipitation, however, no rainfall was recorded during the experiment. Topography and instrument locations were surveyed using a Sokkia® Set230 R3 total station. Sand samples were collected for laboratory analysis at the end of the experiment.

3.2.2 Tide and Water Table Fluctuations

The tide elevation was monitored using a KPSI® Series 730 pressure transducer (PT). The PT was attached to an iron stake that was inserted deep into sand in the surf zone about 70 meters seaward of the berm crest. Six-minute averaged tide records were also obtained from a Texas Coastal Ocean Observation Network (TCOON) gauge at Bobhall Pier, located approximately 1 km north of the study site.

Eight groundwater wells were installed along a shore-perpendicular transect that are parallel to the surface moisture sampling grid and extending from the upper foreshore to the back slope of the foredune. The wells were located at distances of 8, 15, 25, 35, 45, 55, 65 and75 meters from the time-averaged shoreline position, and designated as W1 to W8. Another three wells were deployed in the other side of the moisture grid at the location of 25, 45 and 65 meters, named W9 to W11 (Figure 3.4 and 3.5). The two cross-shore lines are spaced about 20 meters. The wells were constructed from 1.5 meter lengths of 10 cm diameter PVC pipes. The pipes were perforated for sake of free water flow and screened with fine nylon mesh to prevent the entrance

of sand. A KPSI Series 730 pressure transducer was installed at the bottom of each well to monitor water elevation.

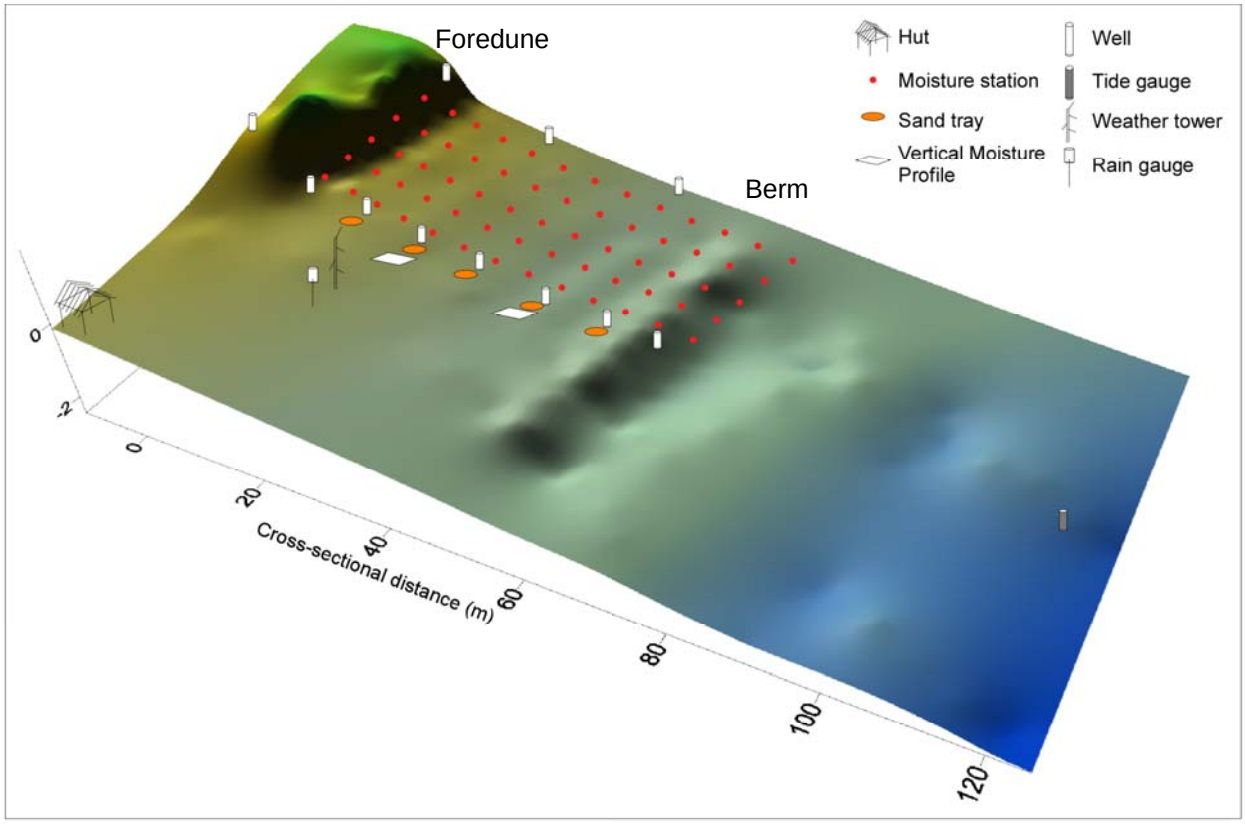

Figure 3.4 Three-dimensional overview of instrumental deployment

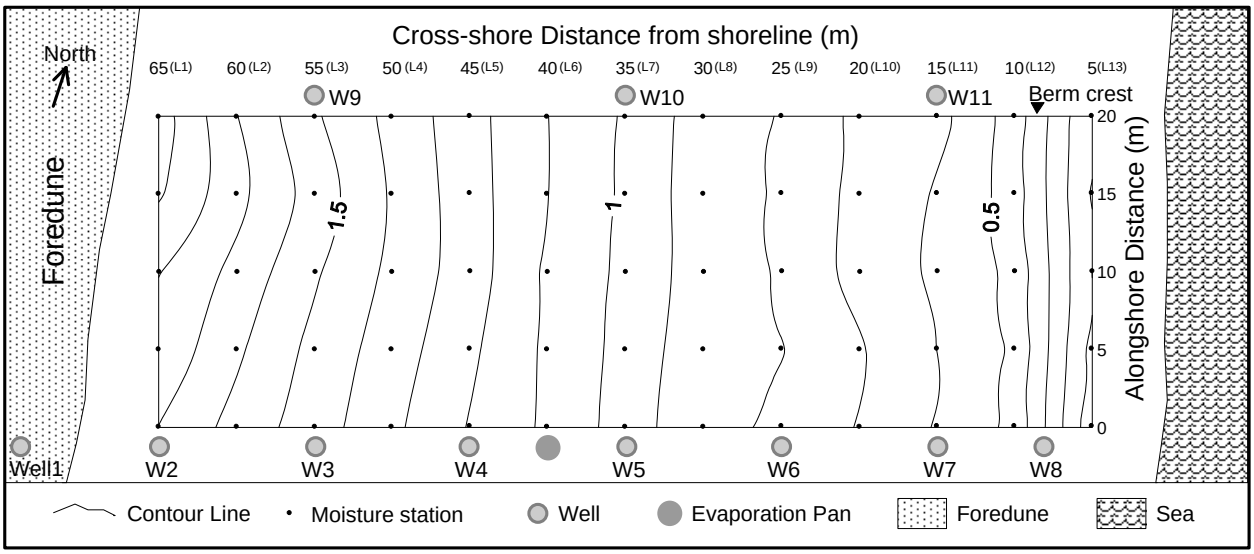

Figure 3.5 Plan-view map of instrument deployment

3.2.3 Soil Moisture

To document spatial variability in surface moisture, a grid of measurement stations was established on the back beach extending from the dune toe to the upper foreshore (Figure 3.4 and 3.5). The grid was comprised of 13 alongshore transects, spaced at intervals of 5 m in the cross-shore direction, extended approximately from the seaward toe of the foredune to the shoreline. Each transect included 5 stations spaced at 5 m intervals. The lines are designated as L1 to L13 (Figure 3.5).

To map surface moisture contents, moisture levels were measured at each grid station using two Delta-T moisture probes spaced 20cm apart on a wooden platform (Figure 3.6). Two probes were employed to allow assessment of the measurement repeatability and to help identify possible errors of the devices. As recommended by Yang and Davison-Arnott (2005), Styrofoam blocks were used to encapsulate the upper 1.4 cm of the probe sensing rods, so that the probes only penetrated 1.4 cm into the surface. Surface moisture was mapped seven times per day (3-hour intervals between 6am and 6pm, and 4-hour interval between 6pm and 10am). At high tide, the seaward most two lines of the grid were submersed by swash. It was presumed that the sediment was saturated and measurements were not collected.

To isolate the effect of groundwater on variations in surface moisture water content, five sand “cores” of about 6 cm depth by 25 cm diameter were collected adjacent to Wells W2, 3, 4, 5, and 6. They were transferred to plastic trays of same size, and replaced in the same spot where samples were initially collected, and leveled to the adjacent area. These “surface” samples ware thus isolated from any groundwater inputs. Moisture readings were collected in the trays and in adjacent areas following each grid sampling run.

To investigate the connection between groundwater fluctuations and surface moisture

Figure 3.6 Photo of moisture probes and the wooden platform used to measure surface moisture content

content, a vertical profile (VP-A), composed of four Delta-T probes was installed at depths of 3, 8, 15 and 30 cm below the surface, closely adjacent to the well W3. Another vertical profile (VP-B), was installed at depths of 3, 5, 10 and 20 cm below surface adjacent to Well 5 (approximate 20 meters landward from the beach face). The vertical profile A was measured from 7:00pm July 29th to 1:30pm August 3rd, and the water table at this location fluctuated between 72 and 83 cm below surface during the experiment. The vertical profile B was measured from 2:00pm August 3rd to 10:00am August 6th, and the water table at this location fluctuated between 34 and 64 cm below surface.

3.2.4 Evaporation and Condensation

Evaporation rate of free water surface was measured using a self-designed instrument, which is composed of a plastic pan of diameter of 63.8 cm as the container to hold water for

evaporation, and a Mitutoyo® digimatic caliper was water-surface-perpendicular installed to measure the elevation of water surface in the pan, with time intervals same as surface moisture measurement.

Naturally dried sand was collected on the surface of dune crest and put into three plastic pans (6 cm depth by 25 cm diameter) in 4:00pm August 3rd. The pans were deployed adjacent to wells W2, W4 and W6. Moisture readings were taken as same time as other moisture measuring runs to estimate the contribution of condensation to the variation of surface moisture content.

The experiment was conducted during 7:00pm July 29th to 10:00am August 6th, 2005, for about eight tidal cycles (approximately 181 hours). All groundwater wells, subsurface moisture probes, and weather instruments were logged with a Campbell® R-23X data logger combined with a Campbell® Multiplexer at 0.5 hertz for 60-second blocks, spaced at 6-minute intervals, while tidal elevation was measured at 5 hertz for 180 second blocks with 6-minute intervals.

3.2.5 Moisture Probe Calibration

The Delta-T probes come with generic calibration functions, but improved accuracy is attained with soil-specific calibrations (Dynamax, 2005). The probes used for subsurface measurements were not modified, so the manufacturer-recommended procedure was used to generate one-point calibrations (Dynamax, 2005). However, the probes used for "surface" moisture measurements were modified by partial encapsulation of the sensing rods, so a more detailed calibration was deemed appropriate. Locations on the beach with moisture contents encompassed the full probe output range (roughly 30mV to 800mV) were identified for each of the two probes, and once the voltage output was recorded a shallow coring ring (of identical diameter and depth to the probe array) was used to collect the actual sediment that generated the reading. These samples were sealed and returned to the laboratory for subsequent drying and

determination of the gravimetric moisture content. Calibration of surface moisture probe A was plotted in Figure 3.7 as an example. Although the relationship between field readings and laboratory-determined gravimetric moisture contents are far from linear, the coefficient of determination (R2) was significantly high as 0.973 (n=50) and the standard error is less than 2%, implying high reliability and repeatability of the probe.

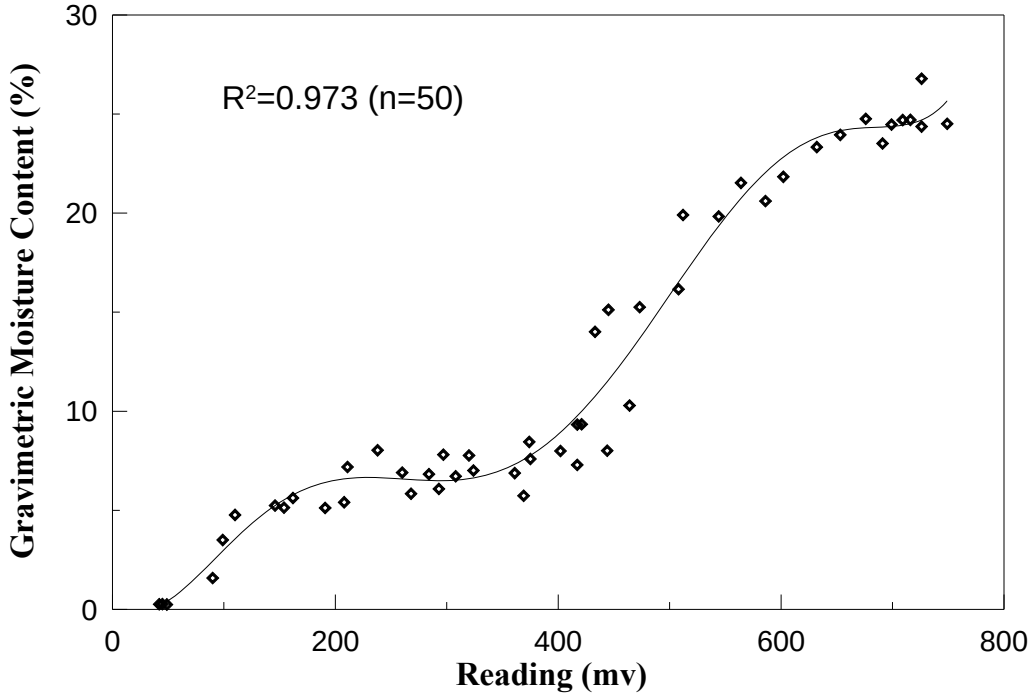

Figure 3.7 Calibration of surface moisture Probe A
(Fit with six-order polynomial equation, see appendix 3.1 for detail)

3.2.6 Pressure Transducer (PT) Calibration

Calibration of the PTs was carried out in the field. A capped length of PVC pipe was filled with water, stood upright, and leveled. Voltage outputs from each of PT were then recorded at depths of 0, 10, 20, 30, 40, 50 and 60 centimeters in both ascending and descending order. A linear regression was then fit to each set of measurements. All had R^2 values higher than 0.999, and the standard error was in all cases smaller than the rated level of error (± 1cm). Calibration of the PT install in the well W2 is shown in Figure 3.8 as an example.

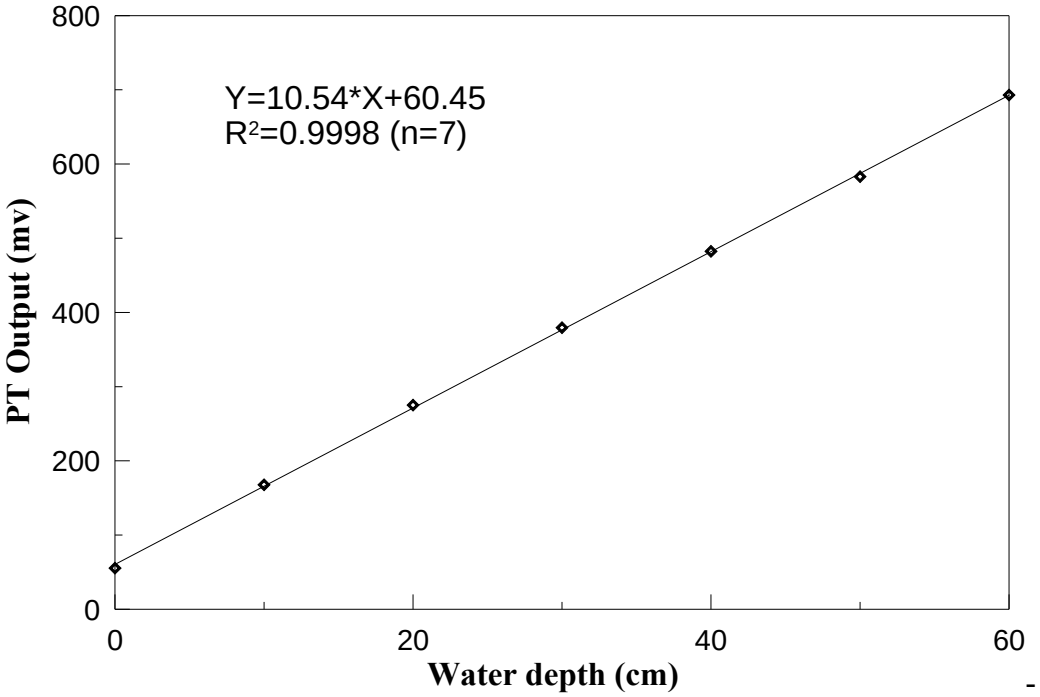

Figure 3.8 Calibration for PT of Well 2

CHAPTER 4 SPATIAL AND TEMPORAL DISTRIBUTION OF BEACH SURFACE MOISTURE

This chapter provides a description of surface moisture dynamics in the beach. Based on field measurements, time series and maps of surface moisture content were obtained. Variations in surface moisture content were examined and analyzed regarding to the variability exhibited in the cross-shore and alongshore directions and over time. Key processes regulating this variability were identified, and the relationships among these processes were further clarified.

4.1 Introduction

The spatial and temporal patterns of beach surface moisture distribution are controlled by factors including topography, precipitation, evaporation, condensation and groundwater table depth, sometimes wind speed and direction. Beaches generally slope to varying degrees, hence surface elevation and the water table depth increase in the landward direction. The landward increasing water table depth is the key factor influencing the spatial distribution of beach surface moisture, particularly for well-sorted and non-vegetated beaches. The groundwater table fluctuations and the daily evaporation-condensation transition, on the other hand, act as regulators affecting the temporal variations in surface moisture content at a certain spot in the beach. Since the evaporation-condensation cycle often shifts diurnally with a period different than the groundwater table fluctuations, the two processes together may further increase the spatially-varying temporal variability in beach surface moisture content.

The major purposes of this study are 1) to measure, analyze and represent the spatial distribution and the temporal patterns of beach surface moisture, 2) to uncover the factors

controlling the variability, such as evaporation, condensation, and groundwater input, and 3) to determine and differentiate the importance of these factors.

4.2 Methodology

During the eight-day study period from July 29th to August 6th, 50 runs in total have been conducted to measure surface moisture contents using Delta-T moisture probes. Figure 4.1 shows the tidal oscillations during the study period and the time of each moisture runs. The measurements from the probes were calibrated using field collected samples. The average of calibrated moisture measurements from two probes was used to represent each point of the moisture grid. The moisture contents in the grid are mapped using the kriging-gridding method in Sufer 8, distributed by the Golden Software Company. The elevations of groundwater table were collected from wells with pressure transducers installed, and referred to the average sea level of the study period. Evaporation was measured directly using a digital caliper and records were transformed into evaporation rates in millimeter per day. Detail of the approaches used and the deployment of instruments can be found in section 3.2 of Chapter 3.

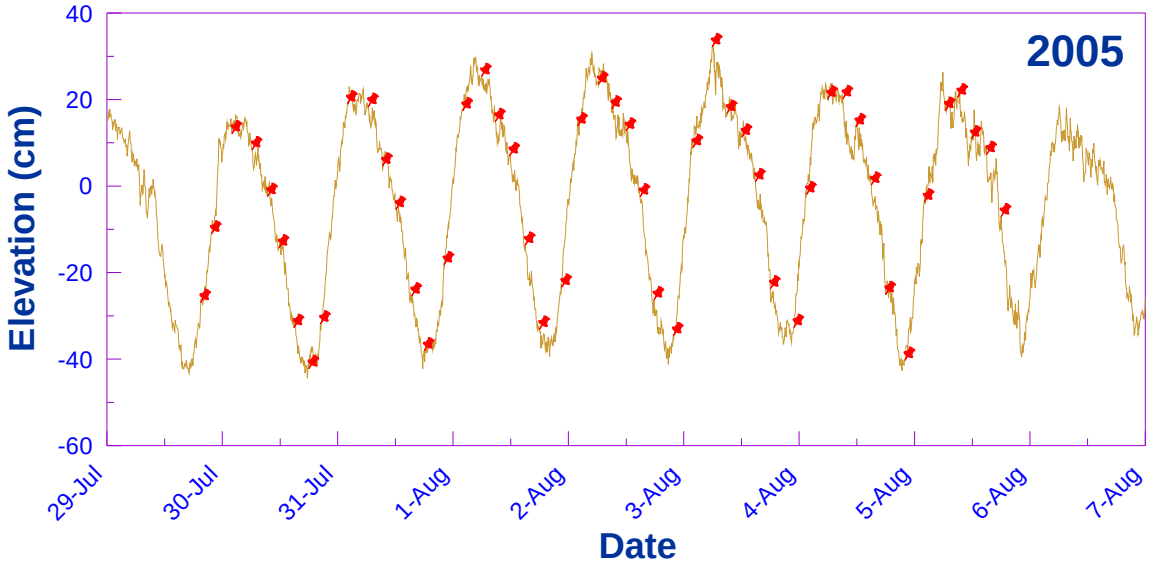

Figure 4.1 Time of moisture runs and tidal level
(The line shows sea level, and Symbols indicate the time of each moisture run)

4.3 Results and Analysis

The spatial variability in beach surface moisture content is evaluated by comparing the moisture maps and the averages and ranges of the moisture contents of each alongshore line in the moisture grid. The temporal variability is assessed using time series of moisture contents of each line, along with the fluctuations of evaporation rates and groundwater table. All moisture contents mentioned in the following sections are in percentage by volume.

4.3.1 Moisture Content Variations among Alongshore Lines

Figure 4.2 plots the minimum, maximum, median, lower quartile, and upper quartile for all records of moisture contents in each alongshore line, and each line has 250 records. The whiskers bounding each box indicate the extreme records (minimum and maximum), the box is defined by the lower and upper quartiles of all records, and the line in the box indicates the median of all measurements. Ignoring of extreme values (which represent 1 of 250 measurements), the lengths of boxes in Figure 4.2 provide a good visual indication of the relative variability in moisture content observed at each line. It shows that Lines 1-5 and 10-13 have relatively low variability (<6%), while other lines have relatively high variability (8-20%). In particular, Lines 7-9 have the highest variability at more than 15%. It also shows that Lines 1-7 have medians (<10%) substantially smaller than Lines 8-13 (35-45%). This large jump is associated with the highest spatial and temporal variability in surface moisture content, which occurs around Line 7.

Based on the variability showed in the lines, the beach can be divided into three parts by the distances from the averaged shoreline, the back beach (45-65 m), the middle beach (25-40 m) and the fore beach (0-20 m). Moisture contents of the back beach have low averages (>5%) with low variability (>3%), the middle beach has intermediate averages (10-30%) but with highest

variability (8-20%), while the fore beach has high averages close to saturation with low variability (>6%). This division provides a simple basis for us to understand the spatial distribution of beach surface moisture and is convenient for further analysis in the following sections.

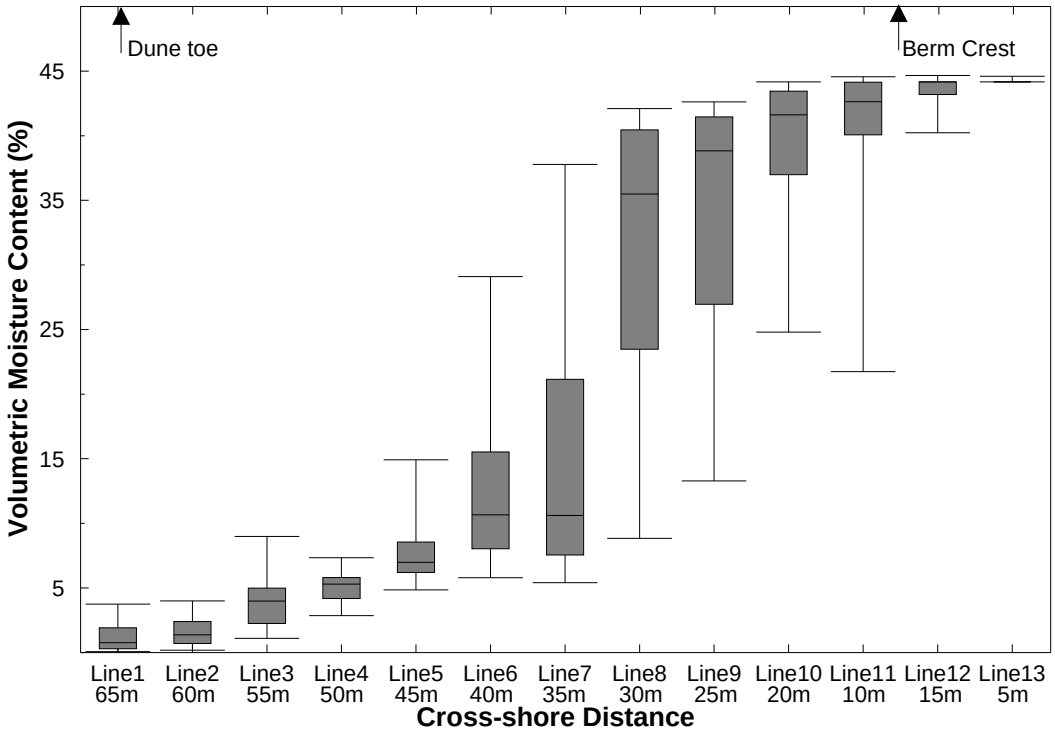

Figure 4.2 Box-Whisker plot for averages of each line from all runs

4.3.2 Moisture Content Variations over Space

Figure 4.3 shows of maps of moisture runs using spatial coordinates of the moisture grid. Only records from Day 4 to Day 5 (Aug 1st 6pm to Aug 3rd 6pm, Run22 to Run36) are shown here for demonstration. The moisture maps indicate that the moisture contents vary not only in the cross-shore direction but also in the along-shore direction (which is implied by curvatures in moisture contours), but the alongshore variability (less than 10% in a line) is substantially smaller than the cross-shore (~0-45%). Over time, the moisture contours move landward and seaward responding to tide rising and falling (which is indicated by the surface areas occupied by

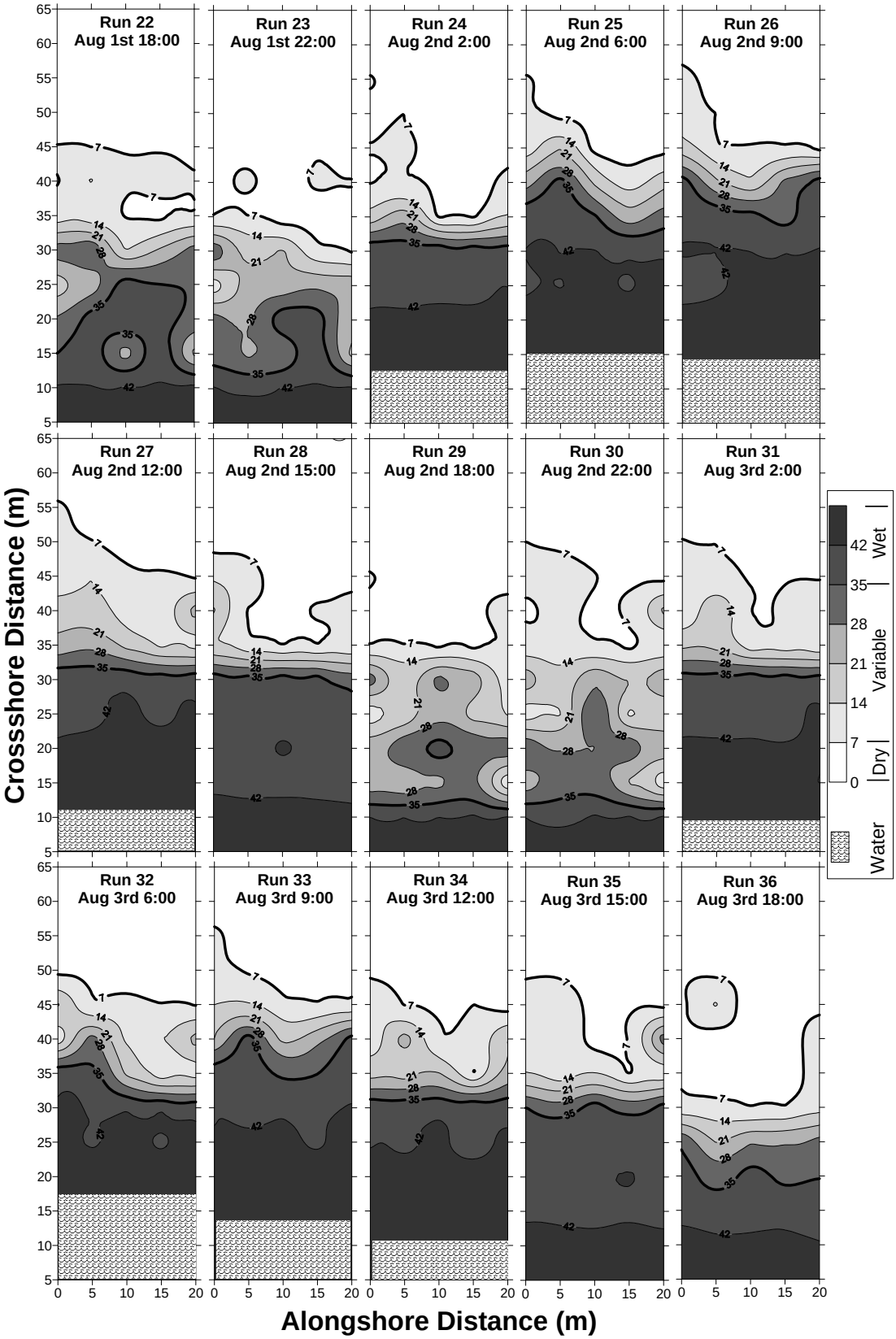

Figure 4.3 Moisture maps of the grid from Run22 to Run36
(Numbers in the maps are moisture content in percentage by volume)

water in the maps), since tidal oscillations directly leads to groundwater table fluctuations and hydraulic pressure changes of beach water profiles, and hence variations in surface moisture content.

The beach surface here is categorized into three zones based on surface moisture contents: dry (<7%), variable (7-35%), and wet (>35%), which are differentiated by the thick lines in the maps in Figure 4.3. Seven percent was selected as the boundary between dry and variable zones because it is often cited as the "critical" moisture content in aeolian transport (e.g., Sherman, 1989). 35 % was selected according to the shape of water retention curve of native sediment (Figure 7.1). The maps indicate that the back beach (45-65 m) remained dry during the study period, except that the corner at the left-hand side (south) and the seaward edge was occasionally occupied by the variable zone when tide was high (Runs 24-28, and Runs 31-35). The dry zone extended to the middle part of the middle beach (35m in Aug 1st and 2nd and 30m in Aug 3rd) when tidal level was low. It is interesting that the seaward boundary of the dry zone (the 7% contour) changed position and shape in the study period, but it was keeping a relatively similar shape during high tide. This stability is likely maintained by beach surface topography (see the same shape showed by the topographical contour in Figure 3.6 and 4.10).

As expected, the middle beach (25-40 m) has variable moisture contents with the widest range. The variable area occupies a relative narrow space (less than 10m) when the tide is relative high (Runs 24-28, Runs 31-35), while it expands to about 20m wide during low tide (Runs 22-23, Runs 29-30, and Run36). The position of the variable area shifts landward or seaward as tide rises or falls. Not surprisingly, the wet zone shifts its landward boundary with the tide. During low tide, the width of the saturated zone was compressed from about 30m to less than 10m, while during high tide it expands once again. This behavior is exactly reverse of the

variable zone. The alternation of viable and wet zone (changes of surface moisture content) occurred in the area between 15 and 30 m is likely caused by groundwater table fluctuations. When the groundwater table falls, the hydraulic pressure decreases, as a result water drainage occurs within the sand column as well as beach surface. Conversely, hydraulic pressure and subsequently surface moisture content increases by recharge through capillary rise as groundwater table elevates.

There are several points worth noting in regard to the spatial patterns of beach surface moisture. First, the boundaries of all three zones shifted landward and seaward in great agreement with tidal level fluctuations, although exceptions existed (e.g. Run33 and dry zone of Run35). Secondly, the rates of zone boundary movement differed between zones because the time lag between tidal level oscillations and surface moisture content response increases with distance from shoreline. The wet-variable boundary thus moves more quickly than the variable-dry zone boundary. Third, large portions of the "dry and wet" zones were spatially stable. The back beach almost always occupied by dry zone, while the foreshore and near the berm crest was wet during most time period, except during low tide. The landward part of middle beach was occupied alternatively by the dry or variable zone while the seaward part was occupied by the variable or wet zone. Although only two days of observations are shown here, these basic trends characterize the entire data set.

4.3.3 Temporal Variability in Beach Surface Moisture Content

Figure 4.4 shows a time series of average moisture contents for the lines adjacent to each well, along with observed evaporation and groundwater table elevations. Moisture contents of all lines demonstrated clearly cyclic changes through the study period. The amplitudes of the moisture fluctuations varied slightly but the averages seemed fairly stable in each cycle. In the

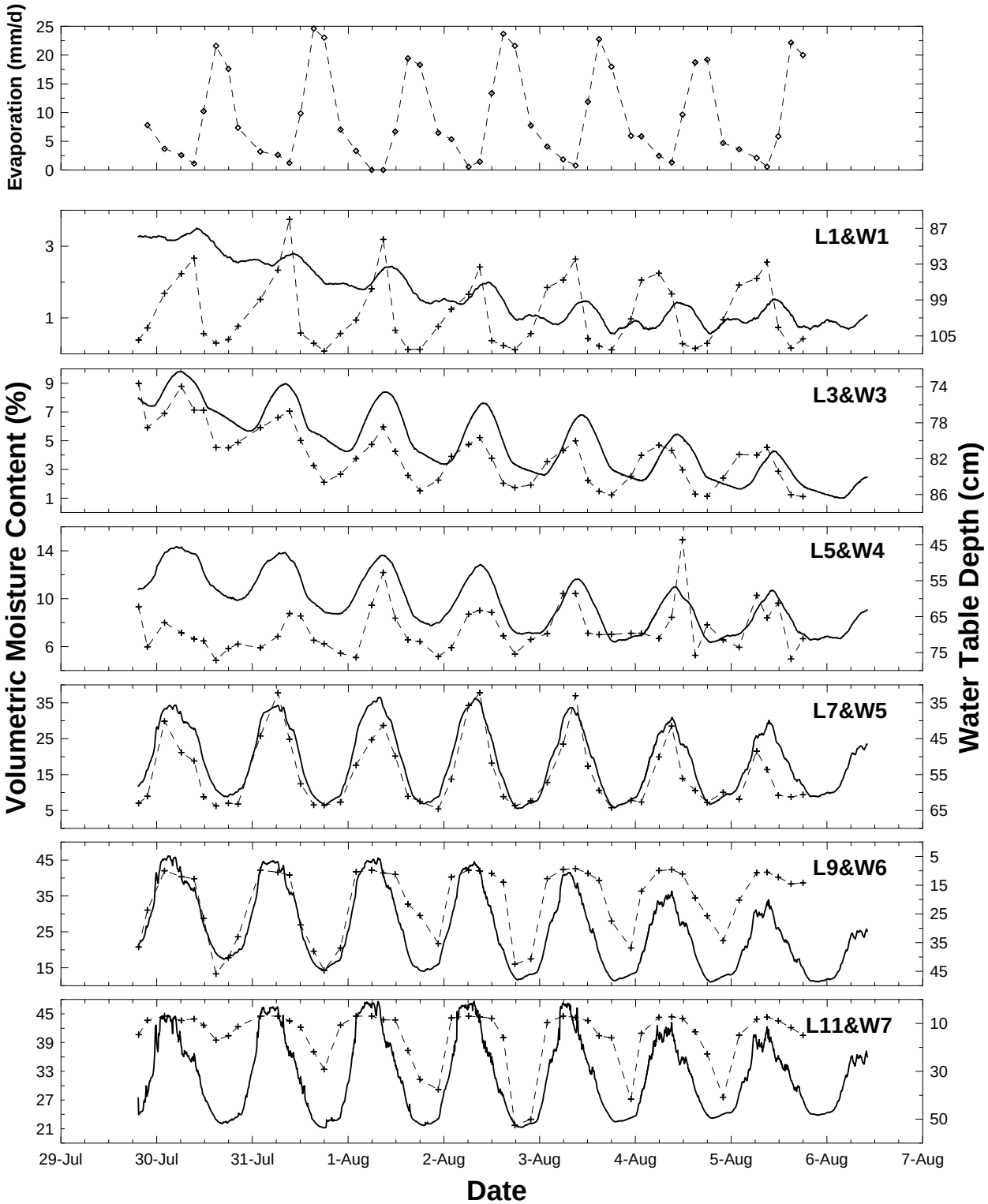

Figure 4.4 Comparisons of measured moisture content, groundwater level and potential evaporation rate over the study period (Dashed line with diamond is evaporation rate (mm/d), dashed lines with crosses are measured volumetric surface moisture content (%), and solid lines are ground water table elevations (cm); each cross symbol represents the averaged value of records from five stations in that line)

back beach from Line1 to Line5, the daily peak values of surface moisture content were usually recorded at 9:00am each day, and the lowest records were usually obtained at 6:00pm except for a few at 3:00pm. In the middle beach, the timing is somewhat more variable. Taking Line7 as example, highest moisture content recorded varied between 6:00am and 9:00am, and the lowest records varied between 6:00pm and 10:00pm. On the fore beach from Line10 to Line12, surface moisture content usually remained saturated or close to saturation but the lowest records were obtained in 3:00pm (Jul 30th), 6:00pm (Jul 31st), and 10:00pm (all other), which correspond to low tides. Although beach surface moisture demonstrated cyclic changes over time in all lines, the variations in the times of the daily peaks and lows may imply different processes involved like cyclic changes of groundwater table, condensation and evaporation. The underlying reasons for these variations will be further analyzed in the following section.

Beach surface moisture content experienced cyclic changes but the shapes of the cycles differed between lines. In the back beach from Line1 to Line5, the fluctuation curves of surface moisture content are skewed forward considerably, spending more time in climbing from daily lows (in the late afternoon at 3pm) to peaks (the morning of next day at about 9am). The skewness indicates a lower rate of moisture recharging than the rate of depletion. The moisture losses in these lines were apparently caused by evaporation because the highest moisture content was less than 10%, implying no direct drainage could occur. The sources of moisture recharging can be both capillary rise and condensation. However, the capillary rise is very likely to play a much more important role in replenishing moisture loss than the condensation, as the moisture contents remained almost same increasing rates after 6:00am each day, when condensation cannot occur (the temperatures of air and land surface increase after sun rise). In the fore beach from Line7 to Line12, no skewness can be clearly identified in those moisture cycles. This

behavior can be attributed to the process of wetting and drainage responding to the position changes of local water table.

4.3.4 Comparison of Surface Moisture Content, Groundwater Level and Evaporation

Examination of the moisture content of Line 1 and water table elevation at Well 1 (the second plot in Figure 4.4) demonstrated that at this location (65 m away from shoreline), surface moisture content varied within the range from 0% to 4% as groundwater level fluctuated around 95 cm below ground surface with a cycle amplitude of about 2 cm. The average water table depth at W1 decreased slightly during the study period. A time lag clearly existed between the cyclic changes of moisture content and groundwater level. More importantly, peaks of moisture content in each cycle always occurred earlier than those of groundwater level. This implies that at Line1 groundwater table fluctuation is not the major factor that is controlling the variations of surface moisture content. Figure 4.5 plots moisture contents of Line1 against evaporation rates. It is worth noting that the evaporation rates are plotted in descending order here. Clearly, surface moisture contents in Line 1 responded much more closely to evaporation than to groundwater table fluctuations: measured moisture contents in each cycle reached its peaks with the lowest evaporation rates between 6:00am and 9:00am, and decreased quickly to lower values when evaporation rates increased.

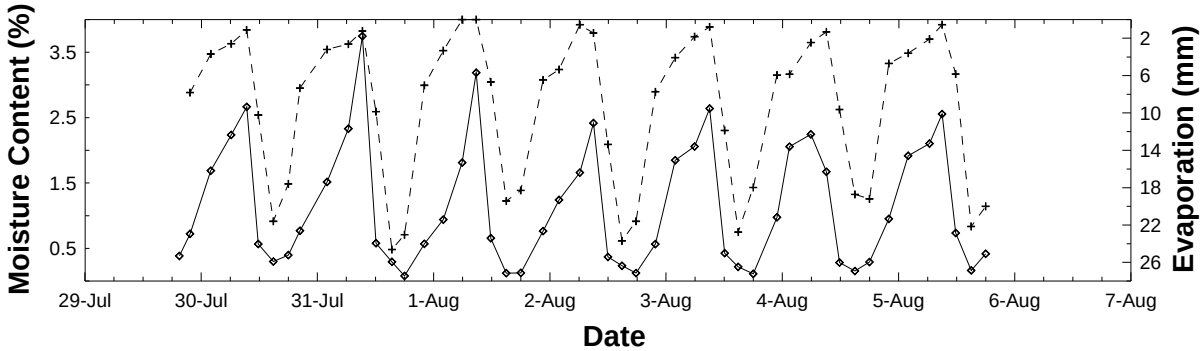

Figure 4.5 Comparison of observed volumetric surface moisture content of Line 1 (solid line with diamonds) and evaporation rates (dashed lines with crosses)

In comparing Line3 and adjacent Well3 (located 50m from shoreline), it is obvious that beach surface moisture content showed a long-term decreasing trend corresponded with the averagely falling groundwater level during the study period (the third plot in Figure 4.4). This indicated that oscillations of groundwater level played a significant role in affecting contents of surface moisture, which was not showed at Line 1 because the water table was considerably shallower at Well 3 (~80 cm in average) than at Well 1 (~95 cm in average). However, the cyclical fluctuations in moisture content again were out of phase with the water table (like Line 1) and corresponded more closely to evaporation rates (Figure 4.6), which means beach surface moisture content started to increase from its lowest value even though the groundwater level was still falling. This implies that at Line 3, daily variations in surface moisture content were dominated by evaporation, while groundwater levels influenced the longer-term average surface moisture content.

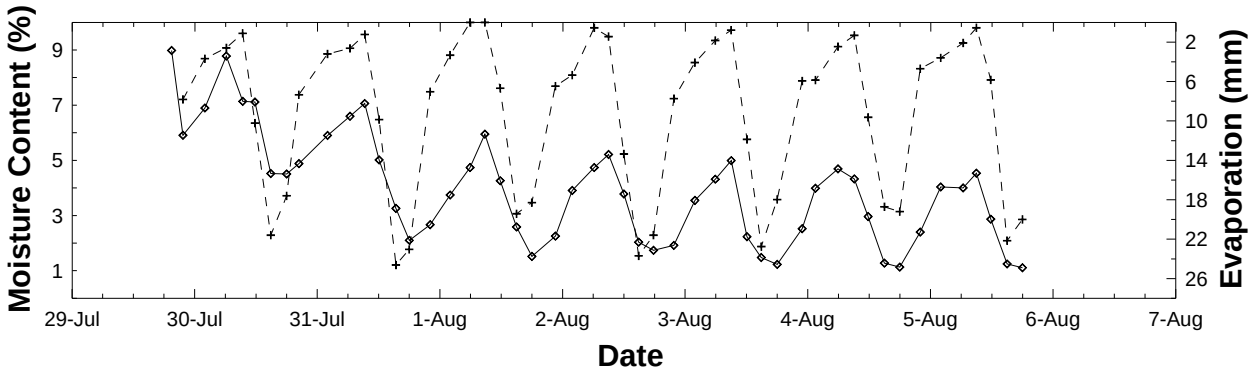

Figure 4.6 Same as Figure 4.5 except for Line3 and evaporation

At Lines 5, 7, 9 and 11, surface moisture content responded closely to groundwater fluctuations (Figure 4.4). Note that the water table is progressively closer to the surface at these lines. Line 9 and 11 in Figure 4.4 indicate that the beach surface was almost saturated when the water table fluctuated to within about 40 cm of the surface. This behavior is likely caused by the existence of the near-saturated capillary fringe. When the water table fluctuates in the capillary

fringe, capillary force is high enough to keep water in soil pores from drainage and the moisture content thus remains saturated. However, the extent to which the beach surface dried during low water table did not exactly correspond with the water table falling depth. Taking Line 11 as an example, moisture content decreased about 3% from saturation in Jul 30th with the water table dropped from about 8 cm to 53 cm below the surface, while in Aug 3rd it decreased about 8% from saturation with water table fell from about 10 cm to 50 cm below surface. This can be attributed to the hysterisis effect in the long-term drying and wetting process the surface experienced, which leads to various moisture contents with same hydraulic pressures. During the spring tide (the study period), the surface moisture actually experienced a number of drying and wetting loops responding to water table fluctuations in each tidal cycle, which provided a perfect situation for hysterisis to play a role. In this case the hysterisis may need to be considered in order to fully understand and accurately model the spatial and temporal variability in surface moisture.

4.3.5 Relationship between Surface Moisture Content and Elevation

Elevation of the beach surface may determine the long-term status of near-surface moisture content. All of the moisture data have shown that relatively high back beach locations usually are drier, while relative low fore beach locations are wetter. Note that it is not the elevation itself that directly determines the moisture status of the beach surface. The depth of the groundwater table (or hydraulic pressure), along with soil properties (e.g., pore-size distribution and hydraulic conductivity) are the controlling factors that affect moisture distribution in the sand body. Generally, the groundwater table has a much smaller slope angle than the beach surface. The depth of water table below surface therefore increases landward closely responding to surface elevations. The elevation of the beach surface thus can be used to calculate water table

depths with known hydraulic properties of native sediment, and in turn as an indicator for surface moisture content if groundwater table data are not available.

Figure 4.7 indicates that the beach surface is almost saturated when the surface elevation is less than ~70 cm (above the mean water level datum) and the water table depth is less than ~40 cm, which means the capillary fringe is about 40cm for this study site. Surface moisture content decreases rapidly from ~40% to ~5% as the surface elevation increases from ~70 to 140cm, and the water table depth increases from ~40 to ~80 cm. Further, the beach is dry (content <2%) when the surface elevation is above 160 cm and the water table depth is below 90 cm. It is worth noting that the relationship between the water table depth and surface moisture content shown in Figure 4.5 might be very close to the soil moisture retention curve, but these measured values also include the effect of evaporation. Nevertheless, these results confirm that the beach surface elevation has a strong, nonlinear relationship with averaged surface moisture content. This relationship provides a basis to assess, quickly and easily, the variability in surface moisture content.

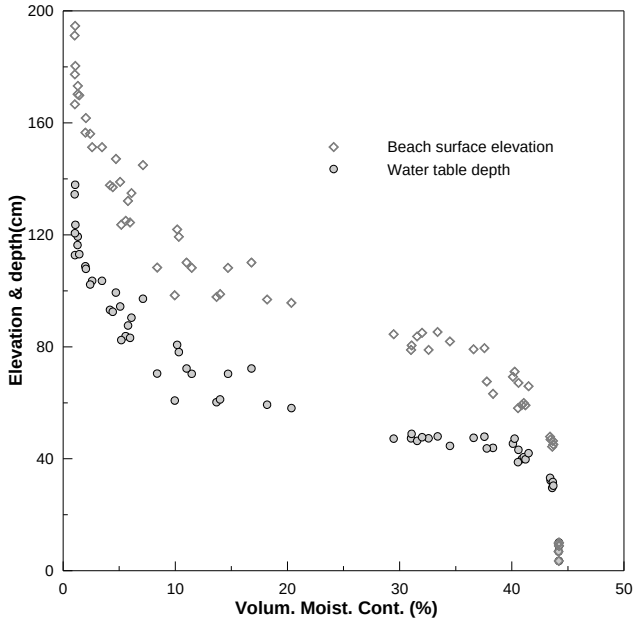

Figure 4.7 Relations of surface elevation and water table depth with averaged surface moisture content obtained at all moisture stations

4.4 Discussion

Tide-induced groundwater fluctuations appear to exert a strong influence on surface moisture content of the beach, particularly the fore beach and middle zones, in determining short-term variations in moisture content where the groundwater table is relatively shallow. Water table depth also appears to control the long-term averaged surface moisture content on the back beach, although daily fluctuations associated with evaporation and condensation strongly modify that signal.

Since the beach material at the study site is well-sorted sand, the beach can be treated as an isotropic sand body, and because the rates of groundwater table rising/falling are relatively low, the hysterisis effect of sand drying and wetting should be negligible (Child, 1969) although it can be possibly identified in the areas close to the shoreline. Moisture content within the sand body, and beach surface as well, can therefore be illustrated and predicted by the soil moisture characteristic curve (or soil water retention curve) (Miyazaki, 1993). The characteristic curves of sand materials are usually steeper in the two ends and much flatter in the middle part than those of clay or loam (van Genuchten, 1980).

Relationships between water retention curves, water table fluctuations and surface moisture dynamics for different parts of the beach (i.e., the back beach, middle beach and fore beach) are schematically illustrated in Figure 4.8. Surface moisture content at a certain location can be considered as the intersection of the surface and the moisture profile above the water table (which is described by the water retention curve). The intersection changes its position along the profile curve as the curve shifts up and down and the water table fluctuates. As also shown in the Figure 4.4(a), water tables in the back beach are relatively deep below surface and vertical fluctuations are of small amplitudes. As a result, surface moisture contents are very low and only

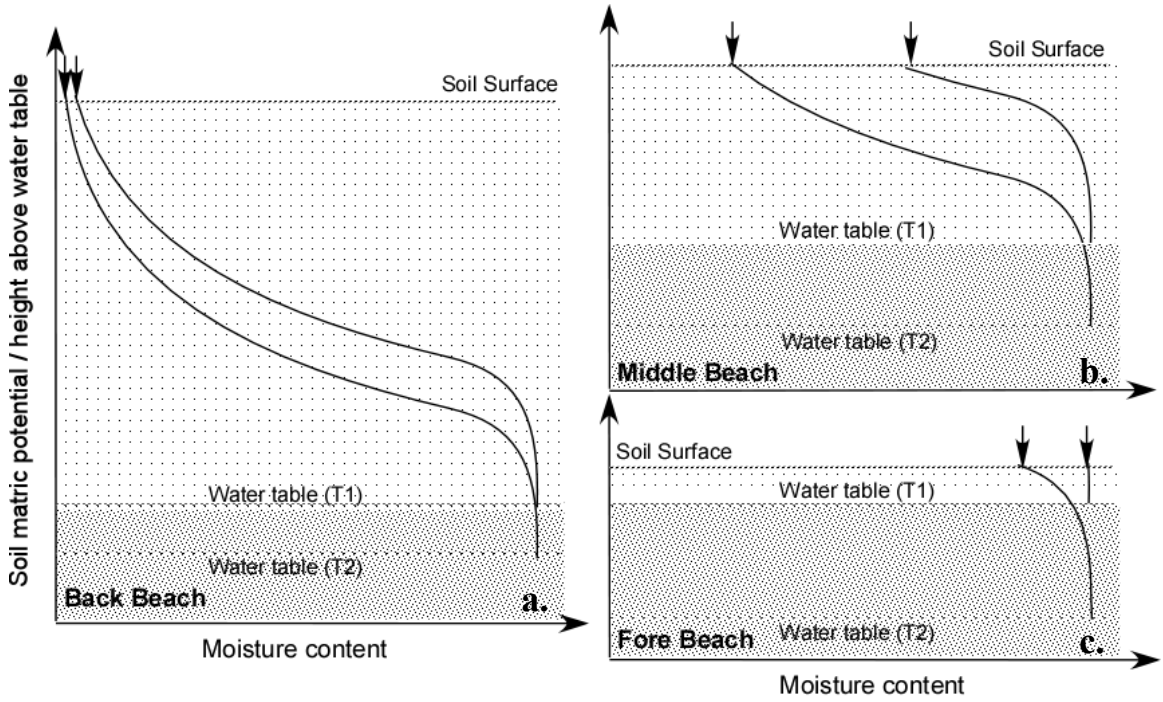

Figure 4.8 Schematic illustrations of the relationship between surface moisture dynamics, water table fluctuations and soil water retention curve in the beach (a. the back beach, b. the middle beach, and c. the fore beach. The effect of hysterisis is not considered here.)

vary within a narrow range because the intersection of the surface and the curve is located in the upper steep end of the profile. At the fore beach, water tables are very shallow and generally close to the surface, so surface moisture contents are extremely high and close to saturation. With the existence of the capillary fringe (extending about 40 cm above the water table at this site), the range of moisture content variations is also very narrow. At the middle beach, surface moisture contents vary within the largest range although the averages are lower than those of the fore beach. This occurs because the elevation of the beach surface above the water table level is located in the flat middle part of the water retention curve, where the moisture content changes most rapidly with depth (a small change in the position of water table will lead to large changes in surface moisture content). At high tide the capillary fringe approaches the surface providing near-saturation contents, but the pores rapidly drain as the tide and water table fall, and the capillary fringe drops away from the surface. As mentioned above, the moisture content in this

zone varies from 10-40 % during a typical tidal cycle (see Line 7 of Figure 4.4). In contrast, variations in surface moisture content during a tidal cycle on the back beach and fore beach are generally less than 5% (see Line 1 and Line 12 of Figure 4.4 respectively).

The diurnal changes in rates of evaporation and condensation, which are produced by the combination of wind speed, humidity, temperature, and solar radiation, can also impose cyclic effects on beach surface moisture content. It is straightforward that beach surface will dry more rapidly (and to a greater degree) if the potential evaporation rate is larger, and will wet if the condensation occurs without consideration of other inputs such as capillary rise or precipitation. The evaporation and condensation in general alternate in a period of a day (24 hours), while the period of tidal cycle usually differs with locations, so that their effects on surface moisture content could therefore be strengthened or diminished by each other in regarding to the period difference between the two cycles. For this study site, the dominant tidal cycles, and groundwater table fluctuations as well, have a period of ~25.6 hr, very close to the evaporation-condensation cycle. Further, all high tides and high water table were recorded during the night when the evaporation rate is small and condensation may occur, on the other hand, high evaporation rates in general were recorded during low tides. Therefore, the effect of evaporation and condensation in controlling surface moisture variations were overlapped with, and cannot be easily isolated from that of groundwater table fluctuations.

The evaporation- and condensation- induced diurnal variations can be explained by the Dry-Soil-Layer (DSL) conceptual model proposed by Yamanaka and Yonetani (1999, see Figure 4.9). The DSL is a layer formed at the surface of a bare, sandy soil. Liquid water transport from deeper soil layers stops at the bottom boundary of the DSL and vapor water transport is dominant. This model was experimentally confirmed by stable isotopic analysis (Yamanaka and

Yonetani, 1999). They argued that with daily variations in solar radiation input, vaporization of soil water and condensation of vapor occur alternatively throughout the entire DSL, not only limited within the bottom boundary of DSL as previous investigators have suggested (e.g. Hillel, 1971; Campbell, 1985). They hypothesized that the DSL primarily acts as an evaporation zone during day time as the temperature increases, and acts as a condensation zone in late afternoon and at night as the temperature drops. This conceptual model is useful to understand the moisture dynamics of a dry sand surface. It implies that the processes of evaporation and condensation alternatively control surface moisture content: moisture content will decrease during the late morning and the afternoon as evaporation occurs due to increasing leads of solar radiation, and will increase in late afternoon and early evening when condensation occurs as solar radiation close to zero.

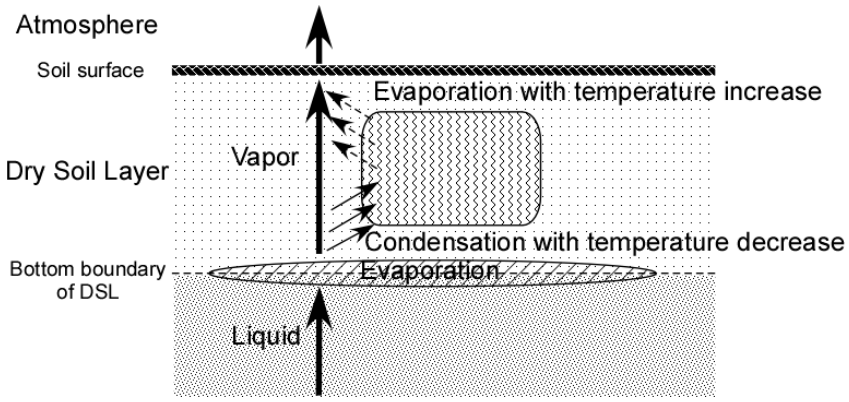

Figure 4.9 Schematic illustration of the conceptual model of sandy surface hydrodynamics (modified from Yamanaka and Yonetani, 1999)

As previously mentioned, the field data show that surface moisture content drops to daily low values around 6:00pm and reaches daily peaks in the early morning around 9:00am (Lines 1 and 3 in Figure 4.4). The evaporation clearly is the dominant process that reduces surface moisture content. However, it is somewhat contradictory that, if the condensation is assumed as the only reason that leads to the moisture content increase in the "dry surface", the increases between 6:00am and 9:00am in turn imply that the condensation still occurs after sunrise.

However, the air temperature increases almost right after sunrise (around 6:00 am), indicating no condensation during this time period. Reasons for this contradiction may be a) that some other processes (e.g., capillary rise) besides of condensation were involved in the moisture content increasing; b) that the "surface" measured was out of the range of the DSL. The thickness of the DSL can vary from millimeters to centimeters or more depending on the intensity of the drying process (Campbell, 1985). In this study, the measured moisture content would have represented the combined layer of the DSL and the sub-layer when the DSL was less than 14 mm thick (the exposed length of moisture probe pins). Such measured moisture contents would be affected by both evaporation process and the movement of the moisture profile. Therefore, more investigations on the definition, identification and determination of the DSL and associated processes must be conducted to enhance the understanding of surface moisture dynamics.

In the cross-shore direction, surface moisture content varies from totally dry (<1%) to saturation (~45%). This cross-shore variability in surface moisture can be linked to the increasing groundwater table depth landward moving from shoreline to dune toe. The relationship between surface moisture content and water table depth determined that the back beach remained dry and the fore beach wet, while the middle beach exhibited highly varying moisture content as the groundwater table fluctuated. In alongshore direction, surface moisture content generally has a smaller variability, less than 10% (Figure 4.3). Almost identical fluctuations of the water table were observed in paired wells at either ends of the sample grid, which were located almost exactly equal distance from the shoreline (e.g., Wells 2 and 9, Figure 3.6). This implies that the fluctuations in groundwater level did not drive alongshore variability of the moisture content. The elevation of beach surface varied substantially in the alongshore direction, up to 25 cm in the back beach and less than 5 cm in the middle and fore beach (see

Figure 4.10a), which means the water table depth varied. Moisture contours were roughly parallel to topographical contours for the back beach and part of the middle during high tides (e.g., Runs 25-27, and Runs 32-34), but stronger curvatures, other than smooth lines in the topographical map, can often be found in contours of those moisture maps (Figure 4.3 and 4.10). Although some other factors associated with spatial heterogeneity in the surface conditions, such as variations of wind speed, temperature, sand texture and packing rate, are commonly recognized as major regulators for the spatial variability, the variations of surface elevation in the alongshore direction do exert significant influence on the alongshore variability in surface moisture content at this study site.

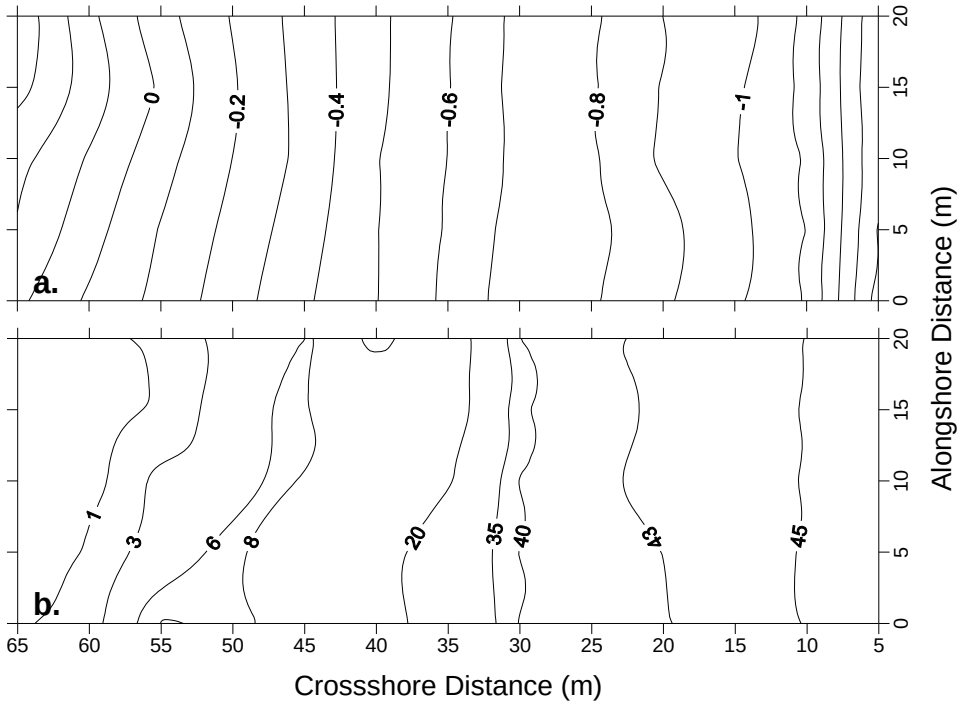

Figure 4.10 Comparison of a. topographical map (numbers are relative elevation in meter), and b. moisture map (numbers are volumetric moisture content in percent of Run 27)

4.5 Conclusions

Results showed that beach surface moisture content generally decreases landward with distance increase from shoreline. Both groundwater table fluctuation and evaporation play a role

in controlling surface moisture content variations. The influence of groundwater decreases landward, both because the groundwater table depth usually increases and because the amplitude of groundwater table fluctuations decreases, moving landward. As surface moisture content decreased, the importance of evaporation increased, finally became the dominant control at Line 1, near the dune toe.

Primarily, beach surface moisture demonstrated a pattern of continuously wet fore beach and dry back beach. The middle beach, however, experienced significant alternations between wet and dry conditions in response to rising and falling of tides and water table levels. In the back beach, where water table depth was usually below 80cm, surface moisture content was usually less than 5% (except for extreme highs) and below 3% on average. Evaporation process played a dominant role in controlling surface moisture content in this zone and content variations of range of ~4% each day. In the middle beach, where groundwater table fluctuated between 80cm and 40cm below surface, surface moisture contents vary in a wide range from less than 5% to higher than 40%. The effect of evaporation was not significant in comparison to the influence of liquid capillary transport. In the fore beach, where both the highest average water table elevations and the largest fluctuation amplitudes are found, relatively high and almost steady moisture contents occur (from ~35% to saturation). The effect of groundwater (along with swash) clearly controlled variations in surface moisture content.

In the alongshore direction, surface moisture content demonstrates a smaller variability than in the cross-shore direction. Overall, surface moisture content varies in a range less than 10% in alongshore lines, which can be attributed to, at least partly, the alongshore variations in beach surface elevation. However, the strong curvatures, in contrast to smooth topographical contours, can be found in moisture maps. This suggests that some other parameters associated

with spatial heterogeneity in beach surface conditions, including texture and packing rate, may also exert significance influences on the alongshore variability.

Temporally, beach surface in general became wetter during flood tide and drier during ebb tide, although a time lag existed between the changes of surface moisture content and tidal level oscillations. In the back beach, surface moisture content usually increased from late afternoon each day to the early morning of the next day and then decreased, along with evaporation process, but its increasing rate was slower than decreasing rate. In the middle beach and fore beach, temporal changes of surface moisture content keep same time pace with groundwater table oscillations instead of evaporation.

These findings may be common for other beach settings. However, for beaches composed of coarser sand (which implies higher hydraulic conductivity and flatter water retention curve), surface moisture content may decreased more rapidly with distance from shoreline and the variable zone therefore will be significant narrower than in this study site. In addition, for beaches of higher energy and larger tidal range, the back beach area (where soil moisture dynamics are dominated by evaporation) can be much larger.

CHAPTER 5 MODELING POTENTIAL EVAPORATION

This chapter focuses on simulating potential evaporation based on field obtained meteorological data. The present study attempts to model evaporation in small time scales (minutes and hours), utilizing the mass-transfer method, represented by the superior equation proposed by Singh and Xu (1997b), and the combination approach, represented by the Penman equation.

5.1 Introduction

Evaporation is a major component of the terrestrial hydrological cycle and its accurate estimation is essential to an array of problems including water balance calculations, irrigation management and ecological modeling in studies of climatology, hydrology, agriculture and ecology (Brutsaert, 1982; Wallace, 1995; Saunders *et al.*, 1997). However, evaporation is usually difficult to estimate owing to interactions between its controlling factors and the complexity of the land-atmosphere system.

Atmospheric parameters including solar radiation, relative humidity, vapor pressure deficit, air temperature and wind speed have long been recognized as major regulating factors for the process of evaporation. However, the relative importance of these parameters varies with specific local conditions and time scales. Based on four-year continuous measurements, Xu and Singh (1998) found that the vapor pressure deficit is most and wind speed is least closely correlated with pan evaporation in all time scales of hours, day, 10-day and month. They also found that solar radiation, air temperature and relative humidity have fairly close relationships with evaporation but systematic differences can be clearly seen for larger time scales. The relevance of these variables to evaporation possibly also changes with environmental settings,

thus giving rise to the large number of evaporation equations available in the literature that have similar or identical structures but different coefficients (Singh and Xu, 1997a).

Besides being directly measured using precise and carefully designed instruments, evaporation can be calculated theoretically by several approaches including: (1) water budget, (2) empirical determination, (3) mass transfer, (4) energy budget, and (5) combination of energy budget and mass transfer (Brutsaert, 1982; Wallace, 1995; Sanders *et al.*, 1997; Singh and Xu, 1997a). The water balance method expresses the conservation of mass, with consideration of evaporation, precipitation, surface and groundwater flow, and water storage, in a lumped or averaged hydrological system. However, water budget method in general is not feasible for evaporation estimation because relatively small but unavoidable errors in measuring precipitation, runoff and water storage can often result in large absolute errors in the ultimately calculated evaporation (Brutsaert, 1982). The empirical methods usually relate evaporation to meteorological factors based on regression analysis, and therefore may have limited applicability due to its lack of process representation and to the specific requirements on model variables (Singh and Xu, 1997b). Although the mass-transfer method is broadly based on Darton's law, the constants of the equations are normally empirically determined and need to be calibrated for site-specific conditions. The approach of pure energy budget does not exist strictly in that the three variables (i.e., the net radiation at surface R_n, is the soil heat flux G, and the sensible heat flux H) used for calculation can usually not be monitored directly or calculated based on measurements in the form of energy. The final option, the combination of energy budget and mass-transfer has been employed widely to simulate or predict evaporation with routine climatic data and generally produce acceptable estimates (e.g. Penman, 1948, 1963; Monteith, 1965; Tanner and Fuchs, 1968; Ben-Asher *et al.*, 1983; Monteith and Unsworth, 1990; Qiu *et al.*, 1998;

Valiantzas, 2006). From a practical standpoint, the method of mass-transfer can be used with the absence of solar radiation records, and the implementation of the combination approach depends on its availability.

Evaporation is most commonly estimated on a weekly, monthly or annual basis, although a few studies have presented applications of daily simulations (Rowntree, 1991). However, modeling at higher temporal resolution of hours or even minutes is necessary for the micro-scale environmental studies due to the high variability of evaporation, particularly in coastal areas. The major purposes of this study are 1) to identify and further examine correlations between evaporation and its five aforementioned controlling factors for coastal areas where usually have unique climatic patterns; and 2) to evaluate accuracy and efficiency of the two widely used approaches (i.e., the mass-transfer method and the combination method) in evaporation estimation at high temporal resolution.

5.2 Evaporation Models

A large number of evaporation models have been developed for specific conditions with concerns of data availability. The mass-transfer method and the combined approach are selected here because they are commonly believed reliable and require only a few inputs that can be routinely obtained.

5.2.1 The Mass-transfer Method

The mass-transfer method, also referred to as aerodynamic method, employs Dalton's law that describes eddy motion transfer of water vapor from an evaporation surface to the atmosphere (Singh and Xu, 1997a, b). Equations based on this method normally have simpler forms and require fewer inputs than the energy-budget based equations. They may be reliable in

the areas and over the periods in which they were developed, however, large errors can be generated when these equations are extrapolated to other climatic areas without recalibration of the various constants. Although a large number of equations have been proposed with different combinations of required input parameters, Singh and Xu (1997b) generalized most of the available mass-transfer equations, and based on a comparative study found a superior form to be:

$$E = a_1(1 + a_2 u)(e_s - e_a)\left[1 - a_3(T_a - T_d)\right] \quad \textbf{(5.1)}$$

in where E is the evaporation rate (mm/d), a_1, a_2 and a_3 are constants need to be recalibrated, u is wind speed (m/s), T_a is the air temperature (℃), T_d is the dew point temperature (℃), and e_a is actual vapor pressure (kPa) given as:

$$e_a = \frac{RH}{100} e_s \quad \textbf{(5.2)}$$

in which RH (%) is relative humidity and e_s is saturation vapor pressure (kPa), which is a function of air temperature (See appendix 2 for calculation)

5.2.2 The Combination Approach

The combination approach is generally believed to be reliable and accurate for practical calculations (Singh and Xu, 1997a). Broadly, it utilizes the structure of the energy budget approach but calculates the sensible heat term using the mass-transfer method. The energy budget can be expressed as:

$$\lambda E = R_n - G - H \quad \textbf{(5.3)}$$

in which λ is latent heat of vaporization (MJ/kg), the combination λE is the latent heat flux (MJ/m^2/d=11.57 Watts/m^2), R_n is net radiation at surface (MJ/m^2/d), G is the soil heat flux

(MJ/m^2/d), and H is the sensible heat flux (MJ/m^2/d) between the atmosphere and water/soil surface.

Although the three parameters in the right-hand side of equation 5.3 are difficult to measure directly, a number of previous studies have provided reliable ways to estimate them from routine meteorological data. The net radiation R_n can be calculated with input of solar radiation and air temperature (e.g., Valiantzas, 2006). The soil heat flux G is usually presumed equal to 5% of R_n when R_n >0 (e.g., Nilsson and Karlsson, 2005). A large number of equations and concepts have been developed to calculate the sensible heat term H (e.g., Monteith, 1965; Priestley and Taylor, 1972; Stagnitti *et al*., 1989). However, when the radiation term dominates and the sensible heat term approaches zero, the equations based on the combination approach usually produce estimates with small differences. For example, Shuttleworth and Calder (1979) found that in areas of low moisture stress, estimates of the Priestley-Taylor model and the Penman's equation were within about 5% of each other.

The Penman (1963) equation, which is widely used as the standard method in hydrological applications to estimate potential evaporation and evapotranspiration, is used in this study to represent the combination method. It can be expressed as:

$$\lambda E = \frac{\Delta}{\Delta + \gamma} R_n + \frac{\gamma}{\Delta + \gamma} 6.43 D f(u) \qquad \textbf{(5.4)}$$

where the first term in the right-hand side is the radiation term and the second is the aerodynamic term, Δ is the slope of the saturation vapor pressure curve (kPa/^{o}C), γ is psychrometric coefficient (kPa/^{o}C), D is vapor pressure deficit (kPa) between actual vapor pressure e_a and saturation vapor press e_s, and $f(u)$ is wind function, which is given by:

$$f(u) = a_u + b_u u \qquad \textbf{(5.5)}$$

where a_u and b_u are the wind function coefficients; and u is wind speed at 2m height (m/s) (See appendix 2 for details of parameter calculation). In the original Penman equation, a_u and b_u were empirically determined as 1 and 0.536 respectively. It should be noted that the aerodynamic term is essentially similar to equation (5.1) except for the exclusion of the air temperature part.

5.3 Methodology and Data

The evaporation modeling approaches used in this chapter require data that include solar radiation, wind speed, air temperature and relative humidity. The latter four variables were directly monitored (see section 3.2 for more information). Measured pan evaporation rates from the field are also presented for comparison. Hourly solar radiation records were obtained from National Park Service (NPS) Gaseous Pollutant and Meteorological Database (ARS, 2005), and were subsequently interpolated linearly at 6-min interval. These data were measured at the Malaquite Visitor Center, Padre Island National Seashore, which is located about 900m south of the study site.

5.4 Experimental Results

Figure 5.1 shows measured solar radiation, wind speed and direction, air temperature and relative humidity. All parameters clearly show diurnal cycles. As expected, air temperature, relative humidity on-shore wind speed have readily identifiable, but highly non-linear relationships with solar radiation intensity.

Solar radiation followed a simple and expected pattern: increasing from sunrise (about 5:45am) to a daily peak value at noon (about 12pm) and then decreasing until sunset (about 6:15pm). The influence of cloud cover is occasionally detectable, for example from 9:00am to 3:00pm in Jul 30th and from 10:00am to 1:00pm in Aug 4th.

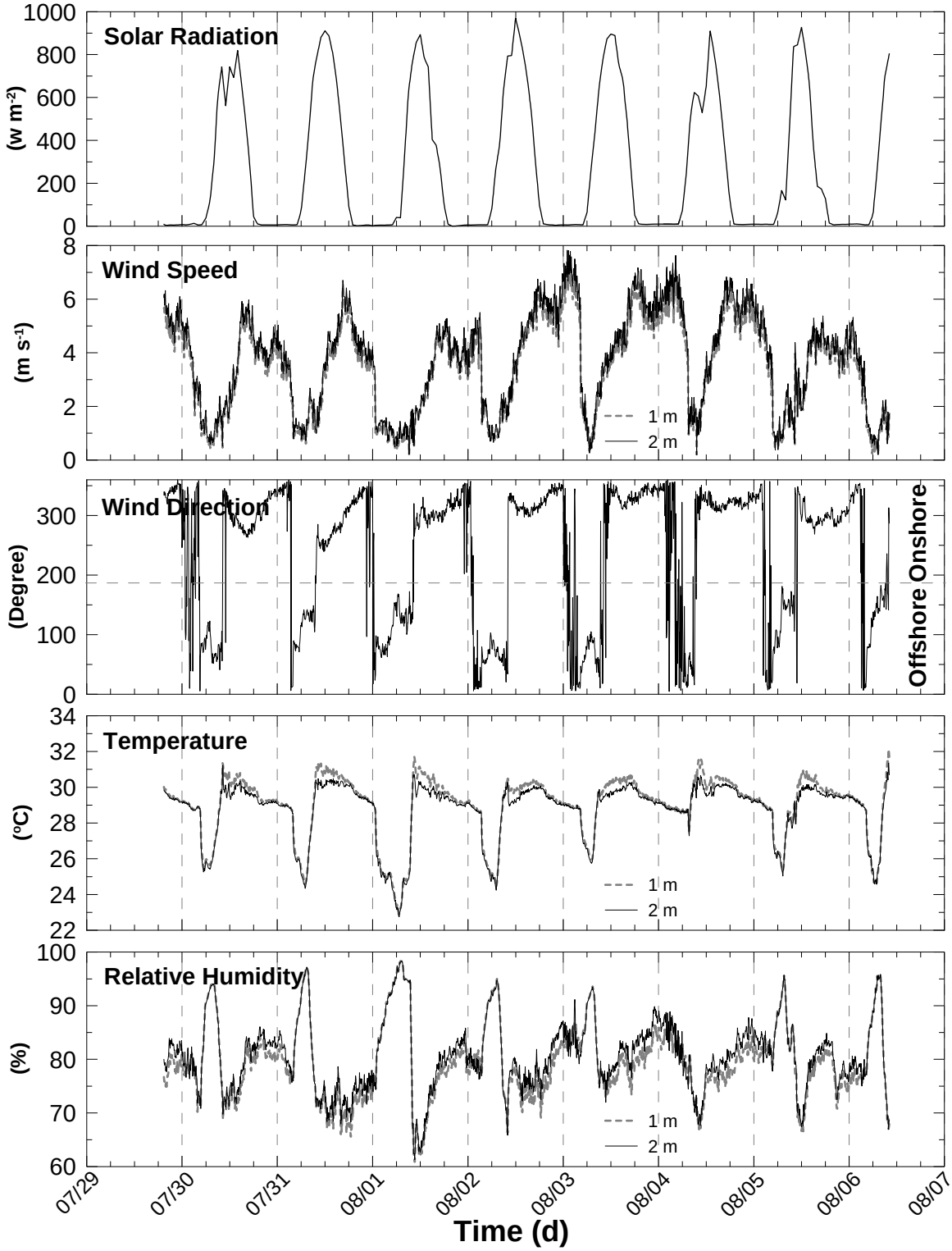

Figure 5.1 Measured 6-minute meteorological parameters. Solar radiation was originally of one hour intervals and subsequently interpolated into 6-minute data. Wind speed, relative humidity and air temperature were measured at two heights of 1m (grey thick dashed line) and 2m (dark thin solid line) above beach surface respectively.

Wind speed varied also exhibited clear, cyclic diurnal patterns. It usually picked and consistently increased from the late morning through the early afternoon, decreased abruptly after about 3:00am, and then stabilized (to a degree) from the midnight through the early morning. In general, on-shore winds had higher speeds than off-shore winds. The difference in wind speed at1 m and 2 m elevation was less than 0.2 m/s throughout the study period.

Wind direction followed a classic day sea-breeze and night land-breeze pattern. Typically the wind shifted onshore between 9:00 and 11:00am and offshore between midnight and 3:00am in the following day. These shifts are driven by atmospheric pressure difference between the air over the land and water surface, which is in turn caused by differences in heat capacities and hence temperature changing rates of the land and water surface.

Air temperature increased rapidly each day from around 5:45 am (dawn), reached its daily peak value around 11:00am, and then decreased gradually until around 4:00 am, and then dropped quickly to its daily lows. It is clear that the variations in air temperature are driven by the solar radiation input. Variations in air temperature can also be related to wind direction shifts. Air temperature essentially represents land surface conditions during prevailing offshore wind and reflects sea surface conditions during onshore wind. Although the solar radiation intensity usually has very low spatial variability (particularly in small space scales), the temperature of the land surface responds more to energy fluxes than that of the sea surface due to the substantially lower average heat capacity of the land surface. This influence is apparent in the timing of daily high air temperatures, which occurred before solar radiation reached its peak at 12:00pm on most days (Figure 5.1). Cooler marine air drawn onshore during the afternoon provided gradually cooling temperatures. The influence of wind direction shifts can also be seen at night, in the rapid temperature drop associated with the shift to offshore winds. Air temperature records at 1

m elevation are closely correlated with and usually higher than that at 2 m. This is because that air at higher elevation is often to a lager degree mixed with cooler air brought by the onshore winds during the afternoon and the evening.

Relative humidity also clearly shows diurnal cycles, which are negatively correlated with variations of air temperature as expected. During on-shore wind, relative humidity measured at 2 m is appreciably higher than that at 1 m. This is very likely owing to the cooler temperature at higher elevation as aforementioned.

In general, solar radiation as the major energy source manipulates the temperature changes of the air and the earth surface below. As the temperature of the land surface responds to energy input more rapidly than that of the sea surface, the atmospheric pressures subsequently differs to various degrees between them. The pressure difference determines the occurrence and the speeds of the winds, and the pattern shifts between land-breeze and sea-breeze. The wind speed and direction controls the rates of air and moisture transfer between the two surfaces and in turn affects variations in air temperature and the correlated relative humidity.

5.5 Comparisons of Observed and Simulated Evaporations

The evaporation measurements reported here actually represent the cumulative evaporation that occurred during each measurement interval. Water levels in the evaporation pan were recorded every three hours during the day and every four hours at night. It is reasonable to assume that the time-averaged measurements represent the real evaporation rate at the center time point for each interval.

5.5.1 Simulations Using the Mass-transfer Method

In the study of Singh and Xu (1997b), the constants a_1, a_2 and a_3 of equation 5.1 varies

climatic stations. The best fits of these constants varied slightly over time for a given station but considerably more between different stations. Clearly, they need to be calibrated for site-specific environmental conditions. To accomplish this, wind speed, air temperature and relative humidity measured at 2m above ground surface averaged for each period of evaporation measurments, and used as input data. The constants a_1, a_2 and a_3 were initially set as 2.25 , 0.15 and 0.034 respectively (the averages obtained in the study of Singh and Xu, 1997b), and iteratively adjusted to achieve the best agreement between observed and simulated evaporations. The best fit was defined by the criterion of minimum sum of squares (Xu and Singh, 1998), which can be described as an objective function:

$$ER = \sum_{1}^{N} (E_{obs} - E_{sim})^2 \rightarrow \text{minimum} \qquad \textbf{(5.6)}$$

in which *ER* is the determining function, *N* is the number of measurements, E_{obs} is observed and E_{sim} is simulated evaporation rate. The best-fitted set of a_1, a_2 and a_3 were eventually found as 7.90, 0.23 and 0.015 respectively.

Figure 5.2 shows observed evaporation rates and simulations from the mass-transfer method (equation 5.1) with recalibrated constants shown above. Although the timing of low evaporation rates is well captured, substantial underestimations during about 11:00am-6:00pm each day and overestimations from 6:00pm to 8:00am are apparent. This discrepancy between observed and simulated pan evaporation rates is owing to the unique atmospheric conditions in coastal areas. During onshore winds, the measured parameters including vapor pressure deficits and air temperature in a large part represented the conditions of the air from the sea surface instead of the land surface, while the observed pan evaporation was controlled by the conditions

near land surface. Therefore, the evaporation rates can not be accurately simulated from these parameters.

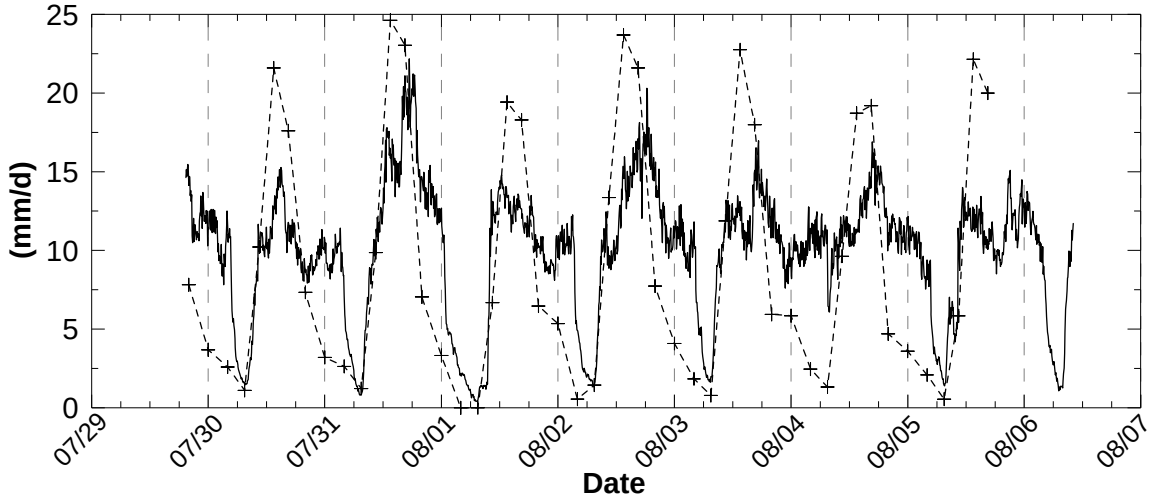

Figure 5.2 Observed (dashed line with cross symbols) vs. simulated (solid line) pan evaporation rates using the mass-transfer method (Eq 5.1)

5.5.2 Simulations Using the Combination Approach

The Penman equation (equation 5.4), representing the combination approach here, requires solar radiation as an input in addition to vapor pressure deficit, wind speed and air temperature. Results calculated directly by the Penman equation are shown in Figure 5.3. It shows the simulated evaporation rates agree with the observed quite well in terms of magnitude. However, the predicted values are clearly offset slightly in the temporal dimension. A second departure from the measured values occurs in the early evening. Predicted values drop to a minimum but measured values remain relative high. This might result from the underestimations by the wind function in the original Penman equation.

5.5.3 Comparison

As recommended by Willmott (1982) and Jacovides and Kontoyiannis (1995), the differences between observed and predicted evaporation can be quantitatively evaluated by mean

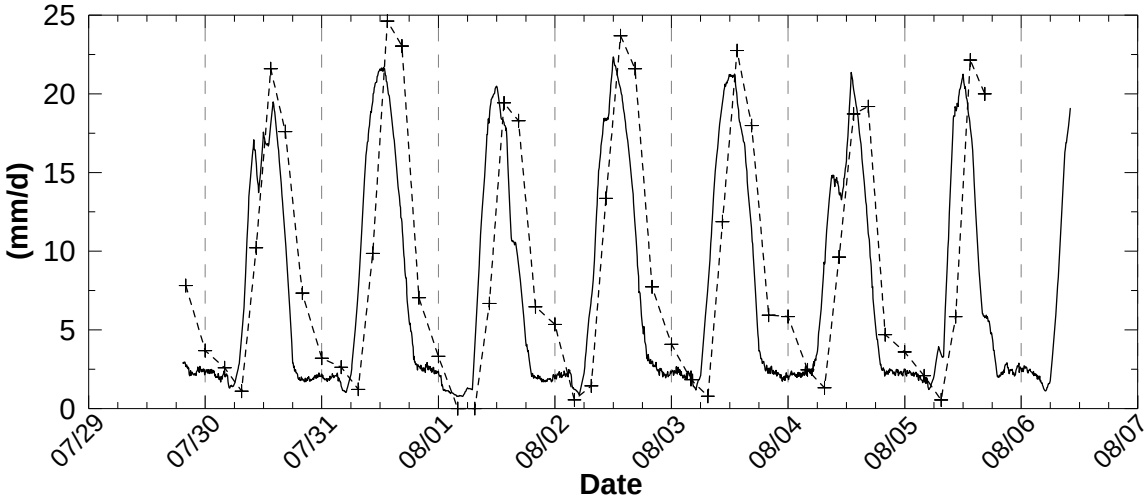

Figure 5.3 Same as Figure 5.2 but using the combination approach (Eq. 5.3)

absolute error (MAE) and root mean square error (RMSE), which are defined by

$$MAE = \frac{1}{N}\sum_{i=1}^{N}\left|S_i - M_i\right| \tag{5.7}$$

$$RMSE = \sqrt{\frac{1}{N}\sum_{i=1}^{N}\left(S_i - M_i\right)^2} \Bigg/ \frac{1}{N}\sum_{i=1}^{N} M_i \tag{5.8}$$

where S and M are paired simulated and measured values respectively, and N is the number of records. The MAE and RMSE (N=50) are 5.11 and 0.64 mm/d respectively for mass-transfer method (Equation 5.1), and 4.72 and 0.62 mm/d respectively for the combination approach (Equation 5.3).

Statistically, the combination approach is slightly better, but almost equivalent to the mass-transfer method in terms of errors. However, it should be noted that the simulations shown in Figure 5.2 are already based on optimizations of constants involved, while those in Figure 5.3 are calculated on the original Penman equation. Therefore, the statistical comparison might be misleading. Visually, the fit of the Penman approach appears much more reasonable, and it can be improved further with shifts in time and slight adjustment in its aerodynamic term.

5.6 Modifications of the Penman Equation

The mass-transfer method is not suitable for this study and will not be addressed further. The combination approach is theoretically reliable, and more importantly, its simulations demonstrate promising agreement with observed values upon examination except for a temporal offset and some underestimation. These can be attributed to the radiation term and aerodynamic term, respectively, of the Penman equation (equation 5.4).

Peak evaporation rates calculated by the combination approach consistently occur about two hours earlier than observed values (Figure 5.3). The Penman equation employed here actually involves two distinct energy sources (radiation and aerodynamics), which may affect the evaporation process in different ways. Energy absorbed by water from radiation is theoretically partitioned into two parts, the first part that is consumed by the evaporation process and the second part is a residual stored as heat to increase water temperature and outgoing long-wave radiation. Water temperature will increase only after incoming radiation energy exceeds the sum of outgoing radiation and the energy demand of evaporation, and will decrease if sufficient incoming radiation is not available. Therefore, a time lag can usually be expected between temporal variations of radiation and water temperature. Because water temperature continues to increase even after solar radiation peaks, the rate of evaporation continues to increase even though solar radiation levels begin to decrease. Strictly, parameters involved in the aerodynamic term do not directly recharge any energy into water body. Rather, they change the diffusivity of water vapor above water surface. A time lag may also exist between the processes of water molecules being removed from the saturated vapor layer above water surface by wind and replenished into it by evaporation. At an hourly time scale Xu and Singh (1998) found that, evaporation lags behind solar radiation about 2-3 hours, but evaporation was closely correlated

with vapor pressure deficit and air temperature and almost no time lag existed between them. This demonstrates that, the time lag between solar radiation and evaporation is detectable, and therefore must be incorporated in the Penman equation for simulations or predictions at high temporal resolution, while the time lag between evaporation and involved parameters, such as vapor pressure deficit and air temperature, may be ignored, at least on an hourly basis. In the present study, the radiation term calculated by the original Penman equation is clearly peaks ~2 hours earlier than observed values (Figure 5.4), but time lags with the aerodynamic term seem negligible, which can be seen in the simulations from the mass-transfer method (Figure 5.2).

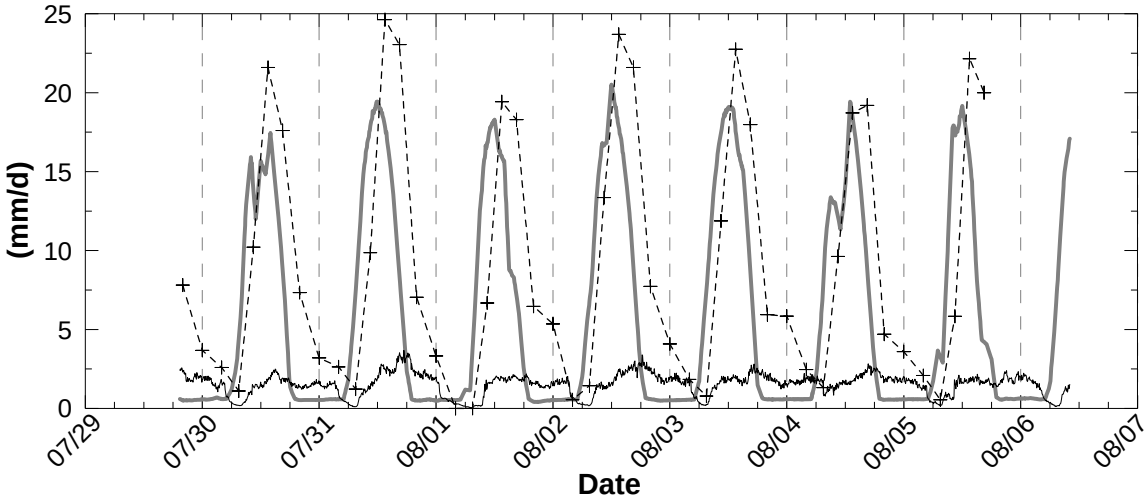

Figure 5.4 Radiation term (grey thick line) and aerodynamic term (dark thin line) of the original Penman equation and observed evaporation (dashed line with cross symbols)

It is worth noting here that the underestimation of the Penman equation can be attributed, at least partly, to the aerodynamic term. These underestimations can be clearly seen from about 8:00 pm to sunrise of the next day (Figure 5.3 and 5.4), and during this period solar radiation was close to zero and supposedly has no direct effect on evaporation. It therefore may not be appropriate to solve the temporal offset problem by shifting predicted values two hours behind, or deal with the problem of underestimation by recalibrating the constants involved in the aerodynamic term. Both problems should be treated together to obtain the best agreement with

observed value. The Penman equation may be modified to estimate instantaneous evaporation rates as follows

$$E' = \frac{1}{\lambda}\left[\frac{\Delta}{\Delta+\gamma}R'_n + \frac{\gamma}{\Delta+\gamma}6.43Df'(u)\right] \quad \textbf{(5.9)}$$

where E' is the real-time potential evaporation rate (mm/d); R'_n is net radiation (MJ/m^2/d) calculated from *dt*-time-offset solar radiation (*dt* is 2 hours in this study); and $f'(u)$ is the modified wind function, in which b_u is equal to 0.86, following the recommendation of Doorenbos and Pruitt (1975), instead of 0.54 as in the original Penman equation. Since the solar radiation values in this study were interpolated from hourly records, the two-hour offset is used here to provide the best fit from the measured records. Note that the time offset from measured solar radiation could be more precisely determined if high-frequency solar radiation records were available.

Figure 5.5 compares the observed evaporation with simulated values using the modified Penman equation (Equation 5.10). Clearly, the modified version performs much better than the original in terms of both timing and magnitude of predicted evaporation rates. The MAE and RMSE (N=50) are 2.85 and 0.32 mm/d respectively for the modified Penman equation, clearly indicative of an improved model performance.

5.7 Summary and Conclusions

The climate in this study site exhibits a classic day sea-breeze and night land-breeze pattern that is common in coastal areas (Figure 5.1). Field measurements demonstrated that the winds shifted directions responding to the atmospheric pressure gradient that is related to the temperature difference between the land and sea surfaces. Onshore winds in general had higher

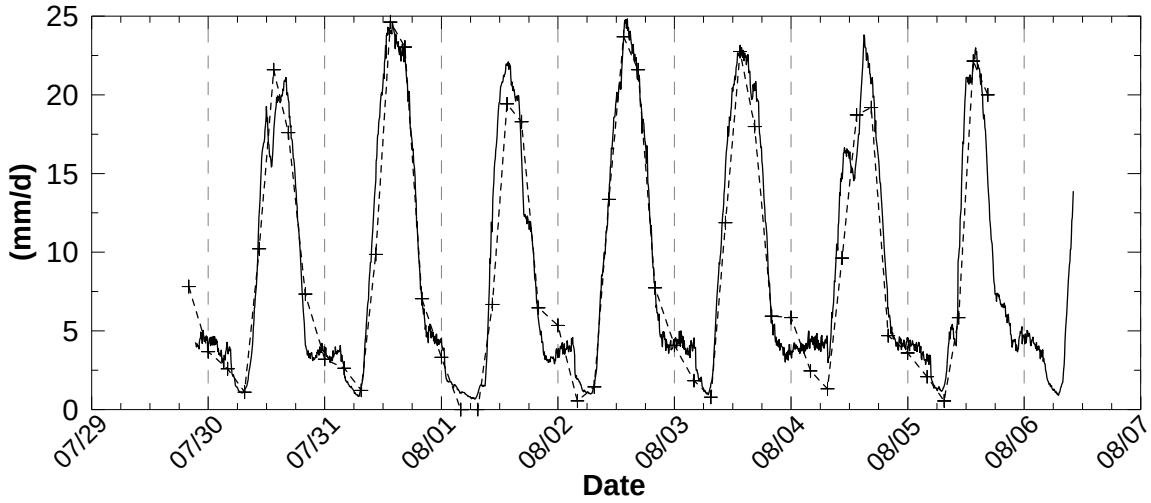

Figure 5.5 Same as Figure 5.2 but using the modified Penman equation (Eq. 5.9)

speeds than offshore winds. During offshore winds (representing land surface conditions), air temperature and relative humidity responded rapidly to the intensities of solar radiation, while they are quite stable during onshore winds (representing sea surface conditions).

Owing, at least in part, to the dominant climatic pattern, the mass-transfer method (which is partly empirically-based), was found unsuitable for evaporation modeling at this study site. Even with optimizations of the constants, it cyclically under- and overestimated the rates of evaporation (Figure 5.2).

The original Penman Equation was found to provide better results except for a time lag error (about two hours in this study) in predictions of instant evaporation rates and some underestimation during the night. This was accounted for by lagging the solar radiation input. It is worth noting that the lag magnitude is specific to this site and may vary for other sites and over different time scales. A simple modification, following Doorenbos and Pruitt (1975), of the aerodynamic component (the second term) of the Penman Equation was found to significantly improves its prediction accuracy, particularly during the time period without solar radiation (Figure 5.5).

Clearly, these conclusions are specifically drawn for coastal areas where atmospheric circulation patterns are rather unique than inland areas. Solar radiation data is a necessary input. Even if field measurements are not available, predictions from existed models must be obtained to estimate evaporation rates for coastal areas.

CHAPTER 6 MODELING GROUNDWATER TABLE FLUCTUATIONS

This chapter deals primarily with simulating beach groundwater table fluctuations forced by tidal signals. Beach groundwater levels were monitored directly in the field and interpreted using spectral analysis. The groundwater-table fluctuations were modeled using the numerical solution of the linearized Boussinesq equation. Separate simulations are conducted for the cases for a vertical beach and a sloping beach. The purpose of the present study is to improve the understanding of groundwater table dynamics in a fine-grained beach dominated by diurnal tides.

6.1 Introduction

The fluctuation of water table as forced by tidal waves in beach systems has been studied extensively (e.g., Nielson, 1990; Gourlay, 1992; Turner *et al.*, 1997; Baird *et al.*, 1998; Horn, 2002, 2006; Chuang and Yeh, 2006). Field observations have demonstrated a number of important characteristics. The beach groundwater table is usually not flat and acts as a damped free wave propagating in the landward direction (Nielson, 1990). Elevation of the groundwater table in a beach is generally higher than tide elevation due to the relatively higher rate of recharging than drainage (Turner, 1993). The beach water table is also asymmetric and skewed in time (Raubenheimer *et al.*, 1999). Emery and Foster (1948) conceptualized the beach as a filter that allows larger or longer waves (e.g., diurnal tides and spring-neap tides) to pass. The magnitude of water table oscillations decreases in the course of propagation in the landward direction from the shoreline (Raubenheimer *et al.*, 1999; Chuang and Yeh, 2006). The landward distance to which the effects of sea water level fluctuation are discernible depends on its frequency (Jackson *et al.*, 1999). Water table oscillations usually lag behind tidal oscillations by a varying length of time. The length of this time lag is mainly controlled by, and negatively

correlated with, the hydraulic conductivity of beach sediments (which is in turn affected by the characteristics of sediment) (Nielson, 1990; Jackson *et al.*, 1999).

A large number of theoretical studies have focused on simulating and predicting the tide-induced fluctuation of the beach water table (e.g., Dominick, 1970, 1971 and 1973; Nielson, 1990; Turner *et al.*, 1993; Li *et al.*, 1997; Teo *et al.*, 2003; Jeng *et al.*, 2005a, b). However, only a very small number of previous studies have been supported by field or laboratory data (e.g. Braid *et al.*, 1998; Raubenheimer *et al.*, 1999). The most widely used beach groundwater models is the linearized or nonlinear Boussinesq equation, which is originally derived from Darcy's Law and the continuity equation (e.g., Dominick *et al.*, 1971; Turner *et al.*, 1997; Horn, 2002 & 2006). The use the Boussinesq equation requires a number of assumptions. First, it is assumed that horizontal flow dominates in the beach groundwater oscillations and that vertical flow can be neglected. This is supported by field studies from Baird *et al.* (1998) and Raubenheimer *et al.* (1999). Second, density gradients are assumed negligible, which is comfirmed by the study of Raubenheimer *et al.* (1999). Third, it is assumed that sand drains instantaneously, which has been shown to be a reasonable approximation (Raubenheimer *et al.*, 1999). Finally, it is assumed that the ground water flow in a shallow aquifer can be described using the Dupuit-Forchheimer approximation (Braid *et al.*, 1998). Theoretical studies based on the numerically or analytically solved Boussinesq equation reasonably provide a reasonable approach to represent and interpret the behavior of real beach groundwater table. Numerical simulations always require specifically measured or defined initial and boundary conditions to achieve higher accuracy. However, analytical solutions in most cases have not satisfactorily matched field observed groundwater-table oscillations due to, at least partly, the inaccurate representation of complex oscillations of sea water level, and the presence of a mixture of tidal and wave cycles of a variety of amplitudes

and periods. The relative error of simulation or prediction in general increases with distances landward from shoreline and time length of the simulation (see Baird *et al.*, 1998; Raubenheimer *et al.*, 1999).

Most previous investigations have been conducted on gravel or coarse-grained beaches dominated by semidiurnal tidal cycles. Few if any studies provide substantial information about groundwater dynamics for fine- or very-fine-grained beaches. The purpose of this study is to improve the understanding of groundwater table dynamics in a fine-grained beach dominated by diurnal tides. The Boussinesq equation is solved numerically and tested against field obtained data. The effect of wave setup, that is, expanding the extent of the moving shoreline and elevating the averaged groundwater level, is also incorporated into the solution to enhance model performance.

6.2 Theoretical Background

The Boussinesq equation is most widely used and is commonly believed to be the most efficient approach in describing groundwater table dynamics. Numerical solutions of the equation generally match field data more accurately but require more information in respect to time-dependent boundary conditions and therefore are usually computationally expensive. Conversely, although fairly easier to calculate, analytical solutions usually generate substantial errors due to simplifications and approximations of initial and boundary conditions.

6.2.1 Boussinesq Equation

One-dimensional saturated groundwater flow in an unconfined, homogeneous, isotropic, and incompressible aquifer can be described by the Boussinesq equation (Liu and Wen, 1997) as:

$$\frac{\partial h}{\partial t} = \frac{K}{n_e}\frac{\partial}{\partial x}\left[h(x,t)\frac{\partial h}{\partial x}\right] \qquad \textbf{(6.1)}$$

where h the elevation of the free water surface (water table) above some lower-bounding aquitard (m), t is time (s), K is hydraulic conductivity (m s^{-1}), n_e is specific yield (dimensionless) , x is horizontal distance (m). Equation (6.1) describes transient horizontal saturated water flow. Under the assumption of prevailing hydrostatic conditions, this one-dimensional equation is sufficient to describe shore-normal groundwater flow (Nielsen, 1990). When the magnitude of water fluctuations is small compared with the depth of the aquifer (H_0, see Figure 6.1a), Equation (6.1) may be linearized to give:

$$\frac{\partial h}{\partial t} = \frac{KH_0}{n_e}\frac{\partial^2 h}{\partial x^2} \qquad \textbf{(6.2)}$$

which can be solved analytically with the boundary conditions:

$$h(0,t) = H_0 + \eta_{tide}(t) \qquad x = 0 \qquad \textbf{(6.3a)}$$

$$\frac{\partial h}{\partial t} = \frac{\partial h}{\partial x} \to 0 \qquad x \to \infty \qquad \textbf{(6.3b)}$$

where $\eta_{tide}(t)$ is the elevation change of tide (Figure 6.1a), Equation (6.3a) indicates that the seaward boundary is fixed at x=0 and bouncing up and down with tidal level. Equation (6.3b) indicates that tidal force has no effect on groundwater table at the landward boundary.

When the landward boundary has a prescribed pressure head (H_2 in Figure 6.1a) and it changes over time, Equation (6.2) cannot be solved analytically. Liu and Wen (1997) provided a discretization scheme of centered finite difference space and a fourth order Runga-Kutta integration technique in time to solve the equation (6.2) numerically, which will be used in the present study.

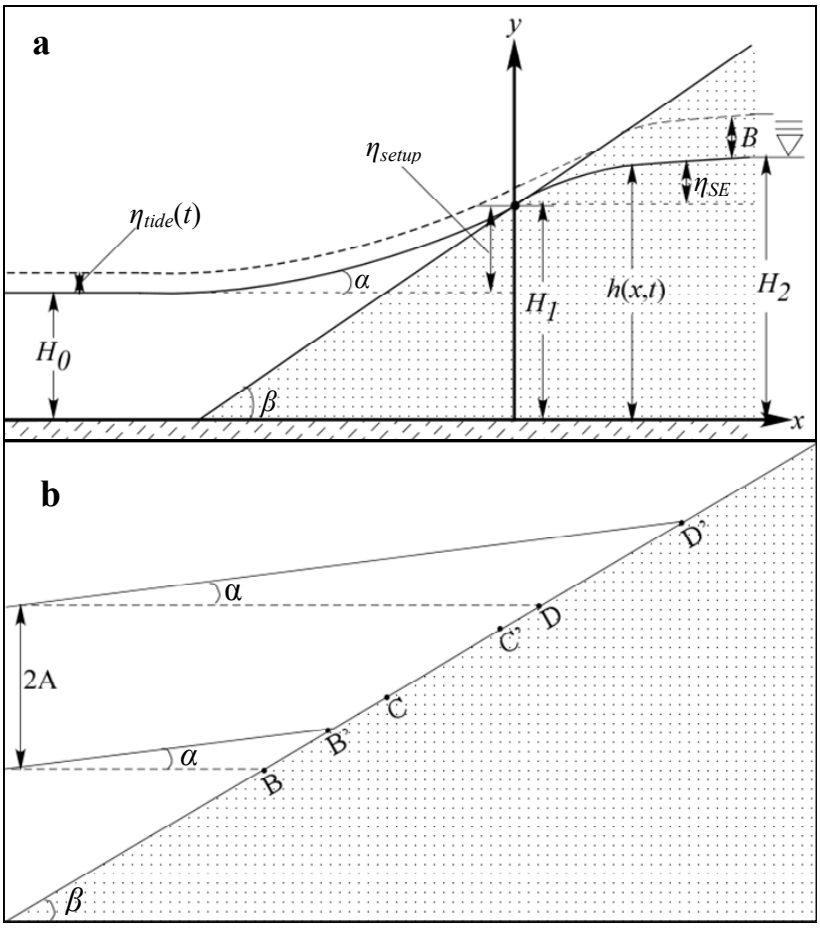

Figure 6.1 Schematic of the effect of sloping beach and wave setup (in (a), $\eta_{tide}(t)$ is the elevation change of tide over time, η_{setup} is the maximum setup height, η_{SE} is the height of superelevation, H_0 is the depth of the aquifer, $H_1 = H_1 + \eta_{setup}$, H_2 is the water table depth of the inland head, α is the setup angle, and β is the slope angle; and in (b), *A* is the amplitude of tidal oscillations, *B*, C and *D* are intersections of beach surface with low, mean and high sea water level (no setup) respectively, B', C' and D' are intersections of beach surface with low, mean and high water level with wave setup.)

6.2.2 The Moving Shoreline and Wave Setup

Equation (6.2) is only valid for the assumption of a vertical beach face, in which x is constant relative to a fixed shoreline. To include the effect of moving shoreline, Li *et al.* (2000) introduced a new variable z as

$$z = x - \frac{\eta_{tide}(t)}{\tan\beta} \tag{6.4}$$

in which β is the slope angle (Figure 6.1a).

Wave setup increases not only the mean water surface in foreshore but also the horizontal range of shoreline (i.e. the seaward boundary of beach groundwater). Figure 6.1b shows that the effect of setup increases the shoreline elevation from *B* to *B'* during low tides, and from *D* to *D'* during high tides respectively. In total, it increases the mean elevation of shoreline from *C* to *C'* and expands the horizontal range of the shoreline from $B - D$ to $B' - D'$. It should be noted that we assume here that tidal level was measured inside of the landward most set-down point (as it was in this study and some previous investigations). Under this assumption, the moving boundary condition of shoreline proposed by Li *et al.* (2000) needs to be further considered because they assumed the moving boundary to be equal to the range of tide oscillation. Assuming the setup height remains constant during the rising and falling of tide, the variable z can be further defined as:

$$z = x - \frac{\eta_{tide}(t)}{\tan\beta - \tan\alpha} \qquad \textbf{(6.5)}$$

in which α is the setup angle, and can be approximated by (see the derivation in Appendix III):

$$\tan\alpha = 0.232\tan\beta \qquad \textbf{(6.6)}$$

and the boundary conditions (Equation 3) can therefore be rewritten as:

$$h(0,t) = H_0 + \eta_{tide}(t) + \eta_{setup} \qquad z = 0 \qquad \textbf{(6.7a)}$$

$$\frac{\partial h}{\partial t} = \frac{\partial h}{\partial z} \to 0 \qquad z \to \infty \qquad \textbf{(6.7b)}$$

Obviously, equation (6.2) is still valid for boundary conditions (equation 6.5 and 6.7) after replacing *x* with *z*. With inclusion of equations (6.5) and (6.7), the numerical solution of Equation (6.2) incorporates the effects of a moving shoreline and wave setup.

6.3 Modeling the Field Data

Figure 6.2 shows the positions of wells, beach profile, average, low and high water level in a cross section of the study site. Beach groundwater systems are usually not only forced by various waves, they are also possibly affected by the fluctuations of inland water head (see Figure 6.1a). In this study, the influence of inland water head is not considered. In the following sections, the spatial characteristics and temporal behaviors of beach groundwater table are documented and modeled numerically.

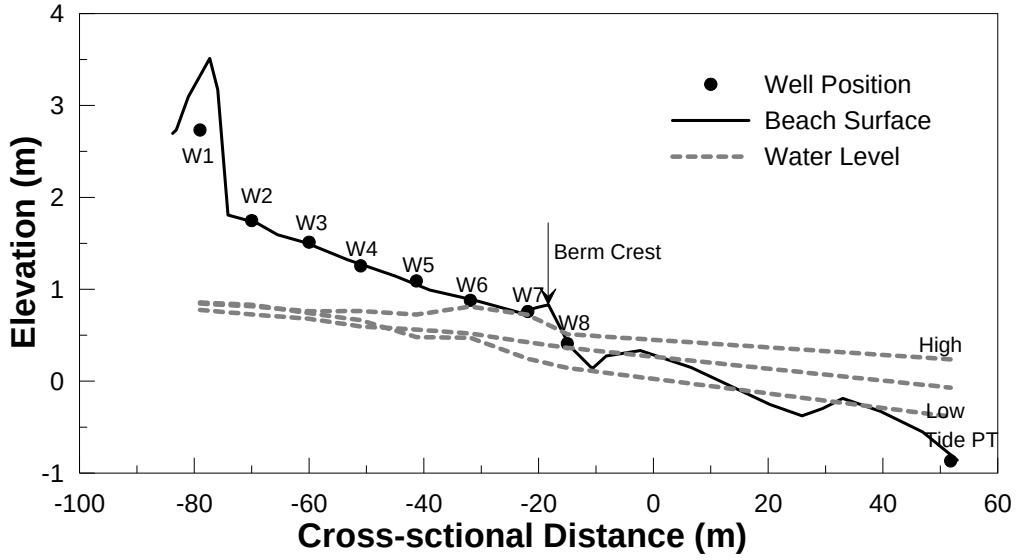

Figure 6.2 Cross-sectional beach profile and instrument deployment

6.3.1 Measured Beach Groundwater Table Fluctuations

The daily average tidal level gently increased during the study period (Figures 6.3 and 6.4). In contrast, the beach ground water experienced substantial drainage, which has been shown in the approximately linear decreasing trend of averaged levels in W1 to W4 (Figure 6.4). This drainage possibly reflects a preceding high water table level associated with a ~1 m high storm surge due to Tropical Storm Emily (see Figure 6.3).

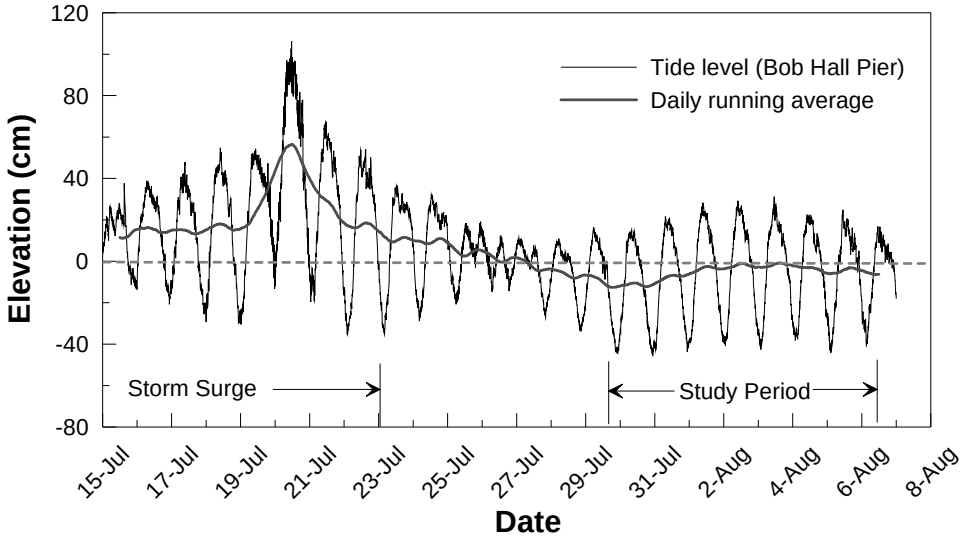

Figure 6.3 Tidal fluctuations in the study site

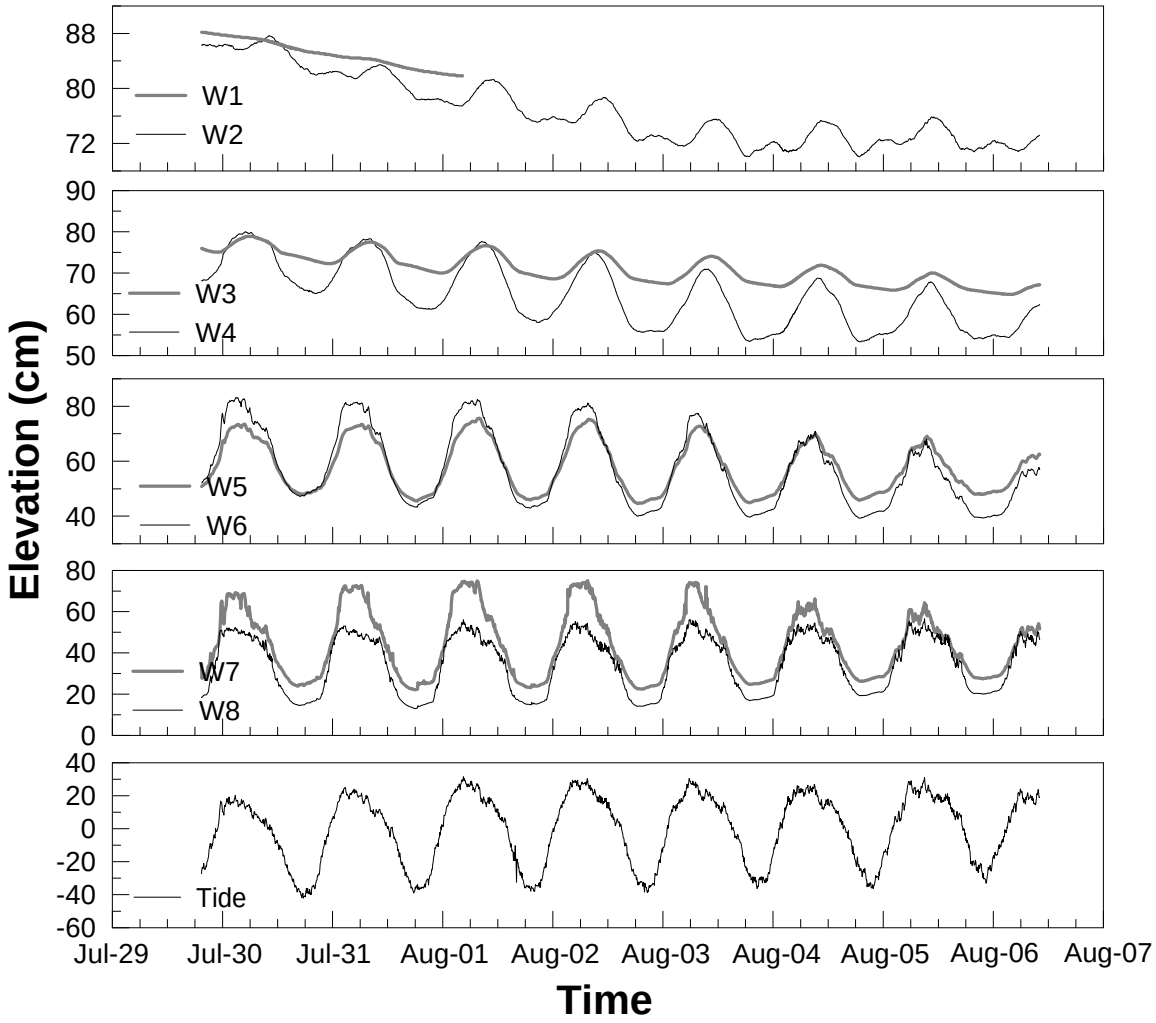

Figure 6.4 Measured groundwater table fluctuations during the study period

Figure 6.4 shows that the measured groundwater table fluctuations corresponded closely with tidal oscillations, as previous authors have reported (e.g., Nielson, 1990; Raubenheimer *et al.*, 1999; Horn *et al.*, 2003). The groundwater table fluctuations forced by tide apparently demonstrated diurnal cyclic changes and those are readily discernable as far as 72 m landward from averaged shoreline (W2). In the landward-most well (W1), which is located approximately 82 m away from shoreline, the tidal signal was almost totally overwhelmed.

6.3.2 Numerical Modeling

Clearly, although the diurnal and higher-frequency signals of tidal oscillations were negligible landward of W1, lower-frequency signals (i.e., the aftermath of the storm surge) still impose substantial influence on groundwater table fluctuations at this distance from the shoreline. In order to include all frequency components in the numerical model, we choose the finite difference scheme suggested by Liu and Wen (1997) to solve the Equation (6.2) in the beach domain, from Tide PT to W2. The iteration procedure in the scheme is limited by a finite difference of 0.01 cm. Time step Δt and cell size Δx used here are set at 6 minutes and one meter respectively to avoid the interference of numerical discretization errors with the dissipation and nonlinearity in the original equation. The observed water table at W2 is selected as the landward boundary, and the seaward boundary (i.e., the shoreline) is determined by Equation (6.7a) alone for the vertical beach domain and equations (6.5) and (6.7a) together for the sloping beach domain. The initial values of each cell are obtained from linear interpolation from observed values in all wells at the beginning of the study period.

Grain-size analyses of samples of surface and subsurface layers indicated that the local sand is well-sorted and its composition does not vary significantly from shoreline to dune toe (Figure 3.3) or from the surface to a depth of 0.5m. Thus, homogeneity of the beach materials

reasonably can be assumed. Since no directly measurement of saturated hydraulic conductivity was obtained, it is estimated using the equation proposed by Alyamani and Sen (1993) as

$$K = 1300\left[I_0 + 0.025(d_{50} - d_{10})\right]^2 \quad \textbf{(6.8)}$$

where K is in m/day, I_0 is the smallest grain size (0.074 mm for local sand of this study area), d_{10} is Hazen's effective grain size in mm, relative to which 10% of the sample is finer, and d_{50} is the median of grain size. The value of K for this site was found to be is 0.0084 cm s^{-1} by equation (6.8). The effective porosity is 0.28, determined by continuous measurements of surface moisture content on the inter-tidal zone. Since the study site located at a barrier island composed mostly of sand, the depth of aquifer H_0 is arbitrarily set at 3 meters (Simulation results vary slightly with different aquifer depths).

Numerically simulated groundwater table fluctuations have been plotted in Figure 6.5 and Figure 6.6 with assumptions of vertical beach and slope beach respectively. Both simulation approaches agree with observed data quite well in terms of amplitude damping with distance landwards and phase lag. In detail, both approaches underestimated groundwater table fluctuations and generated large discrepancies during high tides as high as ~20 cm (W7), particularly for the first five tidal cycles. The discrepancy can possibly be attributed to swash over topping the berm crest during high tide and hence extra infiltration from the transitional ponded surface between the berm crest and W6, which has not been incorporated in the model used in this study. Although the linear Boussinesq equation can easily be expanded for additional water sources (Li *et al.*, 1997), this phenomenon is neither easily described mathematically nor readily monitored because of the complex relationship between hydrodynamics and the morphologic evolution of inter-tidal zone.

In comparison, the simulations with a sloping beach perform better than those with a vertical beach as expected. This is very apparent in comparing simulations as of lower tidal elevations, which provide a good fit for the sloping beach approach but consistently underpredict for the vertical sloping beach. The sloping beach introduced extra nonlinearity in groundwater table fluctuations by changing the distance from the shoreline (x), resulting in higher damping rate during low tides and lower damping rate during high tides. However, this effect decreases in the course of wave propagation.

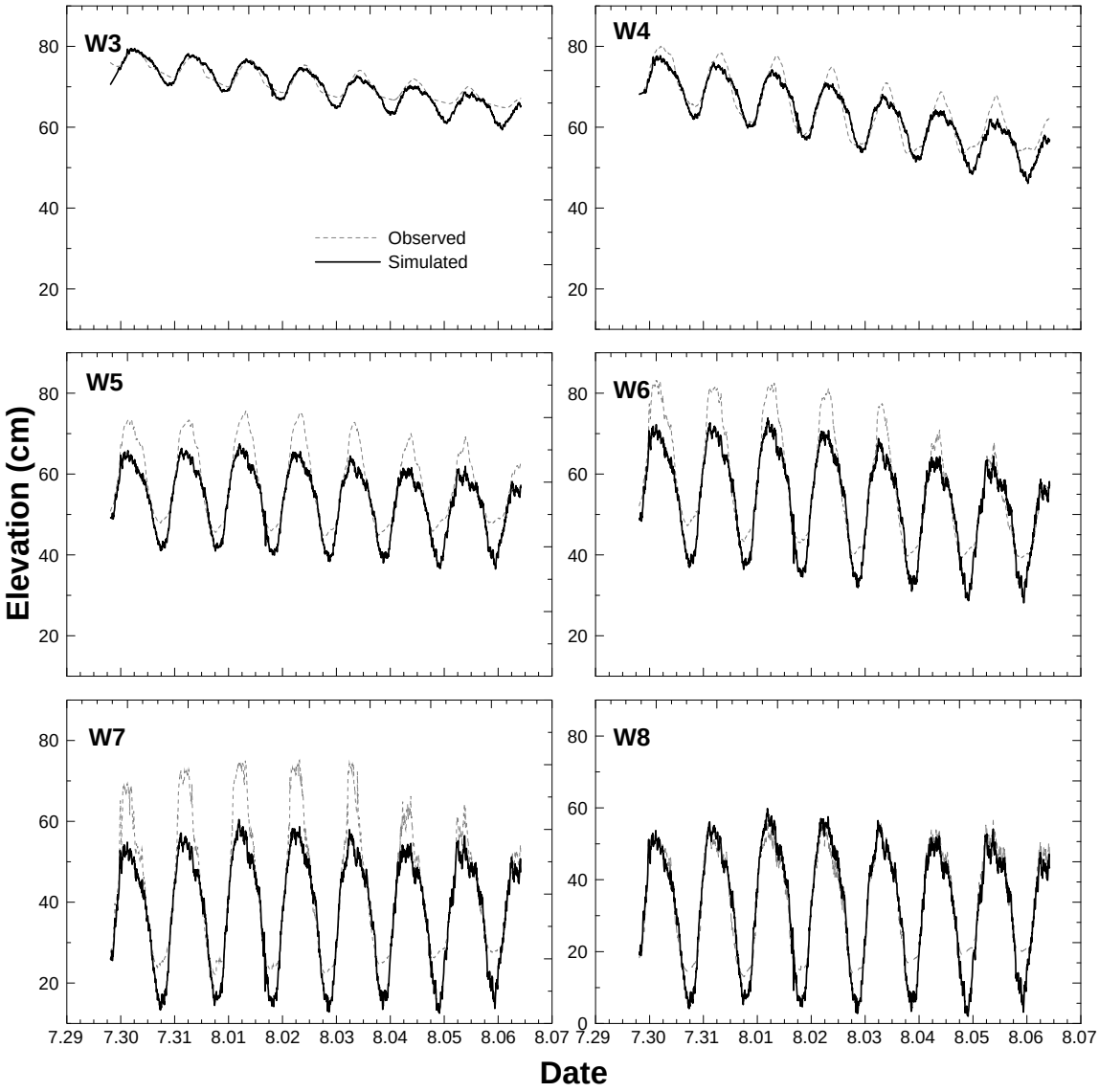

Figure 6.5 Observed vs. numerically simulated groundwater fluctuations with the assumption of vertical beach (thick dark line- simulated, thin grey line-observed)

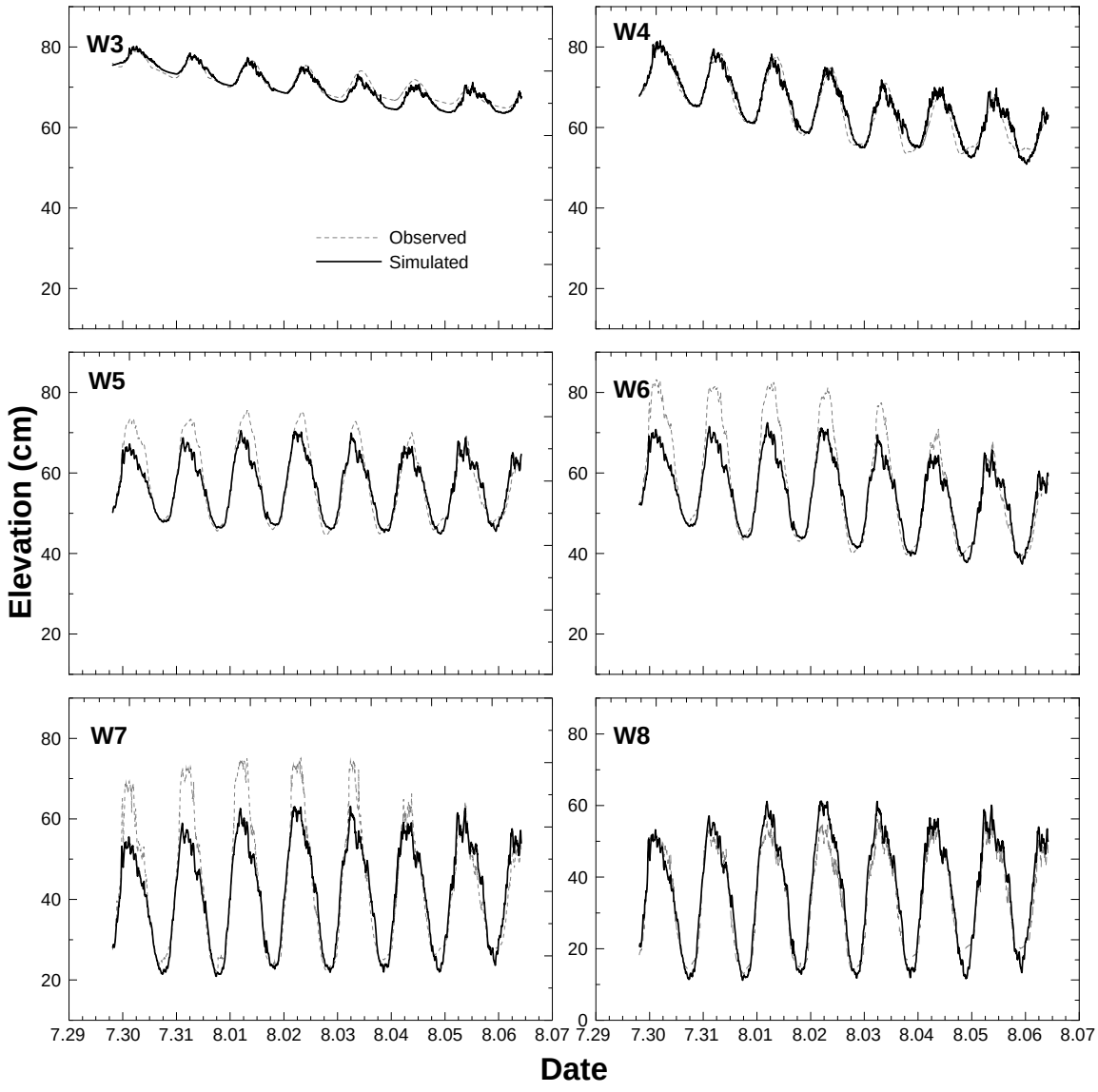

Figure 6.6 Same as Figure 6.5 except with the assumption of sloping beach

Statistically, mean absolute error (MAE) and root mean square error (RMSE) (see definitions and calculations in Chapter 5) are 10.5 and 0.77 cm for the vertical beach approach, and are 5.3 and 0.39 cm for the sloping beach approach, respectively. This indicates that the simulations adopting the sloping beach assumption are significantly better than those adopting the vertical beach assumption in terms of overall accuracy, as showed by visual examination. Again, substantial errors exist in both approaches imply some other processes must be counted.

6.4 Discussion

Tidal oscillations can be described by a range of waves of various periods and amplitudes as:

$$\eta_{tide}(t) = \sum_{1}^{N} A_i \cos(\omega_i t - \delta_i) \quad \textbf{(6.9)}$$

where A_i is the tidal amplitude, ω_i (equals to 2π divided by tide period) is the angular velocity of the tide, and δ_i is the phase difference of the *i*th frequency component of tidal oscillations. Although various tidal cycles together tend to generate additional harmonics in the course of propagation in a sloping beach system (Li *et al.*, 2000), all frequency components act as free waves in the course of propagation, particular for flat beach with relatively large H_0, which was supported by the field work of Raubenheimer *et al.* (1999). The standard solution of equation (6.2) expanding for mixed tide is given by

$$h(x,t) = H_0 + \eta_{setup} + \sum_{1}^{N} A_i e^{-k_{Ri} z} \cos(\omega t - k_{Ii} z - \delta_i) \quad \textbf{(6.10)}$$

where k_{Ri} and k_{Ii} are the real and imaginary parts of the wave number *k*, which represent damping rate and phase lag respectively, are defined by

$$k_R = k_I = k = \sqrt{\frac{n_e \omega}{2KH_0}} \quad \textbf{(6.11)}$$

The wave number *k* (equation 6.11), which is mainly determined by effective porosity n_e, hydraulic conductivity (*K*), and the depth of the effective layer below the MSL and above the impermeable bed (H_0), is generally assumed by most modelers to be a constant thus allowing analytical solutions of the linearized Boussinesq equation (Nielson, 1990; Li *et al.*, 2000 and 2006). The constant wave number leads to landward exponentially increasing damping rates and linearly increasing phase lags of groundwater table oscillations in the landward direction (e.g.,

Jeng *et al.*, 2005a, b). Although k_R and k_I are usually treated as constant and equal to k in most analytical solutions, field evidence indicate that k_R is considerably larger than k_I, possibly due to variable aquifer depth (e.g., Raubenehimer *et al.*, 1999), as well as the effect of capillary fringe (e.g., Barry *et al.*, 1996). Further, Baird *et al.* (1998), Raubenheimer *et al.* (1999) and Horn *et al.* (2003) have reported that the damping rate and phase lags between tide and groundwater table fluctuations are not linearly proportional to the distance from shoreline. The field study of Li *et al.* (2006) also indicated that the simulated groundwater tables are very sensitive to K/n_e and a constant K/n_e usually causes overestimation or underestimation. It is clear that a constant k is not sufficient to accurately predict phase change and damping rate of amplitude.

In this study, although beach materials are highly uniform and the depth of aquifer is at least one order of magnitude larger than the amplitude of tide oscillations (sufficiently to meet the requirement for linearization of the Bounessiq equation), the real damping rates seems not able to be described accurately by any exponential equations. Figure 6.7a shows amplitudes of three major constituent periodicities in measured tidal and groundwater table oscillations. It should be noted that the y axis in Figure 6.7a is logarithmic, which means linear trends in the figure imply exponential trends in regular units. Clearly, the dominant harmonic ($f = 0.039$, T=25.6 hrs and ω=0.245 rad hr^{-1}) damped landward more linearly than exponentially, at least from W7 (x=22 m) to W3 (x=60 m), which indicates that the real part of wave number k_R is not a constant for the dominant harmonic $f = 0.039$. However, the amplitudes rate of the other two constituents (T=12.0, 8.2 hr and ω = 0.524, 0.766 rad hr^{-1} respectively) approximately follow the

exponentially decreasing trend in landward direction. This implies that special attention should be taken in simulating the lower frequency tidal signals.

Figure 6.7b shows the phase lag of the major tidal signal. Apparently, the phase lag increase nonlinearly landward, which implies that the imaginary part of wave number k_I is not constant but nonlinearly increases in landward direction. This confirms the landward increasing trend of the real part of k as discussed above.

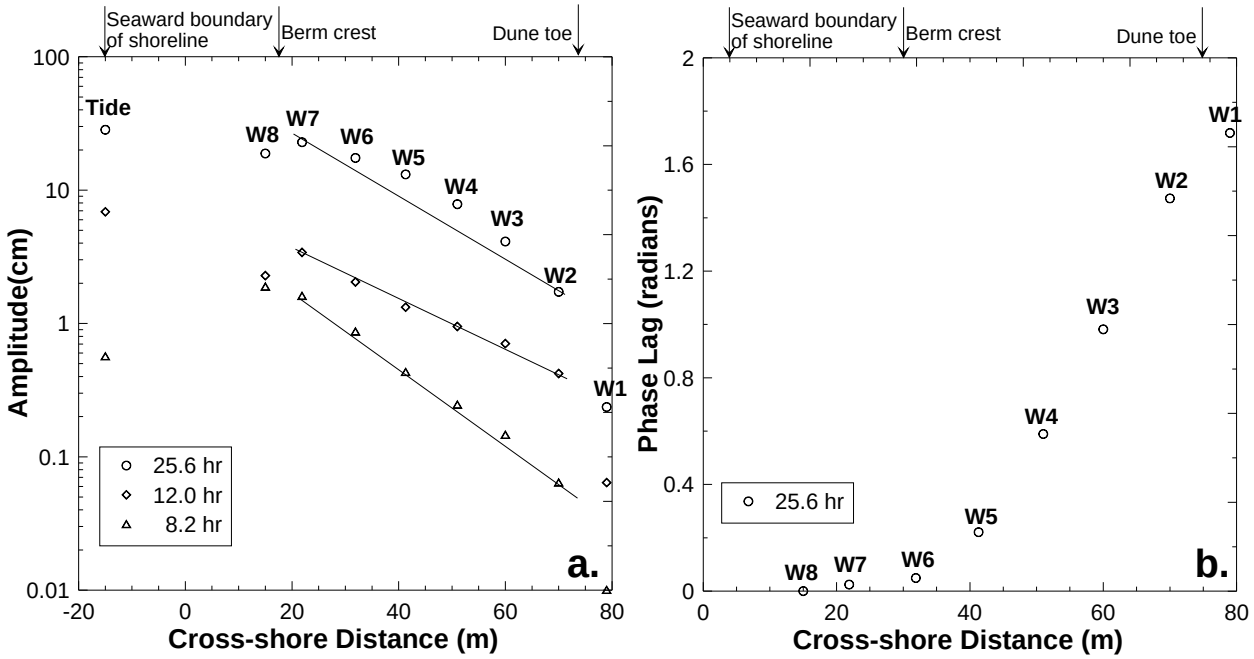

Figure 6.7 Amplitudes (a.) and phase lag (b.) of three major harmonics in observed tide and groundwater table oscillations

Many previous studies have found that k_R is usually larger than k_I, and attributed this to the effect capillary fringe or intermediate-depth aquifer (e.g., Raubenehimer *et al.*, 1999). The gravimetric means of k_R and k_I for the dominant tidal component ($f = 0.039$) is 0.023 and 0.019 respectively. However, no study to date has reported a landward increasing wave number as found in this study (Figure 6.7b). Since the three controlling factors effective porosity and saturated hydraulic are indirectly determined and the aquifer depth is set arbitrarily, no safe conclusion can be drawn to explain the unusual landward increasing trend of and phase lag.

However, speculating in the processes involved in the course of landward wave propagating, this unusual trend is possibly related to the sloped beach groundwater table (the average groundwater table at this beach has a slope roughly equal to the setup angle).

6.5 Conclusions

The beach groundwater table is one of important parameters controlling beach morphological development. The behavior of beach groundwater table can be affected by wave set-up and tidal oscillations, as well as dynamic swash.

The experimental study presented here shows that, beach water table elevations corresponded with tidal fluctuations closely as expected. The amplitudes of beach water table oscillations decreased, and the time lag between water table and tide fluctuations increased, with landward distance from the shoreline. Diurnal and higher frequency tidal signals are indiscernible at ~80 m landward from the averaged shoreline at this study site, but lower frequency sea level oscillations (storm surge) propagate further inland (Figure 6.3).

Beach slope introduces a nonlinear effect to beach groundwater table fluctuations as many researchers have presumed. Wave setup considerably increases the lower boundary of beach water table and introduces additional non-linear effects. The elevation average of the beach groundwater table was significantly affected by prior conditions of sea water level and was found to increase proportionally with landward distance.

Both numerical solutions of the linearized Boussinesq equation based on concepts of vertical beach and sloping beach matched field observed data reasonably well. The sloping-beach solution performs substantially better, particularly during low tides.

Spectral analysis of the field-obtained data indicated that the wave number k, the key parameter in analytical solutions of the Boussinesq equation, is not a constant as many

researchers have presumed. Further investigations are necessary to explain the landward increasing trend in the wave number, particularly for the lower frequency periodicities.

It should be noted these findings may valid only for relative fine-grained beach with low energy input. For coarser-grained beach, the damping rate and phase change of tidal signals can be simulated using analytical solutions as reported by previous investigators. For higher-energy beaches, swash-induced additional infiltration may dominate the groundwater table fluctuations. The accuracy of model simulations may therefore decrease dramatically.

CHAPTER 7 MODELING SPATIAL AND TEMPORAL VARIABILITY IN SURFACE MOISTURE CONTENT

This chapter primarily focuses on simulating diurnal variations in the surface moisture content across the beach. As presented in the previous chapters, beach surface moisture content exhibits high spatial and temporal variability at shore time (hours) and small space (meters) scales. Groundwater table fluctuations through capillary rise and the evaporation-condensation alternation are the two key processes controlling this high variability. In the present study, models that describes evaporation, tide-induced groundwater table fluctuations, and soil water retention characteristics are therefore combined and coupled together to develop a realistic approach to represent this high variability.

7.1 Introduction

Spatial and temporal variations in surface moisture content are of scientific interest as well as of practical importance, and is receiving increasing attention recently from workers in a variety of research areas including hydrology, meteorology, ecology, biology and geomorphology (e.g., Beljaars et al., 1996; Bosilovich and Sun, 1998; Oliveira, 2001; Olyphant, 2003; Chen and Hu, 2004). Of particular concern for the present study, surface moisture has long been cited as an important regulator of aeolian sediment transport (e.g., Chepil, 1956; Belly, 1969; Namikas and Sherman, 1995; Wiggs *et al.*, 2004). Recent studies on instantaneous aeolian sediment transport have shown that a better understanding of the effect of soil moisture content on transport thresholds requires new approaches to comprehensively evaluate and document the spatial and temporal variability in surface moisture in natural environments (Cornelis and Gabriels, 2003). Although a small number of field investigations have provided limited data sets

regarding surface moisture content at various beaches (e.g., Sarre, 1988; McKenna Neuman and Nickling, 1989; Jackson and Nordstrom, 1998; Sherman *et al.*, 1998; Wiggs *et al.*, 2004; Davidson-Arnott and Yang, 2005), no study to date has reported a practical way to represent or simulate the high degree of spatial and temporal variability that characterizes the surface moisture content of real beaches. The inability to represent this variability in a realistic manner is one of the most challenging problems faced in the development of aeolian sediment transport models.

Variations in beach moisture content are the net result of water inputs and outputs including precipitation, evapotranspiration, condensation, wave swash, and groundwater uplift by capillary forces (Namikas and Sherman, 1995; Chen and Hu, 2004; Maxwell and Miller, 2005). Sophisticated computational models are available to predict the movement of water through the unsaturated zone (Ruan and Illangasekare, 1999). Numerous studies based on the combination of unsaturated Richards equation and water retention curve have found that it provides a reasonable basis to numerically or analytically determine the moisture content within a soil body under various conditions. Results of such studies are quite good if water inputs and outputs listed above are either constant or can be described by simple functions (e.g., Suleiman and Ritchie, 2003; Yuan and Lu, 2005). For example, traditional groundwater models often have simplified upper boundary conditions and water fluxes related to infiltration and evapotranspiration (e.g., Charbeneau, 2000; Nachabe, 2002). These fluxes are often uncoupled and may be averaged over time and space, however, very likely missing key dynamics of important land surface processes (Maxwell and Miller, 2005). The problem becomes more difficult for a natural environment like a beach as such fluxes are rarely constant. Rather, they can exhibit large variability over short temporal scales (minutes to hours) and small spatial scales

(meters), which is usually not amenable to simple descriptions or representations (Yang and Davidson-Arnott, 2005). To incorporate the dynamics of the lower boundary, sufficient groundwater models have been developed separately in the previous chapter and further coupled with the evaporation model in this study.

Surface moisture and meteorological phenomena mutually influence one another at various scales of time and space. Evaporation, for example, decreases soil surface moisture content which in turn reduces the rate of real evaporation from the soil surface (Entekhabi *et al.*, 1996). A large number of land surface models have been developed that include consideration of vegetation, surface resistance and snow schemes to calculate spatial and temporal variations in momentum, heat and moisture fluxes with the lower atmosphere (e.g., Sellers *et al*., 1986; Dickinson, 1988; Maxwell and Miller, 2005). However, most previous studies of evaporation have treated surface moisture as constant in time and space for the sake of simplification (e.g., Davies and Allen, 1973; Barton, 1979; Ăcs *et al.*, 1991). Most land surface models to date have a parmeterization at the bottom layer that is user-specified as either a constant or a uniform moisture gradient, and with no attempt to incorporate the influence of groundwater (Chen and Hu, 2004). This study represents a significant advance in the treatment of surface moisture in that it consider dynamics of evaporation and groundwater table oscillations together.

For beaches composed of well-sorted fine sand, groundwater table fluctuations correspond closely to oscillations in sea level such as the tides (e.g., Neilson, 1990; Turner *et al.*, 1997; Raubenheimer and Guza, 1999). Thus, moisture content within the sand matrix and at the surface should vary in accordance with changes in water table elevation (Atherton *et al.*, 2001). Assuming strong enough capillary rise, no hysterisis, horizontal water flow, and no evaporation, surface moisture content can be predicted easily and accurately based on knowledge of i) the

hydraulic characteristics of the sand, ii) the elevation of beach surface, and iii) the water table elevation. However, evaporation rates can be high on a real beach and may exert a significant influence on surface moisture content.

The beach "surface" (i.e., 1-2 cm) represents the interface between the atmosphere and soil system. Changes in surface moisture content resulted from the dynamic interaction between evaporation and unsaturated flow from subsurface layers. However, these dynamics are complex and not well understood, and a satisfactory scheme to model variations in surface moisture content is not yet available. In light of this lack, the objectives of the present study are to: 1) investigate the interrelationship among evaporation, groundwater fluctuations and soil moisture content, and 2) establish mathematical models to simulate and predict the spatial and temporal variations of surface moisture content in a fine-grained beach.

7.2 Model Derivation

Studies of water table fluctuations in relation to the tide, and of evaporation rates from the beach surface, have been developed and presented in the preceding chapters. In this chapter, the problem of moisture transport in the unsaturated zone, from the groundwater table to the surface layer, will be addressed.

7.2.1 The Richard's Equation (RE)

In a homogeneous soil, one-dimensional, isothermal and unsaturated water flow with sources can be described by the Richard's equation (e.g., Yuan and Lu, 2005):

$$C(\psi)\frac{\partial \psi}{\partial t} = \frac{\partial}{\partial z}\left[K(\psi)\left(\frac{\partial \psi}{\partial z} - 1\right)\right] - S \qquad \textbf{(7.1)}$$

with initial and boundary conditions:

$$\psi(z,0) = \psi_0(z) \tag{7.2}$$

$$\psi(0,t) = \psi_s \tag{7.3}$$

$$K(\psi)\left(\frac{\partial\psi}{\partial z} - 1\right) = q(t) \tag{7.4}$$

where ψ is the pressure head (L), $C(\psi) = d\theta/d\psi$ is the differential water capacity (T^{-1}), $K(\psi)$ is the unsaturated hydraulic conductivity function, θ is the volumetric moisture content of the surface layer (L^3L^{-3}), z is the vertical coordinate upward from water table (L), t is the time (T), S is water sources and sinks(LT^{-1}), ψ_s is the prescribed pressure head (L), and $q(t)$ is the water flux at z.

For a surface layer of depth d_1, for z a flux-conservative equation can be obtained by integrating Equation (7.1):

$$d_1 \frac{\partial\theta}{\partial t} = \int_{z_0 - d_1}^{z_0} \left\{ \frac{\partial}{\partial z}\left[K(\psi)\left(\frac{\partial\psi}{\partial z} + 1\right)\right] - S \right\} dz = \frac{1}{\rho_w}(P - E_g - Q) \tag{7.5}$$

with boundary conditions:

$$K(\psi)\left(\frac{\partial\psi}{\partial z} - 1\right)\Bigg|_{z=z_0} = 0 \tag{7.6}$$

$$K(\psi)\left(\frac{\partial\psi}{\partial z} - 1\right)\Bigg|_{z=z_0-d_1} = \frac{Q}{\rho_w} \tag{7.7}$$

$$\int_{z_0-d_1}^{z_0} S dz = \frac{P - E_g}{\rho_w} \tag{7.8}$$

where d_1 is the depth of the surface layer (L); P is the precipitation (LT^{-1}); Q is the water flux between the surface layer and subsurface layer (LT^{-1}); E_g is the rate of soil surface evaporation (LT^{-1}); and ρ_w is the density of water. Equation (7.5), also called the bucket model (Kondo *et*

al., 1992), implies simply that soil water content at any point in time results from the difference between inputs and outputs of water (Wythers *et al*., 1999).

Assuming that the moisture content of the lower boundary of the surface layer is affected only by capillary rise, we obtain:

$$\psi\big|_{z=z_0} = \psi(\theta_i) \tag{7.9}$$

$$\psi\big|_{z=z_0-d_1} = -(z_0 - d_1) \tag{7.10}$$

Eq. (7.7) can therefore be approximated by:

$$\begin{aligned} Q &= K(\psi)\left(\frac{\partial\psi}{\partial z} - 1\right)\Bigg|_{z=z_0-d_1} \\ &= \left[\frac{K(\theta_i) + K\left[-(z_0 - d_1)\right]}{2}\right]\left[\frac{\psi(\theta_i) + (z_0 - d_1)}{d_1} - 1\right] \end{aligned} \tag{7.11}$$

7.2.2 Force-restore Method (FRM)

It is worthwhile to investigate use of more simplified soil parameterizations, in the interest of computational efficiency. The force-restore method (Deardorff, 1977, 1978), which was originally developed for a simple prediction of surface temperature, has been widely used as a model for predicting soil moisture (e.g., Yee, 1988; Noilhan and Planton, 1989; Dickinson, 1988; Savijarvi, 1992; Kondo and Saigusa, 1992; Bosilovich and Sun, 1995, 1998; Pellenq *et al.*, 2003). Although the movement of water is strongly affected by soil hydraulic properties and some uncertainty may be introduced as the moisture content approaches zero (which are not considered in FRM), the force-restore method is still promising as a simple method for prediction of surface moisture content, as Bosilovich and Sun (1998) recommended. The basic relationships of the force-restore method are:

$$\begin{cases} \dfrac{\partial \theta_i}{\partial t} = C_1 \dfrac{E_g - P}{\rho_w D} - C_2 \dfrac{\theta_i - \theta_b}{\tau} \\ \dfrac{\partial \theta_b}{\partial t} = -\dfrac{E - P}{\rho_w d_2} \end{cases} \quad \textbf{(7.12)}$$

in which the last two terms on the right-hand side of the first expression in Equation (7.12) are the force term (net fluxes of water between the soil and atmosphere) and restore term (net fluxes of water between surface soil layer and the subsurface soil layer) respectively; θ_i is volumetric moisture content (L^3L^{-3}) of the surface layer at time t (T); $D = d_1/10$ is an arbitrary normalization depth of 10 centimeters (L); θ_b is mean volumetric moisture content (L^3L^{-3}) of the layer 0-50cm; d_2 is the depth of the bulk layer (L); C_1 is a function of θ_i and C_2 is a constant set at 0.9 (dimensionless); and τ is diurnal period (T). The linear function derived by Deardorff (1978) for C_1 is

$$C_1 = \begin{cases} 0.5 & \theta_g \geq \theta_{fc} \\ 14 - 16.875\left(\dfrac{\theta_i}{\theta_{fc}} - 0.2\right) & \theta_{fc} > \theta_g > 0.2\theta_{fc} \\ 14 & \theta_g \leq 0.2\theta_{fc} \end{cases} \quad \textbf{(7.13)}$$

in which θ_{fc} is the field capacity (L^3L^{-3}), in which θ_s is the saturated water content (L^3L^{-3}).

7.2.3 Evaporation from Soil

The process of evaporation from soil is a function of soil and atmospheric parameters such as surface moisture, vapor pressure, temperature gradients, radiation flux and air turbulence at the soil-atmosphere interface (van de Griend and Owe, 1994). Evaporation from bare soil can be estimated by a simple linear equation (Mahfouf and Noilhan, 1991, citation therein) as

$$E_g = (1 - \sigma_v)\beta E_p \quad \textbf{(7.14)}$$

in which σ_v is the fraction of vegetation cover (dimensionless, equal to 0 for bare soil), E_p is the potential evaporation (LT^{-1}), and β the moisture availability (dimensionless), given as

$$\beta = \begin{cases} \dfrac{\theta_i - \theta_r}{\theta_{fc} - \theta_r}, \theta_0 < \theta_{fc} \\ 1 \qquad\quad , \theta_0 \geq \theta_{fc} \end{cases} \tag{7.15}$$

Details of the calculation of potential evaporation can be found in Chapter 5.

7.3 Methodology and Data

Solar radiation, wind speed, air temperature and relative humidity measurements are utilized in this chapter for evaporation estimation (see Chapter 5). Although groundwater table fluctuations can be predicted based on tidal oscillations (Chapter 6), field data of groundwater table are used directly here. It is worth noting that the direct usage of the field measurements of the groundwater table fluctuation in this study simplifies the computations (much fewer models involved) but not affects the simulation accuracy. Results of grain size analyses are employed to estimate hydraulic conductivity of local sand. See Section 3.2 for details of measurement procedures for all parameters involved.

7.4 Forward Simulation of Surface Moisture Variations

7.4.1 Water Retention Curve and Hydraulic Conductivity

The soil water retention curve, which describes the relation between matric potential and moisture content within a vertical soil profile, provides a simple but efficient way to estimate the soil moisture distribution under steady state. Although a number of models have been developed, the analytical form of the soil hydraulic function proposed by Van Genuchten (1980) is generally

thought to match experimental data more satisfactorily than others (Stankovich and Lockington, 1995; Cornelis *et al.*, 2001). It is expressed as:

$$\Theta = \frac{\theta - \theta_r}{\theta_s - \theta_r} = \left[1 + |\alpha\psi|^n\right]^{-m} \quad \textbf{(7.16)}$$

$$K(\Theta) = K_s \Theta^{\lambda}\left[1 - (1 - \Theta^{1/m})^m\right]^2 \quad \textbf{(7.17)}$$

in which the volumetric water content θ (L^3 L^{-3}) is normalized into the dimensionless water content Θ, that is, the effective saturation (Ruan and Illangasekare, 1999); θ_r is the residual value of volumetric water content (L^3 L^{-3}), α, n are estimated parameter values (dimensionless); $m = 1 - 1/n$ (dimensionless); and $\lambda = 0.5$ is curve shape parameter(dimensionless). Figure 7.1 shows the fitted water retention curve and predicted hydraulic conductivity Padre Island beach sand, in which $\theta_s = 0.443\ \text{cm}^3\text{cm}^{-3}$, $\theta_r = 0.018\ \text{cm}^3\text{cm}^{-3}$, $\alpha = 0.0218$, and $n = 5.701$.

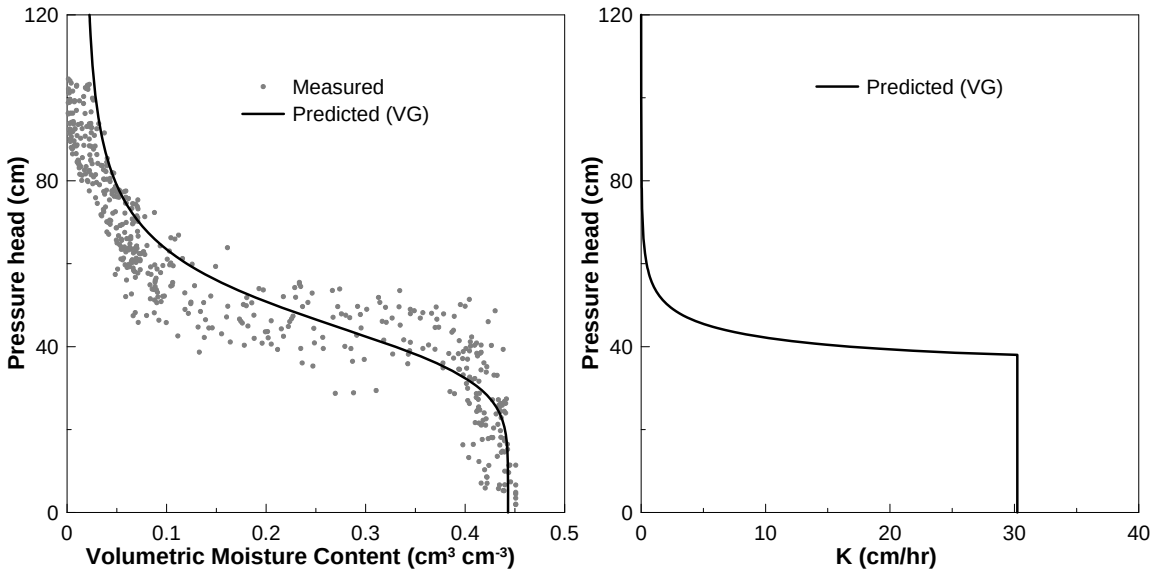

Figure 7.1 Fitted soil water retention curve and predicted hydraulic conductivity using the Van Genuchten (1980) model

Saturated hydraulic conductivity was estimated from the expression proposed by Alyamani and Sen (1993):

$$K_s = 1300\left[I_0 + 0.025(d_{50} - d_{10})\right]^2 \quad \textbf{(7.18)}$$

where K_s is saturated hydraulic conductivity (L T^{-1}), I_0 is smallest grain size (L, 0.074 mm for local sand of this study area), d_{10} and d_{50} are 10th and 50th percentile grain sizes respectively (all determined by graphical method). According to grain-size analyses of local sand samples, K_s has a value of 0.0084 cm s^{-1}. Unsaturated hydraulic conductivities calculated from Equation (7.17) are shown in the right-hand side of Figure 7.1.

7.4.2 Modeling Variations in Surface Moisture Content

7.4.2.1 Comparison of the RE and FRM

Ignoring the effect of hysterisis, and assuming steady-state at each time point, we can calculate the volumetric moisture content and hydraulic conductivity of the lower boundary of the "surface" layer using Equation (7.10), (7.16) and (7.17), given the water table depth (z_0). We designate the depth of the surface layer d_1 as 1.4 cm (in accordance with the depth of "surface" moisture content measurements collected in this study). Equation (7.5), derived from the RE, can then be numerically solved using finite-difference approximation within the explicit scheme of Forward Time Centered Space representation (Press *et al.*, 1988) with boundary conditions given in Equations (7.6)-(7.10) and input of simulated soil evaporation rates.

For comparison with the RE approach, we also simulate the variation of surface moisture content by the FRM method, using Equations (7.12) along with (7.13)-(7.16). For a soil matrix with a slowly fluctuating shallow water table, it is reasonable to assume that the mean bulk moisture content θ_b is affected only by capillary rise, so that θ_b can be approximated and calculated by:

$$\theta_b = \frac{1}{d_2} \int_{z_0 - d_2}^{z_0} \theta(z) dz \qquad \textbf{(7.19)}$$

in which the depth of the bulk layer d_2 is set as 50 cm following previous studies (e.g. Deardorff, 1977, 1978; Noilhan and Planton, 1989; Kondo and Saigusa, 1992; Bosilovich and Sun, 1995, 1998; Pellenq *et al.*, 2003).

Figure 7.2 plots simulated equilibrium surface moisture contents predicted by the RE and FRM approaches with various constant evaporation and steady water table. It is clear that evaporation process exert an influence only when moisture content is in the low range. For the RE, the critical surface moisture contents (below which evaporation begins to impose influences) are about 0.04 and 0.07 for potential evaporation rates of 8 cm/d and 21 cm/d, respectively, which occurs when the water table is at the depth of about 70 cm and 90 cm from the surface. When surface moisture content exceeds these thresholds, it is affected only by groundwater fluctuations. For reference, typical daily maximum and average evaporation rates were around 21 and 8.5 cm/d. For the FRM, similar, the thresholds also exist for the effectiveness of evaporation. They are about at 0.05 and 0.11 respectively. However, FRM simulations exhibit poor behavior near in the saturation end: a dramatic increase in the influence of evaporation (Figure 7.2). This is essentially an artifact of the model and does not reflect the result. With surface moisture contents close to saturation, the restore term of the FRM actually decreases with surface moisture content. This occurs due to the decrease in the difference between surface moisture content and mean bulk moisture content (equation 7.12), while the force term remains constantly equal to potential evaporation as atmospheric demand for vaporization is fully reached. This implies that the FRM is very likely to underestimate surface moisture content and is not be appropriate for use in regions with a shallow water table and high water content.

When compared to the field measurements of surface moisture content, the FRM simulations is nearly as strong as the numerically solved RE from a statistical standpoint. The

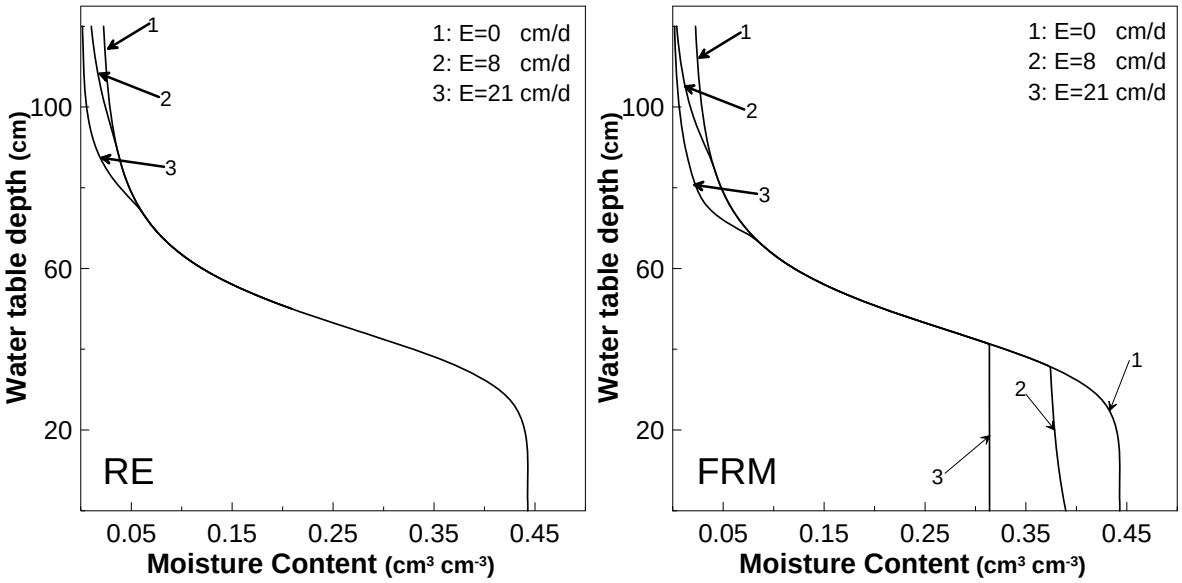

Figure 7.2 Simulated equilibrium surface moisture content by the RE and FRM with steady water table and various steady potential evaporation rates

coefficients of determination (R^2) for simulations by the RE and FRM are 0.92 and 0.90, and the Residual Mean Squares (RMS) are 0.0021 and 0.0022 respectively (Figure 7.3). However, as previously mentioned, the FRM substantially underestimates surface moisture contents close to saturation. Because of this weakness, it was not considered worthwhile to pursue the use of FRM any further.

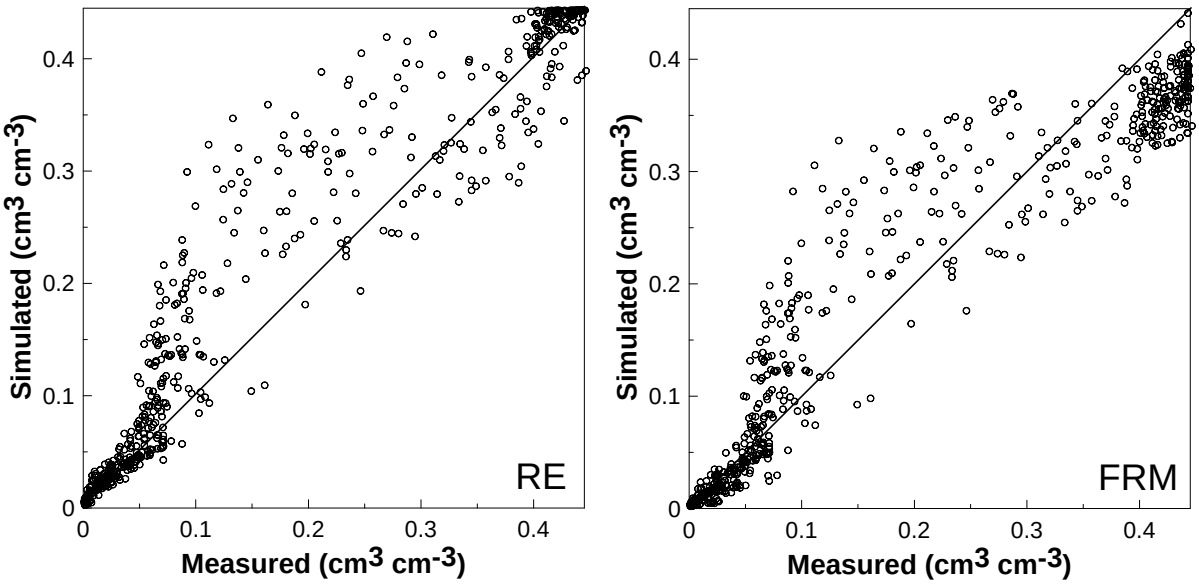

Figure 7.3 Measured vs. simulated surface moisture content by the RE and FRM

7.4.2.2 Simulations of Moisture Content Time Series by the RE

To assess the details of model simulation, simulated time series of the averaged surface moisture content at Lines 1-12 are plotted in Figure 7.4. The numerically solved RE successfully captured the diurnal signals of surface moisture variation in terms of cyclic phase change. Some obvious discrepancies can be identified between measured and simulated moisture content, particularly in the first three days of the study period.

The simulations indicate that the evaporation dominates surface moisture variations in lines close to the dune toe (Line1-Line3), where the beach surface is relatively dry. In this zone, the evaporation induced daily changes of up to 0.04 cm^3cm^{-3}, close to field measurements of Kim (2002), Yang and Davidson-Arnott (2005), and this study. In contrast, groundwater table oscillations only generated content change of ~0.01 cm^3cm^{-3} (see the simulations with and without consideration of evaporation). Water-table-induced fluctuations are dominant for all other lines (the simulations with and without evaporation are overlapped), approximately generating surface moisture variations as much as an order of magnitude up to 0.3 cm^3cm^{-3} each day. Maximum daily changes in surface moisture content were found in midbeach (Line 6 and 7) as Yang and Davidson-Arnott (2005) observed.

The reasonable match between observed and simulated surface moisture content indicates that the numerically solved Richard's equation combined with groundwater and evaporation models can be used as a sufficient approach to model the variability of surface moisture content, and more importantly, it confirms that evaporation and groundwater table are indeed the two key processes controlling the surface moisture content variability in a beach. Overall the surface moisture variations caused by evaporation were very small compared with those caused by water table oscillations. Water table oscillations contribute a large part of the high degree of spatial and

temporal variability in beach surface moisture content. However, evaporation process more important for the back beach, where the water table is relatively low and aeolian sediment transport usually occurs.

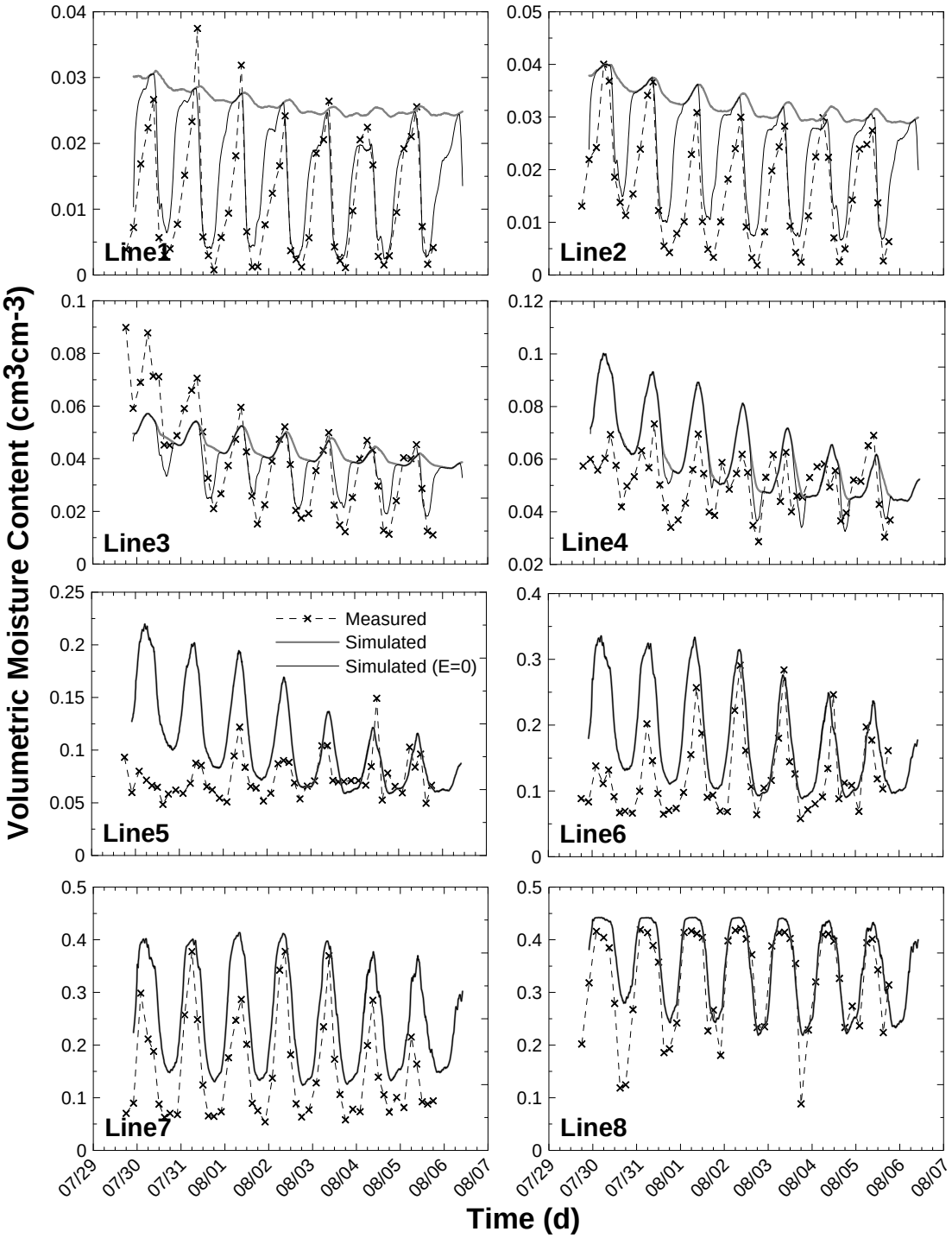

Figure 7.4 Measured vs. simulated time series of averaged surface moisture content for Line 1-12

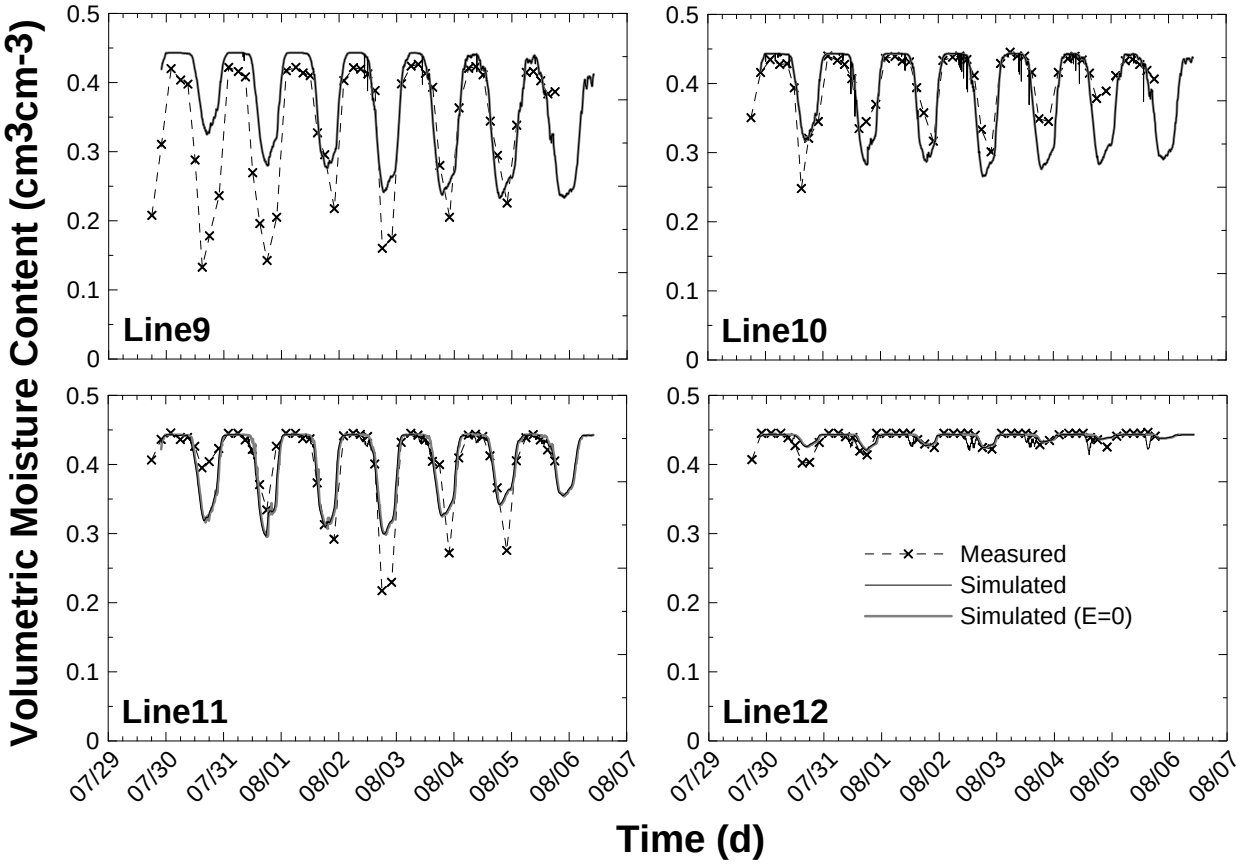

Figure 7.4 Continued

7.4.2.3 Simulations of Spatial Variations in Surface Moisture Content by the RE

Measured and simulated surface moisture maps in Aug 2nd, 2005, were plotted in Fig 10 as an example. The maps were generated using Surfer®, distributed by the Golden Software, Inc. From a visual examination, the simulated maps reasonably match the measured ones in terms of moisture zone shifting and the position of moisture contours. Clearly, some spatial features of the measured moisture maps were not reproduced by the simulation, possibly due to the assumption of homogeneous beach composition (spatial heterogeneity of hydraulic properties of beach surface is not account for). Another problem worth noting is that the width of the moisture "region" 0.14-0.35 is substantially narrower on measured maps than on simulated maps. This implies that in reality moisture content decreases landward more rapidly within this range than

predicted, and that the best-fit water retention curve still does not represent exactly the real relationship between moisture content and pressure head.

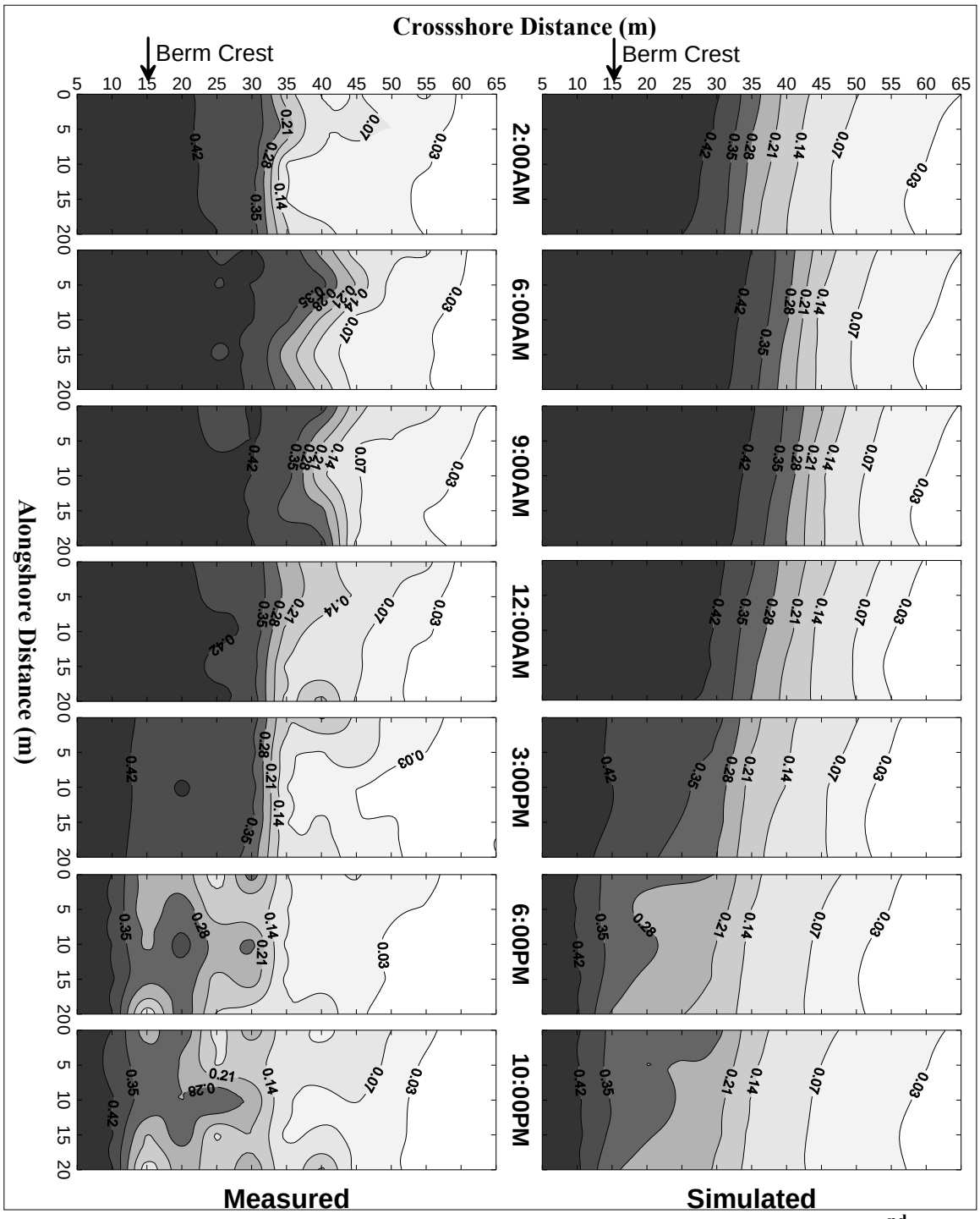

Figure 7.5 Measured vs. simulated surface moisture content maps on Aug. 2nd 2005

7.5 Conclusions

In this study, as no precipitation was recorded throughout the study period, only two temporal parameters (i.e., groundwater table fluctuations and evaporation) that control the variations in surface moisture content are considered. The latter variable is actually a function of four other time-dependent parameters: net radiation, wind speed, air temperature and atmospheric humidity.

The simulations using the numerically solved RE successfully captured the diurnal signals of surface moisture variations in terms of magnitude and timing. This indicates that groundwater table fluctuations and diurnal changes of evaporation are indeed the two dominant processes that determine surface moisture distribution and redistribution for the beach system. The simulations based on the numerically solved RE definitely provides a quite good representation of the evolution of beach surface moisture. The FRM, requiring fewer inputs, was also found as a simple approach to understand and to estimate the variations in beach surface moisture. However, it in general causes underpredictions in the region where the water table is very shallow and the surface moisture content is close to saturation.

Some error generated by the RE simulations were readily identified in the predicted time series and spatial maps of surface moisture content in comparison with measured data. These discrepancies were clearly resulted from the simplification of the beach system, which includes a number of assumptions, such as spatially homogeneous sediment, dominant vertical water flow, hydrostatic state and no hysterisis. These assumptions together provide a reasonable basis to model the spatial and temporal variability of beach surface moisture content with computational convenience. At the same time, they inevitably introduce systematic errors to the simulated results. Note that in general proposed model can never exactly repeat complex behaviors

involved in real, natural systems, but provide approaches to represent those processes for better understanding and practical usages. From this standpoint, the ultimate goal of this study, to achieve a better understanding of beach surface moisture dynamics, is finally achieved by the utilization of the numerically solved RE, along with groundwater, evaporation and soil characteristic models presented in this chapter and preceding chapters.

These combined models can be extrapolated for various environmental settings with specified hydraulic properties. The results are highly useful for relatively wide dissipative beaches with large tidal range (which means large part of the beach is dominated by evaporation process). However, for mud beaches or where native materials has substantial amount of clay, the effect of hysterisis must be included to obtain reasonable model performance.

CHAPTER 8 SUMMARY AND DISCUSSION

8.1 Summary of the Study

In pursuit of the ultimate goal of this project - to model the spatial and temporal dynamics of beach surface moisture-numerous parameters were directly monitored, including beach surface moisture content, evaporation rates, tide and groundwater table elevations, atmospheric conditions (including wind speed and direction, air temperature, and relative humidity), at a fine-grained beach of the Padre Island National Seashore, Texas. Spatial and temporal variability in surface moisture content was documented over an eight-day period. Key factors controlling this variability were identified as groundwater table fluctuations and evaporation (no precipitation was recorded through the study period). These two key factors were successfully modeled independently. Finally, variability in surface moisture content was found to be reasonably represented using the numerically solved Richard's equation, in conjunction with the coupled groundwater model (Boussinesq equation) and the evaporation model (Penman equation), and the soil water characteristic models (van Genuchen model). This study demonstrated that beach surface moisture dynamics can be simulated with data inputs that include tide levels, beach topography, sediment texture, aquifer depth, and routine climatic data (solar radiation, wind speed, air temperature and relative humidity).

Field measurements show that the beach can be classified into three moisture-content zones: the dry back beach, extending from the dune toe to ~45 m (distance from the time-averaged shoreline), the highly-variable middle beach, extending between ~25-45 m from the shoreline, and the wet fore beach, lying in the region from ~25 m to the shoreline. Beach surface moisture content exhibits the highest variability in the middle part of the beach, up to ± 30%

(volumetric) in a day or across a space of ~20 m, while the variability in the back beach and the fore beach is less than ± 6% for the entire study period. In the alongshore direction, surface moisture content also varies quite notably (up to ~10%). The alongshore variability in surface moisture content is controlled, at least partly, by the alongshore variations in beach surface elevation. Over time, the moisture contours shift position in response to tide oscillations, with relatively low speed in the dune side and high velocity in the foreshore side.

To simulate evaporation rates and evaluate the applicability of popular evaporation models to the study site, the mass-transfer method (represented by the Singh and Xu (1998) equation), and an approach combing the energy-budget and mass-transfer methods (represented by the Penman equation), were tested against field-measured evaporation data. Results showed that the mass-transfer method consistently generated large errors in prediction. It appears that the employed parameters are not the key controlling factors for the evaporation in the unique coastal climatic pattern (day sea-breeze and night land-breeze pattern). Simulations generated by the Penman equation provide much better agreement with field measurements, although a clear time offset (~2 hrs) and some underestimation in the early evening were apparent. With modification of the time offset and the constants used in the wind function, the accuracy of the Penman equation improved substantially.

The tide-induced groundwater table fluctuations were simulated using the numerical solutions of the linearized Boussinesq equation. Two approaches were employed, based on assumptions of a vertical beach and a sloping beach, respectively. Both simulations reproduced the signal from the tide quite well in terms of phase change, but the simulation with a sloping beach performed significantly better in regard to the magnitude of the groundwater table fluctuations, particularly during low tides. Underestimations were found in both simulations

during high tides in the second portion of the beach, especially for the first five tidal cycles. These underestimations can be attributed to additional infiltration from swash-induced, transitional ponding on the beach surface near the berm crest. This latter process cannot be included in the Boussinesq equation. The field measurements of ground water table elevations and spectral analyses show that the lower frequency signals in the groundwater oscillations (e.g., diurnal tidal oscillations) do not follow the exponentially damping trend in the landward direction as previous investigators reported. This means the analytical solutions of the Boussinesq equation (which imply an exponential damping rate) are not directly applicable to this study site and similar environments.

Simulated time series and maps of beach surface moisture content both indicate that the numerically solved Richard's equation, combined with models describing the fluctuations of the groundwater table, the evaporation rates and the hydraulic properties of the sediment, provides a reasonable approach to represent surface moisture dynamics. The combination successfully captured most signals from the groundwater table and surface evaporation. However, some systematic errors can also be found by the comparison of the simulated and observed moisture contents.

8.2 Discussion

The systematic errors mentioned above derive mainly from the simplification of the system. Since it is not possible to measure all relevant parameters in appropriate detail for the entire system, some assumptions were made here for the sake of mathematical convenience and simplicity, as is done in all modeling. The simplifications of the system based on these assumptions inevitably introduce some degree of error into the simulated results. It is thus

worthwhile to consider the assumptions used herein. The critical assumptions underlying this study include:

1) The beach is assumed to be composed of homogeneous sediments. Although the beach can be considered as a homogeneous porous medium, beach sand close to dune toe has often been found to be slightly finer with lower bulk density than that close to the shoreline. Further, surface sand often has a lower compaction rate than sand from lower layers. Also, some heterogeneity in surface sand composition usually exists due to unpredictable factors, such as entrapped air, shells, vegetation and sea weed residuals (Faybishenko, 1995; Yang and Davidson-Arnott, 2005). The hydraulic properties (including water retention characteristics and hydraulic conductivity) of the sediment therefore may not remain exactly same for the whole beach (Figure 7.1). It should be noted that even a low degree of spatial heterogeneity in soil hydraulic properties may cause a high degree of the spatial and temporal variability in surface moisture content. Unfortunately, no reasonable approach to date has been reported to represent the subtle heterogeneity of a "homogeneous" medium like a beach. This is an area where further research is necessary and any advances in this problem will greatly improve model performance and accuracy in simulating the surface moisture dynamics.

2) Vertical flows are assumed to dominate the unsaturated water transport within the vadose zone. Although the beach groundwater table is usually gently sloping and fluctuates at very small angles, it is indeed not flat (Nielson, 1990), and this leads to horizontal water flows in the vadose zone. The horizontal flow becomes more evident in the vicinity of the water table and areas where water table is shallow. Horizontal flow may also be important in the area immediately adjacent to the shoreline due to the dynamic swash. Employment of the two-dimensional or three-dimensional version of the Richard's equation may be helpful to better

simulations. However, this scenario can not be achieved until the spatial heterogeneity of required parameters (e.g., groundwater table depths and hydraulic conductivity) is able to be accurately predicted.

3) It is assumed that the sediment has same water retention curves in the drying and wetting cycles. The cyclic movement of the groundwater table results in corresponding movement of the moisture profile above the groundwater table (Stauffer and Kinzebach, 2001). These processes are governed by the water retention curve, which is generally not constant, rather it shows hysteresis effects. That is, the same pressure head usually corresponds with higher water contents during water table falling (drying cycle) than during water table rising (wetting cycle) (Childs, 1969; Kessler and Rubin, 1987). Although well-sorted beach sand usually exhibits only a small hysterisis effect, the hysterisis may still exert some uncertain influences on surface moisture evolution. For example, in Line 6 of Figure 7.4, the measured surface moisture content in July 30th is apparently lower than that in Aug 2nd although the magnitudes of groundwater table fluctuation were almost same. This is possibly due to the hysterisis effect: although the hydraulic pressures were almost same, a long-term drying trend in the area is apparent as the beach experienced substantial drainage during the study period. Carefully-designed laboratory experiments and more field measurements are required to determine the extent to which hysterisis is involved in the evolution of beach surface moisture.

4) The water content profile within the sand column is assumed to be in a steady state with no transient water flow. The assumption of steady state implies that the matric potential on the surface corresponds exactly and synchronously with water table changes. However, realistic matric potential on the surface may substantially lag behind the water table oscillation, and this time lag proportionally increases with the water table depth. Fortunately, for a real beach

environment, the amplitudes of water table fluctuation decrease exponentially with distance from the shoreline as the water table depth increases, which implies the existence of transient water flow may not fundamentally hurt model performance. This was also found to be the case by Raes and Deproost (2003).

5) Atmospheric stresses and demands on evaporation are assumed to be identical for the entire beach. As commonly recognized, potential evaporation is determined by the incoming net radiation, air temperature, humidity and wind speed, which are in turn affected by soil surface conditions (including roughness, albedo and adjacent topography, etc.). Since surface conditions of the beach are not exactly the same, the evaporation potential will also not be spatially uniform. Again, however, this kind of spatial heterogeneity cannot be adequately represented with the current level of knowledge.

6) It is assumed that the real soil evaporation rates respond to surface moisture content variations strictly following the linear relationship given by equation (7.14). Gavin and Agnew (2000) found the surface resistance (to evaporation) of the Penman-Monteith equation is definitely not linearly related the soil moisture content, although their field study has far too few points to generalize a clear relationship. Similar results can also be found in the study of Aluwihare and Watanabe (2003). These results indicate that equation (7.14) may need to be further modified to obtain a more accurate estimation of real soil evaporation, particularly for a dry soil surface. However, such a modification is not currently available. Many researchers have found that the measurements of temperature and humidity of the drying soil surface usually provides a better estimate of real soil evaporation. However, it not possible in practice to measure such information at each point on a grid as large as that employed in the present study. On the other hand, the formation of a dry soil layer (which is usually a few millimeters in depth)

often imposes dramatic influences on the evaporation process (Yamanaka and Yonetani, 1999; Aluwihare and Watanabe, 2003). A more accurate soil evaporation model, particularly for the driest areas, would almost certainly enhance model performance in this study. This is yet an area where further investigations are needed.

The assumptions mentioned above make contributions in varying degrees to the discrepancies that were found between measured and simulated surface moisture contents. Nevertheless, these assumptions are carefully considered and are based on the environmental conditions and field observations. More importantly, they are quite reasonable for balancing the concerns of measurement feasibility, model simplicity, computational convenience, and the complexity of the system. They indeed provide a solid basis to sufficiently simulate the spatial and temporal variability in surface moisture content. However, before this variability is fully understood and improved predictions can be obtained, many more experiments must be conducted to obtain exact information about soil hydraulic properties and more precise functions must be developed to describe the related physical phenomena.

8.3 Model Applicability

Although all model inputs were obtained for a relative short time period and a specific environmental setting, the findings of this study should be fully applicable to other environments where surface moisture dynamics are primarily controlled by evaporation and/or groundwater table fluctuations. As all the models and involved constants are specified physically instead of empirically, associated simulations can be readily conducted with inputs from independent measurements of local atmospheric parameters and hydraulic properties. In addition, all required inputs (e.g., wind speed, air temperature, relative humidity, topography, and grain sizes) are

routine data or can be easily measured. This clearly further enhances the applicability of the model proposed in this study.

For locations where other major water inputs and/or outputs may involve (e.g., precipitation, surface water infiltration, evapotranspiration, etc.), the findings and proposed models of this study can also be easily modified according to the required environmental adjustment. High accuracy of model performance can be expected if those additional fluxes are described accurately.

8.4 Future Work

This study has succeeded in documenting beach surface moisture dynamics, tide and groundwater table fluctuations, and evaporation rates with associated atmospheric parameters. A suite of models describing these processes have been identified and successfully employed. The resulting simulations of temporal and spatial variability in surface moisture content represent dramatic improvement on previous capabilities in this area. However, it should be noted that all modeling and simulations are based on data obtained in an eight-day field investigation. Longer term measurements that reflect a broader range of environmental conditions are highly desirable. Instruments or devices specifically designed for the "surface" layer are needed to achieve better consistency and accuracy in soil moisture content measurements. Specific investigations regarding evaporation from soil, particularly dry soil surface, are required to obtain better understanding of hydrodynamics in the surface layer. Detailed knowledge regarding hydraulic properties of native sediment may be helpful to incorporate the hysterisis effect into the simulation and then enhance the model performance.

REFERENCES

Abbaspour, K., Kasteel, R., and Schulin, R. 2000. Inverse parameter estimation in a layered unsaturated field soil. *Soil Science* 165: 109-123

Abu-Awwad, A.M. 1997. Water infiltration and redistribution within soils affected by a surface crust. *Journal of Arid Environments* 37(2): 231-242

Ăcs, F., Mihailović, D.T., and Rajković. A coupled soil moisture and surface temperature prediction model. *Journal of Applied Meteorology* 30: 812-822

Akiba, M., 1933. The threshold wind speed of sand grains on a wetted sand surface. *Journal of Agricultural Engineering in Japan* 5: 157– 174

Aluwihare, S., and Watanabe, K. 2003. Measurement of evaporation on bare soil and estimating surface resistance. *Journal of Environmental Engineering* 129(12): 1157-1168

Alyamani, M.S., and Sen, Z. 1993. Determination of Hydraulic Conductivity from Complete Grain-size Distribution Curves. *Ground Water GRWAAP* 31(4): 551-555

Anctil, F., Mathieu, R, Parent, L.E., Viau, A.A., Sbih, M., and Hessami, M. 2002. Geostatistics of near-surface moisture in bare cultivated organic soils. *Journal of Hydrology* 260: 30-37

ARS (Air Resource Specialists, Inc.). 2005. Access to National Park Service (NPS) Gaseous Pollutant and Meteorological Data (http://ard-aq-request.air-resource.com/)

Ataie-Ashtiani, B., Volker, R.E. and Lockington, D.A. 1999. Tidal effects on sea water intrusion in unconfined aquifers. *Journal of Hydrology* 216(1): 17-31

Atherton, R.J., Baird, A.J. and Wiggs, G.F.S. 2001. Inter-tidal Dynamics of Surface Moisture Content on a Meso-tidal Beach. *Journal of Coastal Research* 17(2): 482-489

Baird, A.J., Mason, T. and Horn, D.P. 1998. Validation of a Boussinesq model of beach ground water behavior. *Marine Geology* 148: 55-69

Barton, I.J. A prameterization of the evaporation from nonsaturated surfaces. *Journal of Applied Meteorology* 18: 43-47

Bauters, T.W.J., DiCarlo, D.A., Steenhuis, T.S., and Parlange, J.Y. 2000. Soil water content dependent wetting front characteristics in sands. *Journal of Hydrology* 231–232: 244–254

Beljaars, A.C.M., Viterbo, P., Miller, M.J., and Betts, A.K. 1996. The anomalous rainfall over the United States during July 1993: Sensitivity to land surface parameterizations and soil moisture anomalies. *Monthly Weather Review* 124: 362-383

Ben-Asher, J., Matthias, A.D., and Warrick, A.W. 1983. Assessment of evaporation from bare soil by infrared thermometry. *Soil Science Society of America Journal* 47: 182-191

Berg, P. 1999. Long-term simulation of water movement in soils using mass-conserving procedures. *Advances in Water Resources* 22(5): 419–430

Bomar, G.W. 1983. *Texas Weather*. Austin: University of Texas Press. 265p

Bosilovich, M.G. and Sun, W.Y. 1995. Formulation and verification of a land surface parameterization for atmospheric models. *Boundary-Layer Meteorology* 73: 321-341

Bosilovich, M.G. and Sun, W.Y. 1998. Monthly simulation of surface layer fluxes and soil properties during FIFE. *Journal of the Atmospheric Sciences* 55: 1170-1184

Broadbridge, P., Edwards, M. P. and Kearton, J. E. 1996. Closed-form solutions for unsaturated flow under variable flux boundary conditions. *Advances in Water Resources* 19(3): 207-213

Brutsaert, W. 1982. *Evaporation into the Atmosphere: Theory, History, and Applications*. D. Reidel Publishing Co. Dordrecht, Holland. 299p

Campbell, G.S. 1985. *Soil Physics with Basic: Transport Models for Soil-Plant System*. Elsevier, New York, 150p

Cao, J. and Kitanidis, P.K. 1999. Adaptive-grid simulation of groundwater flow in heterogeneous aquifers. *Advances in Water Resources* 22(7): 681-696

Capehart, W.J., and Carlson, T.N. 1994. Estimating near-surface soil moisture availability using a meteorologically driven soil-water profile model. *Journal of hydrology* 160: 1-20

Cartwright, N. and Nielson, P. 2001. Groundwater dynamics and salinity in beaches. Proceedings of Coasts and Ports 2001, *15th Australian Coastal and Ocean Engineering Conference*, Gold Coast, Australia, 441-446

Charbeneau, R.J. 2000. *Ground Water Hydaulic and Pollutant Transport*. Prentice-Hall, Old Tappan, N.J. 593p

Chappell, J., Eliot, I.G., Bradshaw, M.P., and Londale, E. 1979. Experimental control of beach face dynamics by water table pumping. *Engineering Geology*. 14:29–41

Chen, J., Hopmans, J.W., and Grismer, M.E. 1999. Parameter estimation of two-fluid capillary pressure–saturation and permeability functions. *Advances in Water Resources* 22(5): 479–493

Chen, X., and Hu, Q. 2004. Groundwater influences on soil moisture and surface evaporation. *Journal of Hydrology* 297: 285-300

Childs, E. C., and Pulovassilis, A. 1962. The moving profile above a moving water table. *Journal of Soil Science* 13(2): 272-285

Childs, E.C. 1969. *An introduction to the physical basis of soil water phenomena*. John Willey & Sons Ltd, New York. 493p

Childs, E.C., and Poulovassilis, A. 1960. An oscillating permeameter. *Soil Science* 90: 326-328

Chounet, L.M., Hilhorst, D., Jouron, C., Kelanemer, Y., and Nicolas, P. 1999. Simulation of water flow and heat transfer in soils by means of a mixed finite element method. *Advances in Water Resources* 22(5): 445–460

Chuang, M.H. and Yeh, H.D. 2006. An analytical solution for the head distribution in a tidal leaky confined aquifer extending an infinite distance under the sea. *Advances in Water Resources* 30(3): 439-445

Cichota, R., Elias, E.A. and van Lier, Q. de J. 2004. Testing a finite-difference model for soil heat transfer by comparing numerical and analytical solutions. *Environmental Modelling & Software* 19(5), May, Pages 495-506

Conley, D. C., and Inman, D. 1994. Ventilated oscillatory boundary layers. *Journal of Fluid Mechanics* 273: 261-284

Cook, F.J., and Rassam, D.W. 2002. Analytical model for predicting water table dynamics during drainage and evaporation. *Journal of Hydrology* 263: 105-113

Cornelis, W. M., and Gabriels, D. 2003. The effect of surface moisture on the entrainment of dune sand by wind: an evaluation of selected models. *Sedimentology* 50: 771-790

Cornelis, W.M., Ronsyn, J., van Merivenne, M., and Hartmann, R. 2001. Evaluation of pedotransfer functions for predicting the soil moisture retention curve. *Soil Science Society of America Journal* 65: 638-648

Corpus Christi Webside, 2005. http://www.corpuschristiwindsurfing.com/weather.html

Crowea, A.S., Shikazea, S.G., and Schwartz, F.W. 1999. A grid generating algorithm for simulating a fluctuating water table boundary in heterogeneous unconfined aquifers. *Advances in Water Resources* 22(6): 567-575

Davidson-Arnott, R.G.D., and Langham, D.R.J. 2000. The effects of softening on nearshore erosion of a cohesive shoreline. *Marine Geology* 166(1): 145-162

Davies, J.A., and Allen, C.D. 1973. Equilibrium, potential and actual evaporation from cropped surfaces in Southern Ontario. *Journal of Applied Meteorology* 12: 649-657

Deardorff, J.W. 1977. A parameterization of the ground surface moisture content for use in atmospheric prediction models. *Journal of Applied Meteorology* 16: 1182-1185

Deardorff, J.W. 1978. Efficient prediction of ground surface temperature and moisture with inclusion of a layer of vegetation. *Journal of Geophysical Research* 83: 1889-1903

Dickinson, R.E. 1988. The force restore model for surface temperatures and its generalizations. *Journal of Climate* 1: 1086-1097

Dingman, S.L. 1984. *Fluvial hydrology*. Freeman, San Francisco, 383p

Dominick, T. F. 1970. *A mathematical model for tide-induced beach water table fluctuations.* Master thesis, Louisiana State University. 131p

Dominick, T. F., Wilkins, B., Roberts, H. and Ho, C.L. 1973. A study of beach ground-water hydrology and chemistry. *Technical Report 152*, Coastal Studies Institute, Louisiana State University. 5-55

Dominick, T.F. Wilkins, B., and Roberts, H. 1971. Mathematical model for beach groundwater fluctuations. *Water Resources Research* 7: 1626-1635

Doorenbos, J. and Pruitt, W.O. 1975. *Crop water requirement*. Irrigation and Drainage Paper No. 24, FAO, Rome, 179pp.

Duncan, J. R. 1964. The effects of water table and tidal cycle on swash-backswash sediment distribution and beach profile development. *Marine Geology* 2: 186-197

Emory, K.O. and Foster, J.R. 1948. Effect of ground-water on beach erosion. *Journal of Marine Research* 7(3): 644-654

Entekhabi, D., Rodriguez-Iturbe, I., and Castelli, F. 1996. Mutual interaction of soil moisture state and atmospheric processes. *Journal of Hydrology* 184: 3-17

Famiglietti, J.S., Rudnicki, J.W., and Rodell, M. 1998. Variability in surface moisture content along a hillslope transect: Rattlesnake Hill, Texas. *Journal of Hydrology* 210: 259-281

Fang, C.S., Wang, S. N. and Harrison, W. 1972. Groundwater flow in a sandy tidal beach. Two dimensional finite element analysis. *Water Resources Research* 8: 121-128

Farthing, M.W., Kees, C.E., and Miller, C.T. 2003. Mixed finite element methods and higher order temporal approximations for variably saturated groundwater flow. *Advances in Water Resources* 26: 373–394

Faybishenko, B.A. 1995. Hydraulic behavior of quasi-saturated soils in the presence of entrapped air: Laboratory experiments. *Water Resources Research* 31(10): 2421-2435

Fetter, C.W. 1994. *Applied Hydrogeology*. Prentice Hall, N.J. 598p

Fraser, C.J.D., Roulet, N.T. and Lafleur, M. 2001. Groundwater flow patterns in a large peatland. *Journal of Hydrology* 246(1): 142-154

Gardner, C.M.K., J.P. Bell, J.D. Cooper, T.J. Dean and M.G. Hodnett. 1991. Soil water content. In K.A. Smith and C.E. Mullins (ed): *Soil Analysis: physical methods*. Marcel Dekker, Inc., New York, 1-73

Gavin, H., and Agnew, C.T. 2000. Estimating evaporation and surface resistance from a wet grassland. *Physics and Chemistry of the Earth* (B) 25(7-8): 599-603

Gillham, R.W. 1984. The capillary fringe and its effect on water table response. *Journal of Hydrology* 67: 307-324

Gourlay, M.R. 1992. Wave set-up, wave run-up and beach water table: Interaction between surf zone hydraulics and groundwater hydraulics. *Coastal Engineering* 17: 93-144

Grant, W.S. 1948. Influence of the water table on beach aggradation and degradation. *Journal of Marine Research* 7(3): 65-660

Grapher Manual, Version 5.02. 2004. Golden Software, Inc.

Hanks, R.J. 1992. *Applied soil physics: soil water and temperature application* (2nd edition). Springer-Verlag, 1-22

Hanks, R.J. and G.L. Ashcroft. 1980. *Applied soil physics*. Springer-Verlag, New York. 159p

Harrison, W., Fang, C.S., and Wang, S. N. 1971. Groundwater flow in a sandy tidal beach. One dimensional finite element analysis. *Water Resources Research* 7: 1313-1322

Hegge, B.J. and Masselink, G. 1991. Groundwater-table responses to wave run-up: an experimental study from Western Australia. *Journal of Coastal Research* 7(3): 623-634

Held, R.J., and Celia, M.A. 2001. Modeling support of functional relationships between capillary pressure, saturation, interfacial area and common lines. *Advances in Water Resources* 24: 325-343

Hillel, D. 1971. *Soil and Water: Physical Principles and Processes*. Academic Press, New York, 288p

Horn, D.P. 2002. Beach groundwater dynamics. *Geomorphology* 48(1): 121-146

Horn, D.P. 2005. Measurements and modeling of groundwater flow in the swash zone. *Continental Shelf Research* 26: 622-652

Horn, D.P., Li, L. and Holmes, P. 2003. Measurement and modeling of gravel beach groundwater response to wave run-up. In Davis, R.A. (ed). *Proceedings of the International Conference on Coastal Sediments 2003*. CD-ROM published by World Scientific Publishing Corp. and East Meets West Productions, Corpus Christi, Texas, USA. ISBN 981-238-422-7, 11pp

Hwang, S.I., and Powers, S.E. 2003. Estimating unique soil hydraulic parameters for sandy media from multi-step outflow experiments. *Advances in Water Resources* 26: 445–456

Isla, F.I., and Bujalesky, G.G. 2005. Groundwater dynamics on macrotidal gravel beaches of Tierra del Fuego, Argentina. *Journal of Coastal Research* 21(1): 65-72

Iwata, S., T. Tabuchi and B.P. Warkentin. 1988. *Soil-water interactions: Mechanisms and applications*. Marcel Dekker, Inc., New York, 1-380

Jackson, D.W.T. and Cooper, J.A.G. 1999. Beach fetch distance and aeolian sediment transport. *Sedimentology* 46: 517-522

Jackson, N. L., Horn, D. P., Spalding, V. and Nordstrom, K. F. 1999. Changes in Beach Water Table Elevation During Neap and Spring Tides on a Sandy Estuarine Beach, Delaware Bay, New Jersey. *Estuaries* 22: 753-762

Jackson, N.L., and Nordstrom, K. F. 1997. Effects of time-dependent moisture content of surface sediments on aeolian transport rates across a beach, wildwood, New Jersey, U.S.A. *Earth Surface Processes and Landforms* 22: 611-621

Jacovides, C.P. and Kontoyiannis, H. 1995. Statistical procedures for the evaluation of evaportranspiration computing models. *Agricultural Water Management*. 27: 365-371

Jeng, D.S., Li, L. and Barry, D.A. 2002. Analytical solution for tidal propagation in a coupled semi-confined/phreatic coastal aquifer. *Advances in Water Resources* 25: 577–584

Jeng, D.S., Barry, D.A., and Li, L. 2001. Water wave-driven seepage in marine sediments. *Advances in Water Resources* 24: 1-10

Jeng, D.S., Barry, D.A., Seymour, B.R., Dong, P., and Li, L. 2005a. Two-dimensional approximation for tide-induced watertable fluctuations in a sloping sandy beach. *Advances in Water Resources* 28: 1040-1047

Jeng, D.S., Seymour, B.R., Barry, D.A., Li, L., and Parlange, J.Y. 2005b. New approximation for free surface flow of groundwater: capillarity correction. *Advances in Water Resources* 28: 1032-1039

Jhorar R.K., Bastiaanssen W.G.M., Feddes R.A. and Van Dam, J.C. 2002. Inversely estimating soil hydraulic functions using evapotranspiration fluxes. *Journal of Hydrology* 258(1): 198-213

Kessler, A., and Rubin, H. 1987. Relationships between water infiltration and oil spill migration in sandy soils. *Journal of Hydrology* 91: 197-204

Kim, G. Spatial and temporal influences on soil moisture estimation. *Water Engineering Research* 3(1): 31-43

Kim, H., Rao, P.S.C., and Annable, M.D. 1997. Determination of effective air-water interfacial area in partially saturated porous media using surfactant adsorption. *Water Resources Research* 33(12): 2705-2711

Kim, T.H., and Sture, S. 2004. Effect of moisture on attraction force in beach sand. *Marine Georesources and Geotechnology* 22:33-47

Kocurek, G., Robinson, N.I. and Sharp, J.M. 2001. The response of the water table in coastal aeolian systems to changes in sea level. *Sedimentary Geology* 139(1): 1-13

Kondo, J., Saigusa, N., and Sato, T. 1992. A model and experimental study of evaporation from bare-soil surfaces. *Journal of Applied Meteorology* 31: 304-312

Kool, J.B., Parker, J.C., and van Genuchten, M.T. 1987. Parameter estimation for unsaturated flow and transport models - a review. *Journal of Hydrology* 91: 255-293

Li, H., and Jiao, J.J. 2001. Analytical studies of groundwater-head fluctuation in a coastal confined aquifer overlain by a semi-permeable layer with storage. *Advances in Water Resources* 24: 565-573

Li, H., and Jiao, J.J. 2002. Analytical solutions of tidal groundwater flow in coastal two-aquifer system. *Advances in Water Resources* 25: 417–426

Li, H., and Jiao, J.J. 2003. Influence of the tide on the mean watertable in an unconfined, anisotropic, inhomogeneous coastal aquifer. *Advances in Water Resources* 26: 9–16

Li, J. and Islam, S. 2002. Estimation of root zone soil moisture and surface fluxes partitioning using near surface soil moisture measurements. *Journal of Hydrology* 259: 1-14

Li, L. Horn, D.P., and Baird, A.J. 2006. Tide-induced variations in surface temperature and water-table depth in the intertidal zone of a sandy beach. J*ournal of Coastal Research* 22(6): 1370-1381

Li, L., and Barry, D.A. 2000. Wave-induced beach groundwater flow. *Advances in Water Resources* 23: 325-337

Li, L., Barry D.A., Stagnitti F., Parlange, J.Y., and Jeng, D.S. 2000. Beach water table fluctuations due to spring–neap tides, moving boundary effects. *Advances in Water Resources* 23(8): 817-824

Li, L., Barry, D.A. and Pattiaratchi, C.B. 1996a. Modeling coastal groundwater response to beach dewatering. *Journal of Waterway, Port, Coastal and Ocean Engineering* 122: 273-280

Li, L., Barry, D.A. and Pattiaratchi, C.B. 1996b. Numerical modeling of tide-induced beach water table fluctuations. *Coastal Engeering* 30(1): 105-123

Li, L., Barry, D.A., Parlange, J.Y., and Pattiaratchi, C.B. 1998. Reply to Comment on "Beach water table fluctuations due to wave run-up: Capillarity effects". *Water Resources Research* 34(11): 3205-3206

Li, L., D.A.Barry, F. Stagnitti, J.Y.Parlange, and D.S. Jeng. 2000. Beach water table fluctuations due to spring-neap tides: moving boundary effects. *Advances in Water Resources* 23: 817-824

Li, L., Parlange, J.Y., and Pattiaratchi, C.B. 1997. Beach water table fluctuations due to wave run-up: Capillary effects. *Water Resources Research* 33(5): 935-945

Liu, P.L.F., and J. Wen. 1997. Nonlinear diffusive surface waves in porous media. *Journal of Fluid Mechanism* 347: 119-139

Lockington, D.A., Parlange, J.Y., Parlange, M.B., and Selker, J. 2000. Similarity solution of the Boussinesq equation. *Advances in Water Resources* 23: 725-729

Mahfouf, J.F. and Noilhan, J. 1991. Comparative study of various formation from bare soil using in situ data. *Journal of Applied Meteorology* 30: 1354-1365

Massel, S. R. and E.N. Pelinovsky. 2001. Rup-up of dispersive and breaking waves on beaches. *Oceanologia* 43(1): 61-97

Massel, S.R. 2001. Circulation of groundwater due to wave set-up on a permeable beach. *Oceanologia* 43(3): 279-290

Masselink, G. and Pattiaratchi, C.B. 1998. Morphological evolution of beach cusps and associated swash circulation patterns. *Marine Geology* 146(1): 93-113

Maxwell, R.M. and Miller, N.L. 2005. Development of a coupled land surface and groundwater model. *Journal of Hydrometeorology* 6: 233-247

McKenna Neuman, C., and Nickling, W.G. 1989. A theoretical and wind tunnel investigation of the effect of capillary water on the entrainment of sediment by wind. *Canadian Journal of Soil Science* 69: 79-96

McLachlan, A. 1989. Water filtration by dissipative beaches. *Limnology and Oceanography* 34(4): 774-780

Miyazaki, T. 1993. *Water flow in soils*. Marcel Dekker, Inc., New York, 296p

Monteith, J.L. 1965. Evaporation and environment. *Symposia of the Society for Experimental Biology* 19: 205-234

Monteith, J.L. and Unsworth, M.H. 1990. *Principles of Environmental Physics* (2nd ed.). Edward Arnold, London. 291p

Nabelek, P.I., Bartlett, C.D., Baird, A.J., Mason, T., and Horn, D.P. 1998. Validation of a Boussinesq model of beach ground water behaviour. *Marine Geology* 148(1): 55-69

Nachabe, M. 2002. Analytical expressions for transient specific yield and shallow water table drainage. *Water Resources Research* 38(10): 1193

Nachabe, M. Masek, C. and Obeysekera, J. 2004. Obervations and modeling of profile soil water storage above a shallow water table. *Soil Science Society of American Journal* 68(3): 719-724

Namikas, L. S. and Sherman, D.J. 1995. A review of the effects of surface moisture content on aeolian sand transport. In: Tchakerian, V.P. (ed.), *Desert Aeolian Process*, Chapman & Hall, New York, 269-293

NPS(National Park Service). 2005. http://www.nps.gov/pais/naturescience/index.htm

Netto, A.M., Pieritz, R.A., and Gaudet, J.P. 1999. Field study on the local variability of soil water content and solute Concentration. *Journal of Hydrology* 215: 23–37

Neuman, C.M. 2004. Effects of temperature and humidity upon the transport of sedimentary particles by wind. *Sedimentology*, 51: 1-17

Ng, C.O. 1999. Macroscopic equations for vapor transport in a multi-layered unsaturated zone. *Advances in Water Resources* 22(6): 611-622

Nickling, W.G. 1994. Aeolian sediment transport and deposition. In: Pye, K. (ed.), *Sediment Transport and Depositional Processes*. Blackwell Scientific Publications.293-350

Nielsen, P. 1990. Tidal dynamics of the water table in beaches. *Water Resources Research* 26(9): 2127-2134

Nielsen, P. 1999. Comment on "Beach water table fluctuations due to wave run-up: Capillarity effects" by L. Li et al. *Water Resources Research* 35(4): 1323-1324

Nielsen, P. 1999. Groundwater dynamics and salinity in coastal barriers. *Journal of Coastal Research* 15(3): 732-740

Nielsen, P., and Perrochet, P. 2000. Watertable dynamics under capillary fringes: experiments and modeling. *Advances in Water Resources* 23: 503-515

Nilsson, D. and Karlsson, S. 2005. A model for the field drying and wetting processes of cut Flax Straw. *Biosystems Engineering* 92(1): 25-35

NOAA. 2005. http://www.srh.noaa.gov/crp/docs/office/digest.html

Noilhan, J. and Planton, S. A simple parameterization of land surface processes for meteorological models. *Monthly Weather Review* 117: 536-549

Oliveira, M.T. 2001. Modeling water content of a vineyard soil in the Douro Region, Portugal. *Plant and Soil* 233: 213-221

Olyphant, G.A. 2003. Temporal and spatial (down profile) variability of unsaturated soil hydraulic properties determined from a combination of repeated field experiments and inverse modeling. *Journal of Hydrology* 281: 23-35

Otvos, E.G. 1999. Rain-Induced Beach Processes Landforms of Ground Water Sapping and Surface Runoff. *Journal of Coastal Research* 15(4): 1040-1054

Pellenq, J. , Kalmab, J., Bouleta, G., Saulnierc, G.M., Wooldridge, S., Kerra, Y., and Chehbouni, A. 2003. A disaggregation scheme for soil moisture based on topography and soil depth. *Journal of Hydrology* 276: 112-127

Pellenq, J., Kalma, J., Boulet, G., Saulnier, G.M., Wooldridge, S., Kerr, Y., and Chehbouni, A. 2003. A disaggregation scheme for soil moisture based on topography and soil depth. *Journal of Hydrology* 276:112-127

Penman, H.L. 1948. Natural evaporation from open water, bare and grass. *Proceedings of the Royal Society of London*. Series A 193: 120-145

Penman, H.L. 1963. *Vegetation and hydrology*. Technical Communication no. 53, Commonwealth Bureau of Soils, Harpenden, England.

Petrone, R.M., Price, J.S., Waddington, J.M. and von Waldow, H. 2004. Surface moisture and energy exchange from a restored peatland, Quebec, Canada. *Journal of Hydrology* 295: 198-210

Philip, J.R. 1957. Evaporation and moisture and heat fields in the soil. *Journal of Meteorology* 14: 354-366

Pollock, L. W. and Hummon, W. D. 1971. Cyclic changes in interstitial water content, atmospheric exposure and temperature in a marine beach. *Limnology and Oceanography* 10: 522-535

Press, W.H., Flannery, B.P., Teukolsky, S.A. and Vetterling, W.T. 1988. *Numerical Recipes in C: the Art of Scientific Computing*. Cambridge University Press, New York. 735pp.

Priestley, C. H. B. and Taylor, R. J. 1972. On the Assessment of Surface Heat Flux and Evaporation Using Large-Scale Parameters. *Monthly Weather Review* 100 (2): 81-92

Qiu, G.Y., Yano, T., and Momii, K. 1998. An improved methodology to measure evaporation from bare soil based on comparison of surface temperature with a dry soil surface. *Journal of Hydrology* 210: 93-105

Raes, D., and Deproost, P. 2003. Model to assess water movement from a shallow water table to the root zone. *Agricultural Water Management* 62: 79-91

Raubenheimer, B., Guza, R.T., and Elgar, S. 1999. Tidal watertable fluctuations in a sandy ocean beach. *Water Resources Research* 35: 2313-2320.

Roels, S., Vandersteen, K., and Carmeliet, J. 2003. Measuring and simulating moisture uptake in a fractured porous medium. *Advances in Water Resources* 26: 237–246

Rotstayn, L.D. Dix, M.R., Roderick, M.L., and Farquhar, G.D. 2007. Pan Evaporation in 20th Century Global Climate Simulations: Model Implementation and Results for Australia. *CSIRO* (www.csiro.au)

Rowntree, P.R. 1991. Atmospheric Parameterization Schemes for Evaporation over Land: Basic Concepts and Climatic Modeling Aspects. In: Schmugge, T.J and Andre, J.C. (Ed.) *Land Surface Evaporation-Measurement and Parameterization*. Springer-Verlag, New York. p.p. 5-30

Ruan, H., and Illangasekare, T.H. 1999. Estimation of relative hydraulic conductivity of sandy soils based on a sheet flow model. *Journal of Hydrology* 219: 83–93

Russo, D., Russo, I. and Laufer, A. 1997. On the spatial variability of parameters of the unsaturated hydraulic conductivity. *Water Resources Research* 33(5): 947-956

Russo, D., Zaidel, J., and Laufer, A. 2001. Numerical analysis of flow and transport in a combined heterogeneous vadose zone–groundwater system. *Advances in Water Resources* 24: 49-62

Sam Smith, A. W. S. and Trembanis, A. C. 2001. Beach Hardness Variation-New Moisture Related Phenomenon and a Case Study from Byron Bay, Australia. *Journal of Coastal Research* 17(4): 869-876

Sarre, R. D. 1988. Evaluation of aeolian sand transport equations using intertidal zone measurements, Saunton Sands, England. *Sedimentology* 35: 671-679

Saunders, I. R., Bailey, W. G. and Bowers, J. D. 1997. Evaporation regimes and evaporation modelling in an alpine tundra environment. *Journal of Hydrology* 195 (1-4): 99-113

Savenije, H.H.G. 2001. A simple analytical expression to describe tidal damping or amplification. *Journal of Hydrology* 243: 205-215

Savijarvi, H. 1992. On surface temperature and moisture prediction in atmosphere models. *Beitraege zur Physik der Atmosphaere* 65: 281-292

Seigel, D.I. and Glaser, P.H. 1987. Groundwater flow in a bog-fen complex, Lost River Peatland, Northern Minnesota. *Journal of Ecology* 75: 743-754

Sellers, P.J., Mintz, Y., Sud, C., and Dalcher, A. 1986. A simple biosphere model (SiB) for use with general circulation models. *Journal Atmospheric Science* 433: 505-531

Sherman, D.J., Bauer, B.O., Gares, P.A., and Jackson, D.W.T. 1996. Wind blown sand at Castroville, California. In: Coastal Engineering, *Proceedings of 25th International Conference* 1996, Orlando, Florida, 4214-4227

Sherman, D.J., Jackson, D.W.T., Namikas, S.L. and Wang, J. 1998. Wind blown sand on beaches: an evaluation of models. *Geomorphology* 22 (2): 113-133

Short, A.D. and Wright, L.D. 1983. Physical variability of sandy beaches. In: McLachlan, A. and Erasmus, T. (Ed.): *Sandy beaches as ecosystems*. The Hague, Netherlands. pp: 133-44.

Shurbaji, A.-R.M., Phillips, F.M., Campbell, A.R. and Knowlton, R.G. 1995. Application of a numerical model for simulating water flow, isotope transport, and heat transfer in the unsaturated zone. *Journal of Hydrology* 171(1): 143-163

Shuttleworth, W.J. 1991. Evaporation Models in Hydrology. In: Schmugge, T.J and Andre, J.C. (Ed.) *Land Surface Evaporation-Measurement and Parameterization*. Springer-Verlag, New York. p.p. 93-120

Shuttleworth, W.J., and Calder, I.R. 1979. Has the Priestley-Taylor equation any relevance to the forest evaporation? *Journal of Applied Meteorology* 18: 639-646.

Silliman, S. E., Berkowitz, B., Simunek, J. and van Genuchten, M. T. 2002. Fluid flow and solute migration within the capillary fringe. *Ground Water* 40(1): 76-84

Singh, V.P., and Xu, C.Y. 1997a. Evaluation and generalization of 13 mass-transfer equations for determining free water evaporation. *Hydrological Processes* 11: 311-323

Singh, V.P., and Xu, C.Y. 1997b. Sensitivity of mass-transfer equations for determining free water evaporation. *Hydrological Processes* 11: 1465-1474

Song, Z., Li, L., Nielson, P. and Lockington, D. 2006. Quantification of tidal watertable overheight in a coastal unconfined aquifer. *Journal of Engineering Mathematics* 56(4): 437-444

Stagnitti, F., Parlange, J.Y. and Rose, C.W. 1989. Hydrology of a small wet catchment. *Hydrological Processes* 3: 137-150.

Stankovich, J.M. and Lockington, D.A. 1995. Brooks-Corey and van Genuchten soil-water-retention models. *Journal of Irrigation and Drainage Engineering* 121(1): 1-7

Stauffer, F. and Kinzelbach, W. 2001. Cyclic hysteretic flow in porous medium column: model, experiment, and simulations. *Journal of Hydrology* 240: 264-275

Stewarta, J.M., and Broadbridge, P. 1999. Calculation of humidity during evaporation from soil. *Advances in Water Resources* 22(5): 495–505

Suleiman, A.A., and Ritchie, J.T. 2003. Modeling soil water redistribution during second-stage evaporation. *Soil Science Society of American Journal* 67: 377-386

Tanner, C.B. and Fuchs, M. 1968. Evaporation from unsaturated surface: a generalized combination method. *Journal of Geophysics Research* 73: 1299-1304

Teo, H.T., Jeng, D.S., Seymour, B.R. Barry, D.A. and Li, L. 2003. A new analytical solution for water table fluctuations in coastal aquifers with sloping beaches. *Advances in Water Resources* 26: 1239–1247

Thom, A.S. and Oliver, H. R.1977. On Penman's equation for estimating regional evaporation. *Quarterly Journal of the Royal Meteorology Society* 103: 345-357

Tindall, J.A., Petrusak, R.L. and McMahon P.B. 1995. Nitrate transport and transformation processes in unsaturated porous media. *Journal of Hydrology* 169(1): 51-94

Turner, I.L. 1993. Water table outcropping on macro-tidal beaches: a simulation model. *Marine Geology* 115: 227-238

Turner, I.L. 1995. Simulating the influence of groundwater seepage on sediment transported by sweep of the swash zone across the intertidal profile of macrotidal beaches. *Marine Geology* 125: 153-174

Turner, I.L. 1995. Simulating the time-varying extent of groundwater seepage on tidal beaches. *Earth Surface Processes and Landforms* 20: 833-843

Turner, I.L., and Nielson, P. 1997. Rapid water table fluctuations within the beach face: Implications for swash zone sediment mobility? *Coastal Engineering* 32: 45-59

Turner, I.L., Coates, B.P. and Acworth, R. I. 1997. Tides, waves and the super-elevation of groundwater at the coast. *Journal of Coastal Research* 13(1): 46-60

Uchiyama, Y., Nadaoka, K., and Yagi, H. 2000. Submarine groundwater discharge into the sea and associated nutrient transport in a sandy beach. *Water Resources Research* 36(6): 1467-1479

Valiantzas, J.D. 2006. Simplified versions for the Penman evaporation equation using routine weather data. *Journal of Hydrology* 331: 690-702

van de Griend, A.A., and Owe, M. 1994. Bare soil surface resistance to evaporation by vapor diffusion under semiarid conditions. *Water Resource Research* 30(2): 181-188

Van der Kamp, G. and Maathuis, H. 1991. Annual fluctuations of groundwater levels as a result of loading by surface moisture. *Journal of Hydrology* 127: 137

van Genuchten, M.T. 1980. A closed-form equation for predicting the hydraulic conductivity of unsaturated soils. *Soil Science Society of American Journal* 44: 892-898

Vincent, S.D., Williams, R.E. and Bloomsburg, G.L. 1991. Groundwater flow patterns in the vicinity of underground openings in unsaturated rock. *Journal of Hydrology* 127: 1-21

Vogel, H.J., and Roth, K. 2001. Quantitative morphology and network representation of soil pore structure. *Advances in Water Resources* 24: 233-242

Vogel, T., van Genuchten, M. Th., and Cislerova, M. 2001. Effect of the shape of the soil hydraulic functions near saturation on variably-saturated flow predictions. *Advances in Water Resources* 24: 133-144

Walker, J.P., Willgoose, G.R., and Kalma, J.D. 2001. One-dimensional soil moisture profile retrieval by assimilation of near-surface observations: a comparison of retrieval algorithms. *Advances in Water Resources* 24: 631-650

Wallace, J.S. 1995. Calculating evaporation: resistance to factors. *Agricultural and Forest Meteorology* 73: 353-66

Weise, B.R. and White, W.A. 1991. *Padre Island National Seashore: A guide to the geology, natural environments, and history of a Texas barrier island.* Texas Bureau of Economic Geology, Guidebook 17, 94 p. (2nd printing of 1980 edition).

Weisman, R.N., Member, ASCE, Seidel, G.S., and Ogden, M.R. 1995. Effects of water-table manipulation on beach profiles. *Journal of Waterway, Port, Coastal and Ocean Engineering* 121(2): 134-142

Wiggs, G.F.S., Atherton, A.J., and Baird, A.J. 2004. Thresholds of aeolian sand transport: establishing suitable values. *Sedimentology* 51: 95-108

Wiggs, G.F.S., Baird, A.J., and Atherton, A.J. 2003. The dynamic effects of moisture on the entrainment and transport of sand by wind. *Geomorphology* 59: 13-30

Williams, T.A. and Williamson, A.K. 1989. Estimating Water-Table Altitudes for Regional Ground-Water Flow Modeling, U.S. Gulf Coast. *Ground water* 27(3): 333

Willmott, C.J. 1982. Some comments on the elevation of model performance. *Bulletin of American Meteorology Society* 63(11): 1309-1313

Xu, C.Y., and Singh, V.P. Dependence of evaporation on meteorological variables at different time-scales and intercomparison of estimation methods. *Hydrological Processes* 12:429-442

Yamanaka, T. and Yonetani T. 1999. Dynamics of the evaporation zone in dry sandy soils. *Journal of Hydrology* 217(1): 135-148

Yang, Y. and Davidson-Arnott, R.G.D. 2005. Rapid measurement of surface moisture content on a beach. *Journal of Coastal Research* 21(3): 447-452

Yee, S.Y.K. 1988. The Force Restore Method revisited. *Boundary-Layer Meteorology* 43: 82-90

York, J.P., Person, M., Gutowski, W.J., and Winter, T.C. 2002. Putting aquifers into atmospheric simulation models: an example from the Mill Creek Watershed, northeastern Kansas. *Advances in Water Resources* 25: 221–238

Yuan, F. and Lu, Z. 2005. Analytical solutions for vertical flow in unsaturated, rooted soils with variable surface fluxes. *Vadose Zone Journal* 4: 1210-1218

Zhang, H., Baray D.A. and Hocking, G.C. 1999. Analysis of continuous and pulsed pumping of a phreatic aquifer. *Advances in Water Resources* 22(6): 623-632

Zlotnik, Vitaly A. 1998. Comment on "Beach water table fluctuations due to wave run-up: Capillarity effects". *Water Resources Research*, 34(11): 3201-3203

APPENDIX I: FIT REPORT OF PROBE A CALIBRATION (BY GRAPHER®)

Fit Polynomial
$Y=0.911495143-0.07626323823*X+0.001820139858*X^2-1.106137341E-005*X^3+2.909333627E-008*X^4-3.422044472E-011*X^5+1.483354465E-014*X^6$

Degree = 6
Number of data points used = 50
Average X = 395.74
Average Y = 11.952

Coefficients:
Degree 0 = 0.911495143
Degree 1 = -0.07626323823
Degree 2 = 0.001820139858
Degree 3 = -1.106137341E-005
Degree 4 = 2.909333627E-008
Degree 5 = -3.422044472E-011
Degree 6 = 1.483354465E-014

Degree: 0
Residual sum of squares = 3291.6
Coef of determination, R-squared = 0

Degree: 1
Residual sum of squares = 321.283
Coef of determination, R-squared = 0.902393

Degree: 2
Residual sum of squares = 221.468
Coef of determination, R-squared = 0.932717

Degree: 3
Residual sum of squares = 217.175
Coef of determination, R-squared = 0.934022

Degree: 4
Residual sum of squares = 109.647
Coef of determination, R-squared = 0.966689

Degree: 5
Residual sum of squares = 108.213
Coef of determination, R-squared = 0.967125

Degree: 6
Residual sum of squares = 89.3372
Coef of determination, R-squared = 0.972859

APPENDIX II: PARAMETER CALCULATIONS IN THE PENMAN EQUATION

Particularly, Δ can be calculated by

$$\Delta = \frac{4098 \cdot e_s}{T_a{}^2} \quad \textbf{(A.II.1)}$$

in which T_a is air temperature, and e_s is saturation vapor pressure (kPa) estimated by the Clausius-Clapeyron Equation

$$e_s = 0.611 \exp\left(\frac{17.27 T_a}{T_a + 237.3}\right) \quad \textbf{(A.II.2)}$$

λ varies only slightly over a normal temperature range (Valiantzas, 2006) and usually takes a constant value 2.45 MJ/kg for T =20 ^{o}C, but for higher accuracy it can be calculated by

$$\lambda = 2.501 - (2.361 \times 10^{-3})(T_a - 237.3) \quad \textbf{(A.II.3)}$$

γ is usually set as a single constant value 0.0671 (kPa), and can be estimated by

$$\gamma = 0.0016286 \cdot \frac{101.3}{\lambda} \left(\frac{293 - 0.0065 \cdot z}{293}\right)^{5.26} \quad \textbf{(A.II.4)}$$

in which z is the height of other parameters been measured (m). The net radiation R_n is calculated as the difference between the incoming net short wave radiation R_{nS}, and the outgoing net long wave radiation R_{nL} as below (Rowntree, 1991)

$$R_n = R_{nS} - R_{nL} \quad \textbf{(A.II.5)}$$

in which R_{nS} is computed as

$$R_{nS} = (1 - \alpha) R_S \quad \textbf{(A.II.6)}$$

where R_s is measured or estimated incoming solar radiation (MJ/m^2/d); α is reflection coefficient or albedo. For an open water surface, α is approximately 0.07-0.08. However, it is

expected to be somewhat higher for evaporation pan. We use 0.14 here following R_{nL} can be estimated by (Rotstayn *et al.*, 2007)

$$R_{nL} = f\varepsilon'\sigma(T_a)^4 \qquad \textbf{(A.II.7)}$$

Where σ is Stephan-Boltzman constant $= 4.903\times10^{-9}$ (MJ/m2/K4/d); T is mean air temperature (Celsius); ε' is the net emissivity, and f is adjustment for cloud cover. Details for calculations f and ε' can be found in Valiantzas (2006).

APPENDIX III: DERIVATION OF WAVE SETUP ANGLE

Longuet-Higgins (1983) considered the balance between the radiation stress S_{xx} and the on-shore pressure gradient relative to the still water level $h(x)$, and proposed a differential equation,

$$\frac{dS_{xx}}{dx} + \rho g(h_0 + h(x))\frac{dh(x)}{dx} = 0 \qquad \textbf{(A.III.1)}$$

where ρ is the water density and h_0 is the water depth relative to the still water level.

The simple analytical solution provide by Longuet-Higgins (1983) was solved for a semi-infinite domain, but the free surface boundary conditions at the water table and the landward boundaries were not included (Massel, 2001b), therefore has restricted applicability to natural beaches (Li and Barry, 2000). Li & Barry presented a numerical study of the instantaneous, phase-resolved wave motion and resulting groundwater variation in the swash zone due to progressive bore. They also considered the average flow due to wave setup using a simplified representation of the setup gradient.

Using the shallow-water approximation of Longuet-Higgins' equation, Massel (2001a, 2001b) present a formula for the setup-induced water table variation in the vicinity of shoreline,

$$\eta_s(x) = \eta_b + \frac{\gamma^2}{1+\frac{3}{8}\gamma^2}[h_b - h(x)] \qquad \textbf{(A.III.2)}$$

in which γ is the ratio of wave height to water depth (H_b/h_b), η_b is the setdown value at the breaking point, equal to $\gamma H_b/16$.

A coordinate system can be set using the intercept of beach slope and still water level as the origin O, where

$$\eta_s(0) = \eta_b + \frac{\gamma^2}{1+\frac{3}{8}\gamma^2}h_b, \qquad x = 0 \qquad \textbf{(A.III.3)}$$

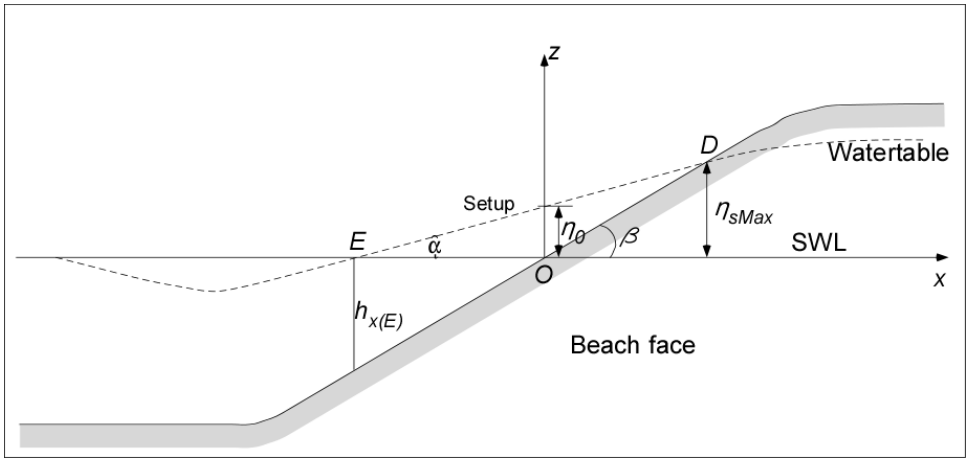

Figure A.III.1 Schematic of wave setup

The point D (water line), where set-up watertable intercept the beach slope, can be illustrated as

$$\eta_{sMax} = \eta_b + \frac{\gamma^2}{1+\frac{3}{8}\gamma^2}[h_b - h(x_D)], \qquad x = \frac{\eta_{sMax}}{\tan\beta} \tag{A.III.4}$$

The point E, where setup watertable intercept the still water level, setup height is 0, can be illustrated as,

$$0 = \eta_b + \frac{\gamma^2}{1+\frac{3}{8}\gamma^2}[h_b - h(x_E)], \qquad x = -\frac{\eta_s(0)}{\tan\alpha} \tag{A.III.5}$$

where is the angle between the setup watertable and still water level (here assumed the setup watertable is linear).

$$h(x_E) = \frac{\eta_b + \frac{\gamma^2}{1+\frac{3}{8}\gamma^2}h_b}{\frac{\gamma^2}{1+\frac{3}{8}\gamma^2}} = \frac{\frac{\gamma^2}{16}h_b}{\frac{\gamma^2}{1+\frac{3}{8}\gamma^2}} + h_b = (1+\frac{8+3\gamma^2}{128})h_b \tag{A.III.6}$$

Since for flat beach $\gamma \approx \frac{1}{1.2}$ (Turner, 1997), $h(x_E)$ hence might be approximated by $1.079h_b$, given:

$$\tan\alpha = \frac{\eta_b + \frac{\gamma^2}{1+\frac{3}{8}\gamma^2} h_b}{\frac{1.079 h_b}{\tan\beta}} = \left(\frac{\gamma^2}{16} + \frac{\gamma^2}{1+\frac{3}{8}\gamma^2}\right)\frac{\tan\beta}{1.079} \qquad \textbf{(A.III.7)}$$

$$= 0.232\tan\beta$$

Therefore, setup angle could be approximated by:

$$\tan\alpha = 0.232\tan\beta \qquad \textbf{(A.III.8)}$$

VITA

Yuanda Zhu was born in Wugang, Hunan Province, of the People's Republic of China. He obtained his bachelor degree of science in environmental protection from the Huazhong Agricultural University in Wuhan, China, in 1998. Immediately after graduation, he began his graduate studies at the same university and was awarded the master of science in soil science in 2001. Between 2001 and 2003, he worked as a Research Associate at the Institute of Geographical Research and Natural Resources Research, Chinese Academy of Sciences. In August 2003, he came to the United States and began a doctoral program at the Louisiana State University. He expects to receive his Doctor of Philosophy degree in geography in fall 2007.